OPTICAL STUDIES OF LONGITUDINAL VIBRATIONS IN CIRCULAR Z-CUT QUARTZ DISCS

BY

ALAN.F.B.WOOD.

THESIS PRESENTED FOR THE DEGREE OF

DOCTOR OF PHILOSOPHY

IN THE

UNIVERSITY OF LONDON

Royal Holloway College June 1955

ABSTRACT

A historical review of the use of powder patterns, polarized light and interferometry to examine small vibrations is given. Suitably cut quartz crystals are used for an examination by these methods of the longitudinal vibrations of thin isotropic discs. Previous calculations of the frequencies and displacements for these modes of vibration are extended and the distribution of stress is computed numerically. The theory underlying the use of the three methods of observation is discussed with particular reference to the examination of these stresses and displacements.

It is found that for sufficiently thin discs the primary stresses and displacements are substantially in agreement with theory, except for the presence in all cases of a coupled flexural mode having a particular symmetry dependent upon the symmetry of the longitudinal mode. Moreover, for those modes which do not have circular symmetry about the disc axis, there are always two frequencies of vibration for which the orientations of the vibratory systems have a particular relation, again dependent upon the particular modal symmetry. A theory is given which

adequately explains the coupling phenomena by reference to the cross shear strains which are due to the particular crystal symmetry of quartz and are not possible for isotropic media.

In connection with the polarized light experiments, a theory of the dependence of the apparent rotatory power of quartz upon stress is developed and agrees well with an experimental test; some phenomena observed by earlier workers are explained on the basis of this theory.

It is shown that there is good correlation between the three methods of observation but that the information yielded by any one method separately is likely to give an oversimplified representation of the state of vibration.

CONTENTS

Note: Figures and Tables are usually placed immediately after the page on which they are first mentioned.

CHAPTER 1

GENERAL INTRODUCTION

The theoretical analysis of the modes of vibration of solid bodies has been completed for a comparatively few cases only, mostly involving one or two dimensional motions. Many of the theoretical results regarding the nodal lines in such cases have been verified experimentally. Some workers have investigated the free vibration of bodies where there is no known theory to predict the motion and have worked out empirical criteria for the types of vibration.

In the case of piezoelectric crystal oscillators for electronic uses, exact solutions of the equations of motion are rarely possible. A great deal of experimental work has been carried out, mostly in the decade 1926-36, with somewhat variable success. Most of these experiments were of an empirical nature and, as the theoretical basis of some of the methods of observation had not been investigated fully, it would be rash to deduce too much about the vibration of a crystalline body therefrom.

The purpose of the present work is to examine systematically a few comparatively simple modes of vibration of a solid body by three of the more prominent methods of observation and to correlate the results as far as possible.

The material chosen for these studies is crystalline quartz; this may easily be excited piezoelectrically into any of its characteristic vibrations, provided the applied alternating electric field is appropriate. In practice this means that as long as the field is not precisely symmetrical, any mode may be excited by increasing the magnitude of the field sufficiently.

The problem will be treated throughout as one of free vibrations with little, if any, reference to the piezoelectric properties of the crystal. This is justified since the coupling coefficient in quartz is small. The forced vibrations of a quartz crystal at a frequency far removed from resonance are so exceedingly minute that even the use of multiple-beam interference under the most favourable conditions would be quite inadequate for their detection. At resonance, the amplitude of vibration is increased by many orders of magnitude and a large alternating electric field is set up within the crystal, by virtue of the direct piezoelectric effect. The resultant potential difference is many times greater than that applied to the crystal but, as it is considerably smaller than that required to force vibrations of the same amplitude and therefore results in second order effects only, its effect on the form of the vibration may be ignored. The experiments of Colwell and Hill (1937) are interesting in this connection

as these workers found that, at a given frequency, a quartz plate displayed the same Chladni figures whether excited piezoelectrically or mechanically (by contact with a rod excited by the magnetostriction effect).

Although a study of the vibrations of quartz crystals is of interest for its own sake, owing to the technological importance of such vibrations, in the present studies every endeavour is made to simulate isotropic conditions by cutting the quartz normal to the optic axis and choosing an appropriate series of characteristic vibrations. The reason for this is that, although the ultimate purpose of this work is to advance the knowledge of the vibrations of crystalline bodies, the author feels that there is scope for a great deal of preliminary work on isotropic bodies. Were it transparent, and capable of taking an optical polish, a homogeneous piezoelectric substance, such as barium titanate, would be in many ways superior to quartz. Thus a large part of the work is concerned with trying to isolate the effects of crystal structure from those due to the phenomena under investigation.

The modes of motion chosen for this investigation are the longitudinal vibrations of thin circular discs, first discussed theoretically by Love (1927). They have been investigated quite successfully by Petrzilka (1932,1935a), although he observed certain discrepancies which will be

discussed later. The methods of observation used by the present author are:

1) By scattering lycopodium powder on the surface
2) By polarized light
3) By multiple-beam interferometry

The first method is more mechanical than optical, but since it gives a visual picture of the motion, it falls within the scope of the thesis title. To avoid confusion the three methods will usually be treated separately, until the final chapter. Historically, they were developed in the order listed above but it will be more convenient to vary this order in the theoretical and experimental sections.

PART I HISTORICAL REVIEW OF PREVIOUS STUDIES OF SMALL VIBRATIONS.

CHAPTER 2

THE USE OF POWDERS TO INDICATE MODES OF VIBRATION

2.1 Flexural vibrations

The use of fine powders to reveal the motion of a vibrating body dates back to the classic experiments of Chladni (1787) who sprinkled sand on vibrating brass plates and thus revealed the nodal systems. His experiments have been repeated on many occasions and have gained additional interest from the theoretical calculations (by Kirchoff (1850), Ritz (1909), and others) of the modes of flexural vibration of circular and rectangular plates.

Various methods for the excitation of vibrations have been used in these investigations. For example, Chladni and others used bowing. Schulze (1907) excited a circular microscope coverslip, resting on a wire gauze, by sounding a Galton whistle beneath it, the nodes being indicated by fine sand.

Wachsmuth and Auer (1928) and Doerffler (1930) used piezoelectrically excited flexural waves in quartz plates to show the transition from flexural to shear wave propagation as the wavelength became small compared with the thickness of the plate. Petrzilka (1932) used circular tourmaline plates cut normal to the optic axis, and excited piezoelectrically, to examine flexural vibrations. Krista (1939) carried out

a similar study using rectangular Z-cut quartz plates. The patterns observed in these cases were very similar to those of isotropic plates, in agreement with theory.

Colwell (1931) excited vibrations by a telephone receiver, or a moving coil loudspeaker unit, in an extensive investigation of the flexural vibrations of circular and rectangular plates. As mentioned in Chapter 1, Colwell and Hill (1937) showed that the patterns observed on a vibrating quartz plate were the same whether the plate was excited piezoelectrically or by external means. Pavlik (1936) used a stainless steel disc and excited it directly by virtue of the magnetostriction effect, using a very high frequency magnetic field (up to 700 Kc/s).

Finally Waller (1937,1949) excited flexural vibrations in variously shaped steel plates by contact with a piece of solid carbon dioxide. Most of the papers quoted here are parts of series by their respective authors and many other workers have also studied flexural vibrations.

In the case of flexural vibrations, the observed patterns have agreed closely with theory, although they are often distorted when the particular flexural mode under examination is coupled to another of slightly different natural frequency. However, this apparent distortion is due to the failure of the mathematical theory to predict the

motion, not of the experimental method to depict the nodes. The reason for the sand or other powder moving to the nodes has been discussed at some length by Andrade and Smith (1931), but the views of Rayleigh (1894) on this subject seem to be quite adequate, namely 'If a grain be situated elsewhere than at a node it is made to jump by a sufficiently vigorous transverse motion. The result may be a movement either towards or from a node; but after a succession of such jumps the grain ultimately finds its way to a node as the only place where it can remain undisturbed.'

2.2 Longitudinal vibrations

The experimental work on the investigation of longitudinal vibrations by powder methods has been less successful than that on flexural vibrations and anomalies are the rule rather than the exception. As long ago as 1820 Savart found that a horizontal glass strip vibrating in the fundamental longitudinal mode showed more than the solitary central node which he expected from theory. Furthermore the pattern produced on the other side, when the glass strip was turned over, was different, the two sets of nodes alternating along the length, with certain exceptions. Savart postulated the existence of a flexural mode of high order coupled to the longitudinal mode and producing the anomalous nodes, although his explanation of their formation is far from clear. It

contains, however, the essence of the complementary nature of the patterns on the two sides, namely, that at a particular point on the length of the strip a given longitudinal movement, e.g. away from the centre of the strip, is accompanied by a motion normal to the plane of the strip, due to the flexure, which is outwards on one side and inwards on the other.

Terquem (1858) repeated Savart's work and gave a clearer explanation of the motion of the sand particles. Lissajous (1858) also observed the same type of patterns on a bar which was clamped at each end.

The study of longitudinal waves in quartz or other piezoelectric crystals has been mainly empirical and directed towards the ascertainment of the types of motion rather than a verification of theoretically predicted vibrations. This is inevitable in view of the difficulty of the theoretical treatment of anisotropic bodies.

Harding and White (1929) studied the longitudinal vibrations of quartz blocks empirically and were able to relate certain general types of lycopodium pattern to the air currents emitted from the corresponding faces of the block. Wright and Stuart (1931) also used the lycopodium method to study the vibrations of rectangular and circular quartz plates, cut either normal to the X-axis or normal to a line in the XY-plane making an angle of 30° with the X-axis, that is, the Y-axis.

They made an empirical examination of some of the modes of vibration, mainly longitudinal, of these plates and noticed that the nodes indicated by the lycopodium were not all of the same nature, as the powder tended to move along some of them. It is not possible to comment further on this work as there is no theory to predict the displacements involved in the modes which they studied.

By using crystals cut in such a way as to behave as if isotropic towards particular types of stress, Petrzilka was able to apply the theory of longitudinal vibrations in thin isotropic circular discs given by Love (1927). Using Z-cut tourmaline discs (1932) Petrzilka successfully showed the existence of Love's dilatational (type A) and rotational (type B) modes and later (1935 a), using Z-cut quartz discs, was able to excite vibrations at the expected frequencies of the composite (type C) modes. The frequencies were in good agreement with theory for the quartz, and a few percent in error for the tourmaline. In all cases, however, the lycopodium patterns showed too many nodes and were so complex for the type C modes that he did not think the calculation of the displacements for the latter modes worthwhile. In the case of the tourmaline experiments, he noticed that the patterns on the two faces of the crystal were complementary, but did not say whether this was so for the quartz. In the

1932 paper he had also examined the flexural modes, which should be the same as those for isotropic discs, as already mentioned. The nodes were found to consist solely of diameters and circles as given by Kirchoff's theory (1850) but the frequencies were badly in error. Petrzilka carried out further experiments (1935 b) on longitudinal vibrations using rectangular Z-cut quartz crystals, Lissütin (1930) having already published a theoretical paper on the subject. These plates may again vibrate in dilatational, rotational or composite modes, and although the frequencies were in good agreement with theory the patterns were disturbed in much the same way as before.

In a critical review of Petrzilka's work, Lonn (1937) considered the sources of error in the calculated frequencies and concluded that the frequency errors for the flexural vibrations of tourmaline were primarily due to the fact that the crystals were too thick for secondary effects (e.g. rotational inertia) to be ignored. He considered that for the longitudinal vibrations, the crystals, both quartz and tourmaline, were thin enough for the frequencies to be correct within the experimental errors, and that the errors in the case of the tourmaline were due to inaccurate values for the elastic constants. Finally he considered that the observed lycopodium patterns were complicated by flexures and referred

to Terquem's work (1858).

In 1938 Petrzilka (in collaboration with Zacek) published a further paper on the longitudinal vibrations of Z-cut quartz crystals, this time using circular annuli. Once more, although the frequencies were correct, the lycopodium patterns were complicated by extra nodes, superfluous to the theory. Petrzilka referred to Lonn's comments but did not agree that the supposed coupled flexure could account for all the observed discrepancies.

CHAPTER 3

THE USE OF POLARIZED LIGHT

The stress-optic effect was discovered by Brewster (1815), who found that glass became birefringent under stress, and suggested examining glass models of mechanical structures by polarized light to determine the stresses. In 1841 Neumann gave a satisfactory explanation of the stress-optic effect in isotropic media. Although Brewster (1818) had recorded the stress-optic effect in crystals, soon after his first experiments with glass, and many other workers including Moigno and Soleil (1850) and Bücking (1883) obtained further results with crystalline media, it was not until 1889 that Pockels gave the mathematical theory for the effect. He assumed that the changes in the optic parameters of the index ellipsoid were linear functions of the six components of stress or strain in the medium, and discussed the effect of crystal symmetry on the number of stress-optic coefficients required to express these relationships.

The linear electro-optic effect, that is a change in optical properties caused by an electric field which changes sign with sign of the field, was discovered almost simultaneously by Röntgen (1883) and Kundt (1883). Again Pockels (1890) gave a mathematical theory involving a linear

relation between the change in the optical parameters and the three components of electric polarization.

Tawil (1926) made the first application of the stress-optic effect to the examination of a vibrating body. An X-cut quartz crystal was placed between crossed polarizer and analyser and observed along the X-axis, the natural birefringence being compensated for by a second X-cut quartz plate with its axes at right angles to those of the first. On exciting the quartz into vibration by means of a valve oscillator connected to transparent electrodes on the X-faces, the initially dark field lit up in certain regions and as the frequency was varied a different pattern was seen for each mode of vibration. Tawil also examined the crystal along the Z-axis; initially the field had a uniform tint, due to the rotatory dispersion of quartz (presumably no compensating plate of opposite hand being used) and on exciting the quartz, the field lit up in patches with substantially white light, thus reducing the saturation of the colouration already present in these regions. Tawil assumed the effects to be due to the superposition of an additional birefringence upon the natural birefringence of quartz. Later, in 1929, he used the stress-optic effect to show that quartz can be excited piezoelectrically into vibrations along the Z-axis. This work is open to serious objection, however, since his reasoning depends upon a comparison of the optical effects produced by

stresses in different crystallographic directions and he takes no account of the anisotropy of the quartz.

Ny Tsi Ze (1927) carried out a series of experiments to test the mechanical and optical effects of electric stress in quartz, using various interferometric methods of observation. The field was always applied along the X-axis by two semi-transparent silver coatings on the major faces. He made allowances for the effect of the change of dimensions, due to the field, on the observed retardations but did not allow for the contribution of the stress-optic effect due to these changes of dimension. Pockels (1890) had previously found the true electro-optic and the induced stress-optic effect to be of the same order of magnitude when quartz is subjected to an electric field. Moreover Ny Tsi Ze found a variation of the extraordinary refractive index, an effect which the symmetry of quartz does not allow, according to Pockels.

Moens and Verschaffelt (1927) performed some experiments on vibrating quartz using a different method from Tawil's. An X-cut quartz plate excited into vibrations along the X-axis was mounted between crossed Nicols and illuminated by white light, the emergent light being examined by a spectrometer. When observations were made along the X or Y-axes the spectrum

was channelled by dark bands, these corresponding to wavelengths for which the retardation between the two waves was a whole number of wavelengths. When the quartz vibrated, these broadened and grew less distinct, as might have been expected. When observing along the Z-axis, however, a most striking effect was noticed. Due to the rotatory dispersion of quartz, a broad extinction band was seen in the middle of the spectrum (for the 12 mm thick crystal used there would be two others in the extreme red and the extreme blue). On vibration of the quartz, this band became less distinct and moved bodily towards the red. The band could be restored to its initial position by rotating the analyser. The effect was remarkable as it indicated an increase of rotation which did not change sign with reversal of the stress directions. Moens and Verschaffelt were at a loss to explain the effect, except for saying that the fading was due to a change of birefringence, but Cady (1946) considered that it was due to the change in birefringence under stress and not to a change in true rotatory power, this being unaffected by stress. Moens and Verschaffelt said in conclusion that the effect could not be produced by either a static stress or a static electric field and that the failure of the electric field to produce any effect probably confirmed Ny Tsi Ze's observation that the length parallel to the Z-axis hardly alters when an electric

field is applied. This phenomenon will be discussed more fully in Chapter 17.

Günther (1932) carried out a similar investigation to that of Ny Tsi Ze and his results were in fairly good agreement with those of Pockels. Petrzilka (1931) repeated Tawil's experiments using a rectangular X-cut quartz plate and showed that in the neighbourhood of the thickness vibration there was a multitude of modes, none of which could be definitely identified as the true thickness vibration. He also observed the vibrating quartz in the direction of the optic axis by means of the interference rings formed in convergent plane polarized light. According to Kundt (1883), these rings are deformed into ellipses by the application of an electric field in the XY-plane, their axes being parallel to the X and Y-axes when the field is along the Y-axis, but at 45° to these directions when the field is along the X-axis, the major and minor axes interchanging when the field is reversed. For an oscillating electric field the axes interchange periodically to give diffuse lemniscates. Petrzilka considers that the observed figures are due to the electric field but, as has already been mentioned in Chapter 1, in the case of resonant vibrations the electric field is of secondary importance only. This method of observation, using convergent polarized light, can only give an idea of the direction of principal stresses in

very simple cases, as the observed figures are the integrated result of the transmission of light through the whole crystal.

Pan Tcheng Kao (1935) published the results of an investigation made some years previously. He observed a quartz plate by plane polarized light along the optic axis and compensated for the rotation of the plane of polarization by reflecting the light back through the quartz. The original plane of polarization was thus restored, irrespective of the wavelength of the illumination,so that a dark field could be obtained by using a crossed analyser. On exciting the quartz by a field along the X-axis, the quartz became illuminated in certain regions, this illumination being coloured. For high order modes the colouration took the form of red and green spots in regular alignment. It was claimed that this regularity was upset by any slight lack of homogeneity in the quartz. However,no explanation was given for these phenomena, which were substantially the same as those observed by Tawil.

Bruninghaus (1935) carried out a fairly systematic investigation of the modes of vibration of X-cut quartz plates, using Tawil's method, the length and breadth being parallel to the Z and Y-axes. He considered pure longitudinal vibrations parallel to the edges of the plate, the frequency constants being given by Hund's formulae (1926). Where the frequencies of overtones of the vibrations in two or more directions

approached each other, Bruninghaus expected to find combination modes. The vibrations were generally more complicated than expected and the frequencies were not very close to the predicted ones. This was not surprising in view of the fact that he had taken no account of elastic coupling between vibrations in the three dimensions.

Eichhorn (1936) made an investigation of the flexural vibrations of X-cut quartz bars, their lengths being in the Y-direction and the flexural displacements occurring in the Z-direction. The bars were observed along the X-axis by Tawil's method, using similar bars with length along the Z-axis to compensate for the natural birefringence. The crystals used resonated at frequencies of the order of 20 Kc/s, and so it was possible to make an efficient stroboscope using a Kerr cell and a phase shifter, enabling the vibrations to be examined at any time in the cycle. He observed the isoclinic along the neutral axis and by using an Ehringhaus compensator with a white light source, the variation of stress was shown up as a variation of tint over the surface of the crystal. He was thus able to make an estimate of the variation of stress although had he used monochromatic light, the stress would presumably have been too small to cause the appearance of the first order stress fringe. He showed the difference

between the types of stress at the centre and outer nodes when the bar was vibrating in the first overtone; he also showed that the longitudinal stress was a linear function of the distance from the neutral axis and gave a graph showing the variation of the longitudinal stress along the length of the bar. Using Pockels' data he made an estimate of the magnitude of these stresses.

Ny Tsi Ze and others (1936) examined the vibrations of hollow quartz cylinders with their axes in the Z-direction, a reflection system being used similar to that of Pan Tcheng Kao (1935). The observed patterns for radial, circumferential and longitudinal modes were very much as they expected from theory. As the crystals were very thick in the direction of the light path (often several centimeters) nothing corresponding to isoclinics would have been indicated (see sections 7.5, 14.4 on this point).

Murray (1941) carried out a similar investigation to Eichhorn's using stroboscopic illumination, but he used a bakelite cantilever excited mechanically at very low frequencies, retardations of several wavelengths being set up.

Bergmann (1949) investigated the vibrations of thick glass cylinders by plane and circularly polarized light. The cylinders were observed along their axes and the vibrations

were excited by resting the curved surface on a suitable quartz vibrator. Of the large number of modes observed, Bergmann selected the pure radial vibrations for a comparison with the mathematical theory worked out by Airey (1913). The observed zero order stress fringes were in good agreement with the calculated values and Bergmann also explained the formation of the dark cross which delineates the isoclinic for a given setting of polarizer and analyser.

CHAPTER 4

THE USE OF INTERFEROMETRY

4.1 Two-beam interference

The method was first used by Dye in 1927, this work being published posthumously in 1932. He examined the piezoelectric vibrations of circular and rectangular X-cut quartz plates by observing the two-beam interference fringes localized in the gap between one polished face of the crystal and a slightly inclined glass reference flat. On setting the crystal into vibration, the fringes broadened, owing to the normal displacement of the surface, the nodal regions of the latter being clearly defined. Alternatively, by using very flat crystals and adjusting the dispersion of the fringes until a minimum of intensity covered the whole surface of the crystal, the antinodal regions alone were illuminated when the crystal vibrated, thus giving a striking presentation of the nodes as black lines on a bright background. By using a helium discharge lamp driven from the same oscillator as that used to drive the crystal, the resulting stroboscopic illumination showed the distorted fringes at maximum displacement.

Thomas and Warren (1928) used the interference fringes formed between a reference flat and a glass coverslip cemented to a reed to examine the vibrations of the latter. They

argued that on vibration the visibility of the broadened fringes becomes zero when the amplitude is $(2n+1)\lambda/8$, n being an integer and λ the light wavelength, and reaches a maximum again for amplitudes of $n\lambda/4$. By counting the reappearances of the fringes as the amplitude increased they were able to measure the amplitude of the reed to an accuracy of 1% or more up to about 8λ, after which the general visibility deteriorated.

Osterberg (1929,1932) used two-beam interference in reflection to examine the vibrations of a quartz crystal, but he obtained the fringes by using the polished quartz face as one mirror of a Michelson interferometer. He noticed the complexity of the patterns and found a non-linear relationship between the crystal amplitude and the exciting voltage. The amplitude was measured by Thomas and Warrens' method but Osterberg used a theoretically calculated formula for the critical amplitudes corresponding to maximum and minimum visibility and showed the previous authors' empirical formula to be incorrect.

Later (1933) Osterberg used a compound Michelson interferometer in which he was able to observe the relative motion of different faces of a quartz block by an ingenious system of mirrors. He also used a refracting interferometer (1934) in which the quartz crystal under investigation was placed in one arm of a Michelson interferometer so that

changes of refractive index due to the vibrations produced a fringe broadening. The broadening due to the change of refractive index was found to be large compared with that produced by the change of thickness, which could therefore be ignored. He hoped to find a value for some of the stress-optic coefficients by comparing the observed fringe shift with the measured surface amplitude (found by using his earlier interferometric methods) for a known type of motion and then to compare these results with Ny Tsi Ze's static determinations (1927), but this work was not followed up. He also found that it was impossible to excite true longitudinal vibrations along the thickness of thin X or Y-cut crystals.

Cortez (1934) used Osterberg's original method (1929) to examine the vibrations of a quartz crystal, but he used white light illumination so that only a central black fringe could be seen when the crystal was at rest. The angle of the quartz surface relative to the incident light beam having been adjusted until this fringe was very narrow, the latter split into two faint brown fringes when the quartz vibrated, and Cortez assumed that these corresponded to the extreme normal excursions of the surface. By positioning the quartz crystal suitably, the black fringe could be shifted to any region of the surface, thus allowing the amplitude to be measured there by comparing the fringe shift with that produced

when the quartz surface was advanced a known distance by a calibrated screw. He measured the amplitude for various strengths of excitation and found this to be proportional to the R.F. current flowing in the oscillatory circuit across which the crystal was connected.

Straubel (1933) also used Osterberg's method but he used a very flat quartz crystal and adjusted the angle of the face until it was exactly normal to the light beam and in such a position as to give darkness over the whole face when at rest. On vibration, the nodal system was revealed as black lines on a bright background, as in Dye's case. In a further paper (1934) he used Osterberg's method (1929) for calculating the amplitude of vibration and, like Osterberg, found that the amplitude was not proportional to the applied voltage, although he did not make very extensive measurements.

Schumacher (1937) used Dye's arrangement to investigate the compressional vibrations of Y-cut quartz plates. He discussed the effect of boundary conditions and showed that a given interference pattern was distorted if the quartz was clamped in an antinodal region.

Kotlyarevski and Pumper (1941) reviewed the previous work on interference and, by using Dye's method of examination, showed that similar quartz plates had the same set of vibratory modes and that the symmetry or otherwise of the observed

patterns indicated the homogeneity of the crystal. Furthermore these patterns were little altered by external conditions.

Borodovskaya and Salomonovich (1951) used Osterberg's method (1929) to measure the amplitude of a vibrating quartz crystal but, contrary to the results of Osterberg and Straubel, found a linear relationship between crystal amplitude and applied voltage.

4.2 Multiple-beam interference

Tolansky and Bardsley (1948,1951) made the first application of multiple-beam interference to the study of vibrations. The multiple-beam method offers many advantages over the two-beam methods; the fringes, being very narrow compared with their separation, retain a sharp envelope when vibrating, even if they overlap. Bardsley (1951) made an estimate of the probable error in the amplitude of vibration as measured by the width of the moving fringe envelope and this will be discussed in Section 6.3. He used the multiple beam method in an examination of the vibrations of variously cut quartz plates and bars and Z-cut quartz rings. He also investigated the amplitude of vibration as a function of the crystal current and obtained a linear relationship between them.

By placing reference flats on each side of a quartz disc two sets of fringes were formed and, if the fringes were arranged to be approximately at right angles to one another, the field of view was covered by bright spots where they intersected. On vibration, the spots traversed lines joining the extreme positions of the intersections of the moving fringes. Knowing the direction of increasing wedge gap on either side of the crystal, the orientations of these short lines showed the relative phases of the two surfaces at various points on the crystal and by this means Bardsley was able to distinguish between flexural and compressional vibrations.

Stroboscopic observations were made by using a mercury discharge lamp or Kerr cell illumination. More interesting, however, is a phenomenon noticed by Bardsley in which the crystal acts as its own stroboscope. While endeavouring to observe strain patterns in the vibrating quartz, (which was still set up for interference observations) by placing it between two polaroids, he noticed that for certain orientations of the polarizer and analyser, one side or the other of the oscillating fringe envelope could almost be removed, and near these settings the strain pattern could be seen either as dark lines on a bright background or vice

versa. Although no explanation of the effect was offered, a qualitative explanation is simple when it is remembered that although the change of optical properties is equal and opposite for alternate extremes of the vibratory cycle, the resultant birefringence is not, since no compensation for the natural birefringence was used. Hence a setting of the polaroids may always be found for which the intensity of the transmitted light will be greater at one extreme of the cycle than at the other, thus producing a partial stroboscopic effect.

Bardsley made a multiple-beam version of Osterberg's refracting interferometer by forming interference fringes between the two silvered surfaces of a crystal. He found that on vibration, the fringes, which were double owing to the birefringence of quartz, had a different intensity distribution from that of the vibrating fringes formed between one surface of the crystal and a reference flat. An interpretation of the interferometric picture obtained would be difficult, as he used an obliquely cut plate (GT) and a large number of stress-optic coefficients would have to be considered.

Apart from one observation on a composite metal-quartz vibrator, Bardsley used transmitted multiple-beam fringes exclusively. The reflected fringes suffer from the disadvantage that the visibility decreases as soon as the

fringes oscillate. Bruce, Macinante and Kelly (1951) have used multiple-beam interference in reflection to measure the amplitude of vibration of a tuning fork but, by removing the first reflected beam, transmission like fringes were obtained. This method, however, can be used easily only where the whole surface moves parallel to itself, as otherwise the first reflected beam is dispersed as soon as vibration sets in.

PART II THEORY OF THE VIBRATIONS TO BE STUDIED AND THE METHODS OF OBSERVATION.

CHAPTER 5

THE MATHEMATICAL THEORY OF LONGITUDINAL VIBRATIONS IN CIRCULAR DISCS

5.1 Plane stress in an isotropic medium, and in quartz.

For an isotropic medium, the six components of strain at any point may be expressed in terms of the six components of stress by two independent elastic constants:

5.1
$$x_x = [X_x - \sigma(Y_y + Z_z)]/E \quad (1) \qquad y_z = 2(1+\sigma)Y_z/E \quad (4)$$
$$y_y = [Y_y - \sigma(Z_z + X_x)]/E \quad (2) \qquad z_x = 2(1+\sigma)Z_x/E \quad (5)$$
$$z_z = [Z_z - \sigma(X_x + Y_y)]/E \quad (3) \qquad x_y = 2(1+\sigma)X_y/E \quad (6)$$

where E and σ are Young's modulus and Poisson's ratio. Considering now a thin lamina parallel to the XY-plane, if there are no external tractions acting over the faces, the stresses having components parallel to the Z-axis, namely Z_z, Y_z, Z_x, become vanishingly small as the thickness decreases, as also do the differential coefficients, with respect to z, of the remaining stresses. These conditions define a state of plane stress and eqns 5.1 reduce to:

5.2
$$X_x = E(x_x + \sigma y_y)/(1-\sigma^2) \quad (1)$$
$$Y_y = E(\sigma x_x + y_y)/(1-\sigma^2) \quad (2)$$
$$X_y = \tfrac{1}{2}Ex_y/(1+\sigma) \quad (3)$$
$$z_z = -\sigma(x_x + y_y)/(1-\sigma) \quad (4)$$

Before proceeding further, the application of the

theory to Z-cut quartz laminae will be discussed. In general, 21 independent coefficients are needed to express the strain components of an anisotropic medium in terms of the stress components, or vice versa. This number is reduced by crystal symmetry, and for quartz only six independent coefficients are required, the equations equivalent to 5.1 being:

5.3
$$x_x = s_{11}X_x + s_{12}Y_y + s_{13}Z_z + s_{14}Y_z \quad (1)$$
$$y_y = s_{12}X_x + s_{11}Y_y + s_{13}Z_z - s_{14}Y_z \quad (2)$$
$$z_z = s_{13}X_x + s_{13}Y_y + s_{33}Z_z \quad (3)$$
$$y_z = s_{14}X_x - s_{14}Y_y + s_{44}Y_z \quad (4)$$
$$z_x = s_{44}Z_x + 2s_{14}X_y \quad (5)$$
$$x_y = 2s_{14}Z_x + 2(s_{11} - s_{12})X_y \quad (6)$$

Applying the conditions for a plane stress system, we find

5.4
$$X_x = (x_x - (s_{12}/s_{11})y_y)/s_{11}(1 - (s_{12}/s_{11})^2) \quad (1)$$
$$Y_y = (-(s_{12}/s_{11})x_x + y_y)/s_{11}(1 - (s_{12}/s_{11})^2) \quad (2)$$
$$X_y = \tfrac{1}{2}x_y/s_{11}(1 - s_{12}/s_{11}) \quad (3)$$
$$z_z = (s_{13}/s_{11})(x_x + y_y)/(1 + s_{12}/s_{11}) \quad (4)$$
$$y_z = s_{14}(X_x - Y_y) \quad (5) \qquad z_x = 2s_{14}X_y \quad (6)$$

Since $1/s_{11} \equiv E$ and $-(s_{12}/s_{11}) \equiv \sigma$ for stresses in the XY-plane, the conditions as regards the latter stresses are the same as for an isotropic medium but the extensional strain normal to the lamina is proportional to $(s_{13}/s_{11})/(1 + s_{12}/s_{11})$ instead of to $(s_{12}/s_{11})/(1 + s_{12}/s_{11})$, the value required for equivalence to the isotropic case. Numerically, $s_{13}/s_{11} = -0.121$ and $s_{12}/s_{11} = -0.133$. In the derivation of the equations of

vibration (Section 5.2), the kinetic energy associated with the displacements in the Z-direction is ignored, so that the theory for an isotropic lamina is directly applicable as regards these equations. It is seen, however, that the shear strains y_z and z_x, acting in planes normal to that of the lamina, do not vanish, and these result in mechanical coupling between the longitudinal modes of vibration under discussion and flexural modes. This effect will be disregarded until Chapter 17, the vibrations of a truly isotropic lamina being considered until then. Lonn (1937) has shown that for a quartz disc with a ratio of thickness to diameter as large as 0.15 (used by Petrzilka, 1935a), the effect of all the disregarded strains can alter the frequency of the lower modes by only 0.1%

5.2 Longitudinal vibrations of a lamina

The differential equations of motion for small displacements u,v, w of an element of an elastic body are

$$5.5 \qquad \partial X_x/\partial x + \partial X_y/\partial y + \partial Z_x/\partial z + \rho X = \rho \partial^2 u/\partial t^2$$

together with two similar equations obtained by changing X,x,u, etc. cyclically. In these equations ρ is the density of the medium and X,Y,Z are body forces, for example, gravitational forces. Ignoring these body forces, the only operative forces in the present case are X_x, Y_y and X_y; considering an element $\delta x \times \delta y \times 2h$ of a lamina,

thickness 2h, we have:

5.6 $$2h\rho\partial^2u/\partial t^2 = \partial T_x/\partial x + \partial S_{xy}/\partial y \quad (1)$$

$$2h\rho\partial^2v/\partial t^2 = \partial S_{xy}/\partial x + \partial T_y/\partial y \quad (2)$$

where T_x, T_y, S_{xy} are the stress resultants, that is, the tractions acting over unit length of the cross section due to the stresses X_x, Y_y and X_y. Using the values of these stresses given by eqn 5.2 and expressing the strains $x_x = \partial u/\partial x, x_y = \partial v/\partial x + \partial u/\partial y$ etc. in terms of the areal dilatation $\Delta = \partial u/\partial x + \partial v/\partial y$ and the rotation $\omega = \frac{1}{2}(\partial v/\partial x - \partial u/\partial y)$, eqns 5.6 become:

5.7 $$\partial\Delta/\partial x - (1-\sigma)\partial\omega/\partial y = (\rho/E)(1-\sigma^2)\partial^2u/\partial t^2 \quad (1)$$

$$\partial\Delta/\partial y + (1-\sigma)\partial\omega/\partial x = (\rho/E)(1-\sigma^2)\partial^2v/\partial t^2 \quad (2)$$

Differentiating these with respect to x and y respectively and adding:

5.8 $$\nabla^2\Delta = (\rho/E)(1-\sigma^2)\partial^2\Delta/\partial t^2 \quad (1)$$

and by differentiating with respect to y and x and subtracting:

5.8 $$\nabla^2\omega = 2(\rho/E)(1+\sigma)\partial^2\omega/\partial t^2 \quad (2)$$

where $\nabla^2 = \partial^2/\partial x^2 + \partial^2/\partial y^2$

Since the solution will be periodic in t we may write:

5.9 $$\nabla^2\Delta + k^2\Delta = 0 \quad (1) \qquad \nabla^2\omega + k_1^2\omega = 0 \quad (2)$$

where $k^2 = (\rho/E)(1-\sigma^2)p^2, k_1^2 = 2(\rho/E)(1+\sigma)p^2$ and p is the angular frequency of vibration. Δ and ω may be found from eqns 5.9, and substituting these values in eqns 5.7 gives u and v. Finally, substituting u and v in eqns 5.2 and

using the requisite boundary conditions for the stresses, namely, that at the periphery of the lamina the shear stress X_y and the component normal to the periphery of the tensile stresses X_x and Y_y vanish, the frequency equation for longitudinal vibrations in the plane of the lamina is obtained.

5.3 Application to a circular disc

In this case it is convenient to use cylindrical coordinates (r,θ,z), the axis of the disc being the z-axis and the middle plane the $r\theta$-plane. If U and V are the displacements along and perpendicular to the radius at (r,θ), the equations for the stress resultants in the $r\theta$-plane may be transformed as follows (see Love,1927 p.56):

5.10 $$T_r = 2Eh[\partial U/\partial r + \sigma(U/r + (1/r)\partial V/\partial\theta)]/(1-\sigma^2) \quad (1)$$

$$T_\theta = 2Eh[\sigma\partial U/\partial r + (U/r + (1/r)\partial V/\partial\theta)]/(1-\sigma^2) \quad (2)$$

$$S_{r\theta} = Eh(\partial V/\partial r - V/r - (1/r)\partial V/\partial\theta)/(1+\sigma) \quad (3)$$

and in cylindrical coordinates, eqn 5.9(1) becomes:

5.11 $$\partial^2\Delta/\partial r^2 + (1/r)\partial\Delta/\partial r + (1/r^2)\partial^2\Delta/\partial\theta^2 + k^2\Delta = 0$$

Now Δ is periodic in θ and may therefore be written as $\Sigma\Delta_n\cos(n\theta+\alpha_n)$ where Δ_n is a function of r only. Substituting this value in eqn 5.11, the resulting differential equation can only hold good if it is satisfied for each value of n separately; hence:

5.12 $$\partial^2\Delta_n/\partial r^2 + (1/r)\partial\Delta_n/\partial r + (k^2 - (n/r)^2)\Delta_n = 0$$

giving as a solution:

5.13 $\Delta_n = A_n J_n(kr)\cos(n\theta)$ (1), and similarly:

$\omega_n = B_n J_n(k_1 r)\sin(n\theta)$ (2) where A_n and B_n are arbitrary constants.

The relative phase of Δ_n and ω_n as regards θ is arbitary at the moment, but it will be seen that the value chosen fits the boundary conditions. On expressing eqns 5.7 in cylindrical coordinates and substituting the values of Δ_n and ω_n from eqns 5.13 we find:

5.14 $U = \left[A\partial J_n(kr)/\partial r + (n/r)BJ_n(k_1 r)\right]\cos(n\theta)$ (1)

$V = -\left[(n/r)AJ_n(kr) + B\partial J_n(k_1 r)/\partial r\right]\sin(n\theta)$ (2)

where A and B are arbitrary constants, connected with A_n and B_n in such a way that:

5.15 $\Delta_n = -k^2 AJ_n(kr)\cos(n\theta)$ (1)

$2\omega_n = k_1^2 BJ_n(k_1 r)\sin(n\theta)$ (2)

Substituting for U and V in the expressions for T_r and $S_{r\theta}$ and equating the latter to zero at $r = a$, the radius of the disc, gives:

5.16 $A\left[(1/a)(1-\sigma)dJ_n(ka)/da + \left(k^2 - (n^2/a^2)(1-\sigma)\right)J_n(ka)\right]$

$- nB(1-\sigma)\left[(1/a)dJ_n(k_1 a)/da - (1/a^2)J_n(k_1 a)\right] = 0$ (1)

$2nA\left[(1/a)dJ_n(ka)/da - (1/a^2)J_n(ka)\right]$

$- B\left[(2/a)dJ_n(k_1 a)/da + (k_1^2 - 2n^2/a^2)J_n(k_1 a)\right] = 0$ (2)

Since $k_1 = k\sqrt{2/(1-\sigma)}$, these equations may be used to find possible values of k and hence the natural frequencies of vibration (using the relations given after eqn 5.9). The value of A/B for these frequencies may also be found, and used to calculate the displacements and stresses.

This completes the formal solution to the problem, the method and notation used here being substantially those used by Love (1927). The form of the vibration for the various modes is only briefly discussed in the next section; a fuller account is given in the relevant experimental chapters.

5.4 Types of vibration

a) Symmetrical modes. If n = 0, then either A or B must be zero to satisfy eqns 5.16. If $A \neq 0$, then V = 0 and U is independent of θ, the frequency equation being:

5.17 $$(1/a)(1-\sigma)dJ_0(ka)/da + k^2 J_0(ka) = 0$$

The displacements in the $r\theta$-plane are entirely radial and the shear stress resultant $S_{r\theta}$ vanishes. The motion involves no rotation about the z-axis.

If $B \neq 0$, then U = 0 and V is independent of θ. The frequency equation is:

5.18 $$(2/a)dJ_0(k_1 a)/da + k_1^2 J_0(k_1 a) = 0$$

The displacements in the $r\theta$-plane are everywhere tangential and only the shear stress resultant is finite; there is no areal dilatation.

In each of these cases the nodes of the longitudinal displacements are a series of concentric circles. Following Petrzilka's nomenclature they will be referred to as types A and B respectively.

b) Compound modes (Petrzilka's type C). When n is not zero the motion may be regarded as compounded of both types A and B. The ratio A/B has a different value for each mode and is determined from the frequency equation as already mentioned. The nodal systems of U and V each consist of a set of circles together with n diameters, so arranged that each set of diameters bisects the angles between the diameters of the other set. Both dilatation and rotation are present and all the stress resultants are finite. The motion is very complex and is discussed in the experimental chapters.

CHAPTER 6

THE USE OF MULTIPLE-BEAM INTERFEROMETRY

Of the methods of examination employed in the present work, the use of the multiple-beam Fizeau fringes formed between the crystal and a reference flat is of outstanding interest in that the results obtained depend on a single variable - the normal surface displacement. The general principles of interference techniques have been fully described previously, but a brief review of the relevant details will facilitate the discussion of their application to the particular problems encountered here.

6.1 Multiple-beam interference

If two, nearly parallel, highly reflecting surfaces, in close proximity, are illuminated by parallel monochromatic light, the multiply-reflected beams interfere, giving rise to a set of interference fringes localized in the plane through the line of intersection of the surfaces which is normal to the incident light beam (Brossel,1947). If viewed in transmission, fine, bright fringes are seen against a nearly dark background, the distribution of intensity being given by

$$6.1 \qquad I = I_o/(1 + F\sin^2\delta/2) \qquad \text{(Airy,1831)}$$

where δ is the phase difference between successively reflected beams and $F = 4R/(1-R)^2$, R being the intensity reflecting

coefficient. I_o is the peak intensity and depends on the transmission coefficient of the surfaces, but the distribution of I does not.

Equation 6.1 is based on a constant path difference between successive beams, this being the case when the surfaces are parallel; for a finite wedge angle and normal incidence, which results in fringes localized in the interferometer gap itself, the path difference between the direct and n^{th} reflected beam is approximately $2nt - 4n^3 t\epsilon^2/3$, where ϵ is the small angle between the surfaces. For high values of n, the second term may become so great as to be of the order of a half wavelength of light, in which case the fringe definition will suffer. Tolansky (1948) has given the maximum tolerable values of t for various wedge angles and, for most of the wedge angles used in the present work, the separation of the surfaces was well below the corresponding critical value.

6.2 Dielectric multilayers as reflecting coatings

Owing to the use of Z-cut crystals in this work, the exciting electrodes were arranged round the periphery of the discs, and would have been short-circuited by metallic reflecting coatings on the major surfaces. For this reason, dielectric multilayers were used exclusively as reflecting coatings. Mechanically, they are far superior to silver coatings and some

of them hardly deteriorated after months of use, whereas silver coatings become scratched as soon as the interferometer surfaces are brought into contact.

The properties and production of such layers have been fully described by Belk, Tolansky and Turnbull (1954). Fig.6.1 shows how the correct phase relation is achieved for the variously reflected beams; obviously these conditions hold good for a particular angle of incidence only. For the work described in Chapters 13 and 15, three layers of zinc sulphide (high μ) were used, alternating with two layers of cryolite (low μ). The theoretical reflectivity of this arrangement is 87%, at normal incidence, but as the thicknesses of the layers were estimated by the colour change method (described in Chapter 11) it is doubtful whether the reflectivity ever exceeded 80%. For some of the photographs included in this work the reflectivity was evidently less than this.

6.3 Oscillating multiple-beam fringes

If one surface of the interferometer is moved parallel to itself with a periodic sinusoidal displacement, the observed fringes move across the surface in synchronism, and the effect recorded by a photographic plate or the naked eye is a set of broadened fringes of reduced intensity. Owing to the extreme sharpness of multiple-beam fringes, the fringe

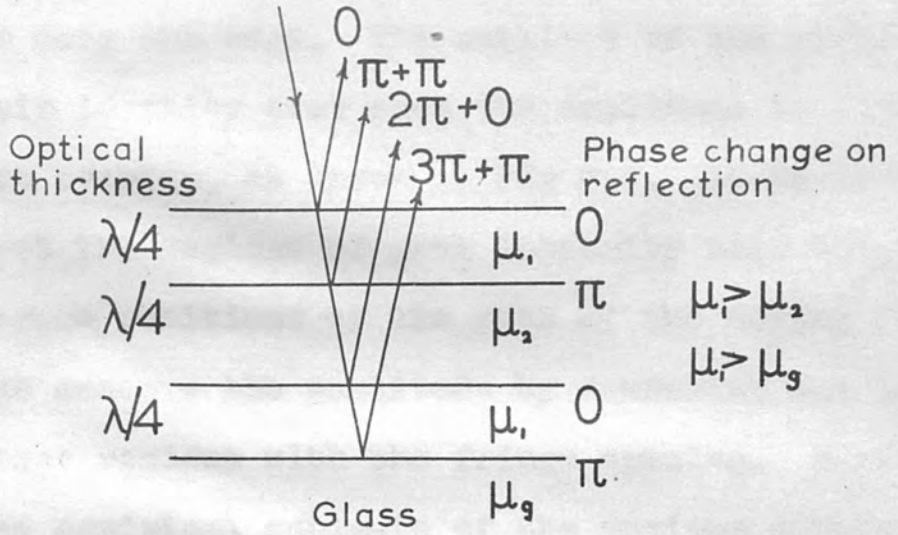
0
π+π
2π+0
3π+π
Optical thickness
Phase change on reflection
λ/4
λ/4
λ/4
μ₁
μ₂
μ₁
μ_g
0
π
0
π
μ₁>μ₂
μ₁>μ_g
Glass

6.1

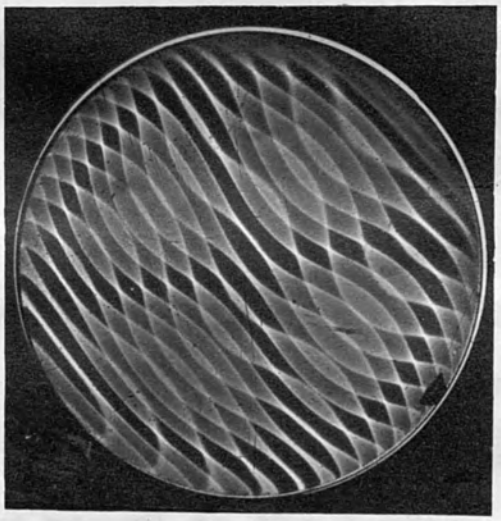

6.2

envelopes are clearly defined, and since the velocity of a moving fringe is zero in the extreme position, the intensity is greater near the edge. The outlines of the envelopes retain their identity even when the amplitude is sufficient for them to overlap, as shown in Fig 6.2. It is tempting to interpret the regions of peak intensity near the edges as the extreme positions of the peak of the moving fringe, and thus to measure the amplitude by comparing the distance between these regions with the fringe spacing. Bardsley (1951) has made an empirical estimate of the maximum divergence of the intensity peak from the true extreme position of the peak of the moving fringe and concludes that it can be no more than twice the half width of the stationary fringe. In view of the false conclusions reached by Thomas and Warren (1928) regarding the intensity distribution of oscillating two-beam fringes, it was thought worthwhile to check this result mathematically.

The calculation is made by putting $\delta = 4\pi(\epsilon x + Y\sin pt)/\lambda$ in eqn 6.1, where x is the distance from the wedge apex, measured along the line of greatest slope and Y the amplitude of the vibration normal to the surface, and finding the mean intensity over a period $pt = 2\pi$, but the resulting expression cannot be integrated directly. However, members of the Mathematics Group of the Admiralty Research Laboratory have

kindly computed the intensity distribution near the maxima for two particular cases. The value of Y is $3\lambda/16$ in each case so that the intensity distribution of the fringes is roughly as shown in Fig 6.4; Fig 6.3 shows the fringes under static conditions. The chosen value of Y gives a phase change of $\pm 135^\circ$ at the extremes of the cycle. The phase change corresponding to the intensity peaks is $\pm 123^\circ$ for $R = 0.7$ and approximately $\pm 132^\circ$ for $R = 0.9$. The half-width of a static fringe, that is the distance between the points at which the intensity has half its maximum value, is given approximately by 6.2 $W = (1-R)/\pi\sqrt{R}$ as a fraction of the distance between orders. Expressing this as the corresponding phase change gives $W = 40^\circ$ or 12° in the two cases. The displacements of the intensity peaks are thus much less than the maximum discrepancies allowed for by Bardsley, but this may not be so when the fringes just overlap.

6.4 The effect of dispersion

Although a high dispersion (that is, very few fringes per centimetre) gives the greatest sensitivity and the biggest lateral shift for a given normal displacement, it is generally undesirable in the study of vibrations for two reasons. Firstly, the fringes can only give information concerning the regions they cross; if the number of fringes is small

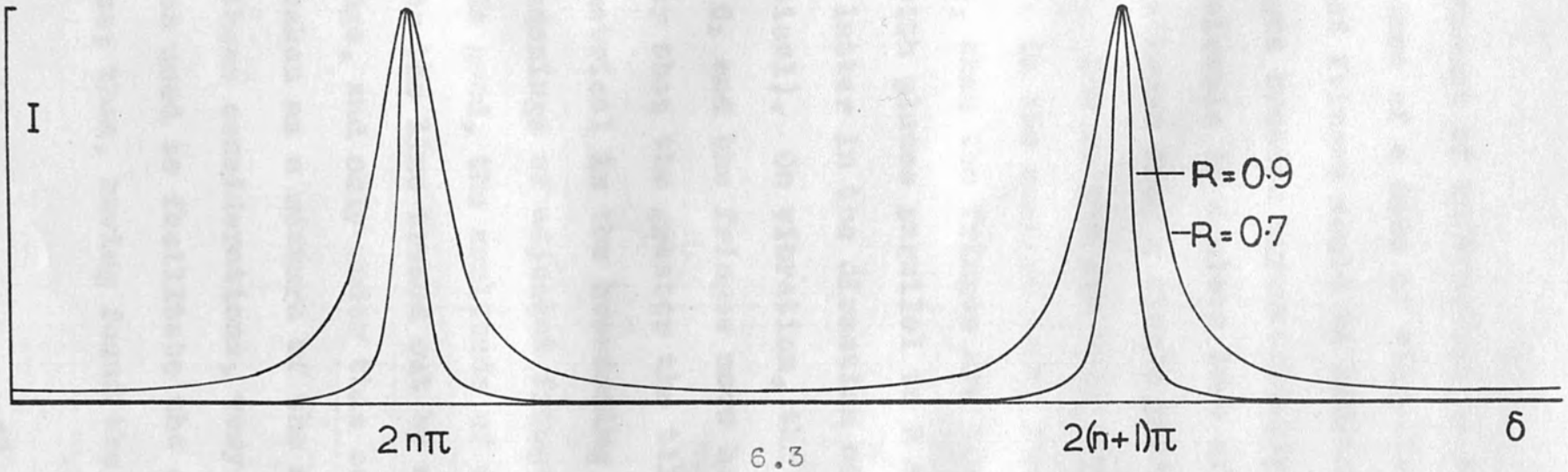

6.3

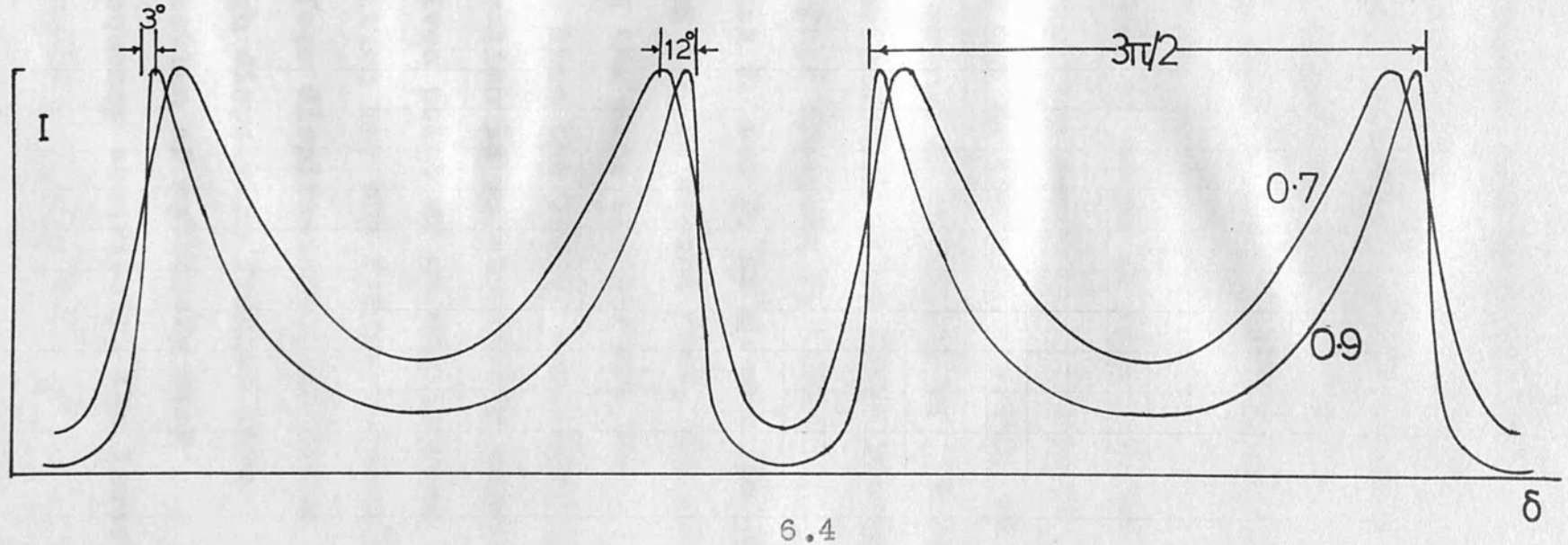

6.4

Figs 6.3-4

the amount of information is correspondingly limited. The presence of a node of vibration falling between two widely spaced fringes would be undetected. Secondly, widely spaced fringes broaden asymmetrically on vibration, and this is undesirable if a clear idea of the surface displacements is to be gathered from a single photograph.

The reason for this asymmetry is shown in Figs 6.5 and 6. If C_0 is the surface under investigation and R the reference flat, then the fringes are traced out by the intersections of C_0 with planes parallel to R and spaced at multiples of $\lambda/2$ from the latter in the direction of the incident light (here assumed vertical). On vibration, the surface distorts between C_1 and C_2 and the fringes move between P_1 and P_2 as shown. It is clear that the greater the tilt of the reference flat, the more symmetrical is the broadening and the more similar are the broadenings of adjacent fringes. When the latter condition holds good, the amplitude of vibration is substantially constant along the line traced out by a given point of an oscillating fringe, and only under this condition may the fringe broadening be taken as a measure of the surface displacement. In spite of these considerations, very high dispersion fringes were often used to facilitate the detection of extremely weak modes; then, having found the frequency accurately, the lower

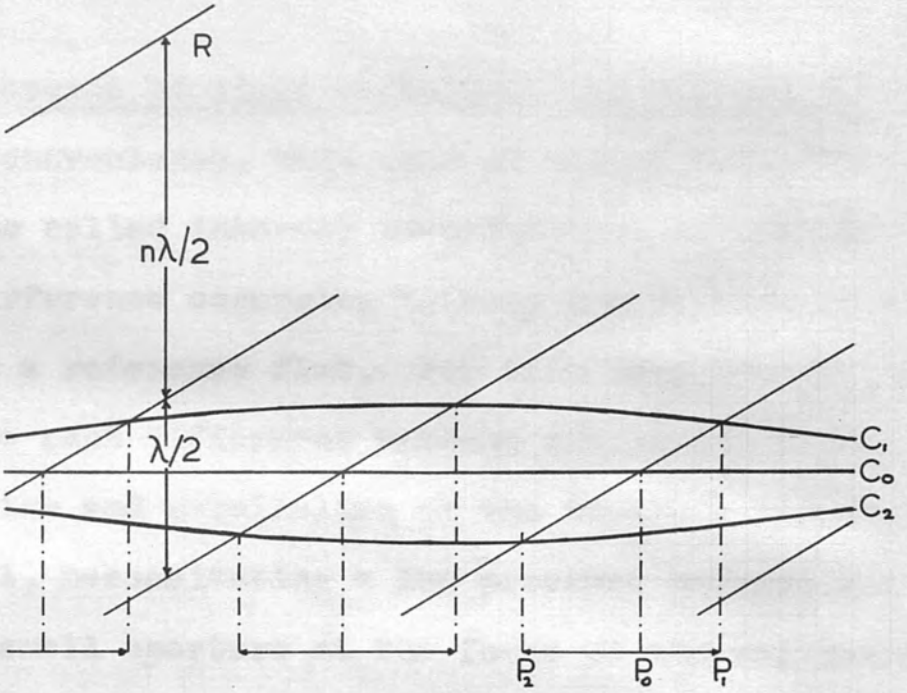

6.5

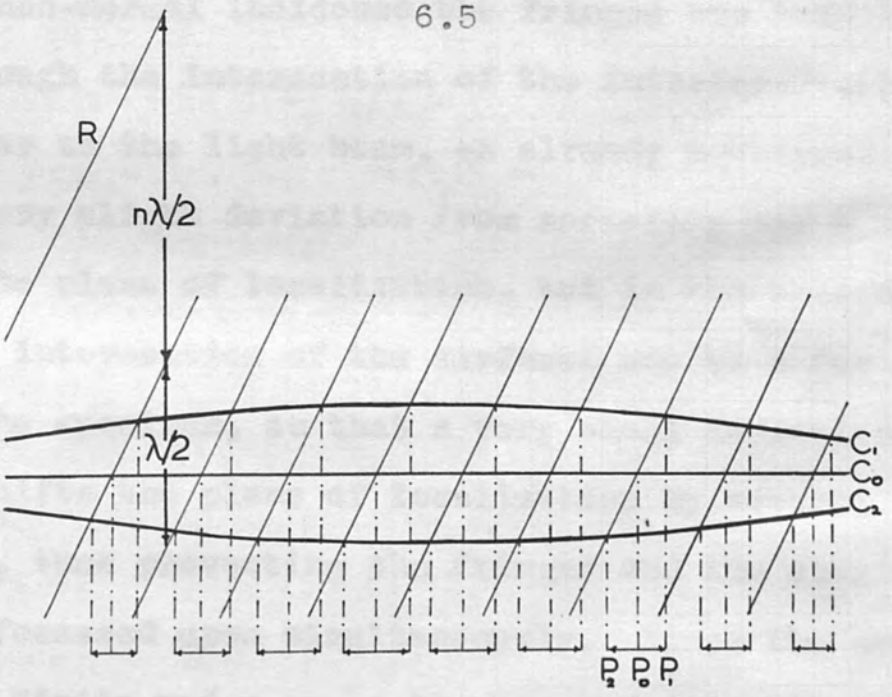

6.6

dispersion was used to examine the vibrations.

6.5 Interference of light reflected from the two crystal faces

For convenience, this type of interference will hereafter be called internal interference, as opposed to the simple interference occurring between one surface of the crystal and a reference flat. For such interference, owing to the great path difference between successive beams, the monochromatism and parallelism of the incident illumination are critical, necessitating a low pressure mercury arc source and a very small aperture at the focus of the collimator lens. For non-normal incidence the fringes are localized in a plane through the intersection of the interferometer surfaces perpendicular to the light beam, as already mentioned. For small gaps any slight deviation from normality has a negligible effect on the plane of localization, but in the present case the line of intersection of the surfaces may be a few metres away from the specimen, so that a very small deviation from normality shifts the plane of localization by several centimetres, thus preventing the fringes and the specimen from being focussed upon simultaneously. Since the crystal must have a finite wedge angle to secure a suitable fringe dispersion, the crystal used for most of the experiments did not fulfil the critical conditions (mentioned earlier) for

obtaining sharp fringes, owing to its large thickness (2 mm). In spite of this, however, the fringes obtained were vastly superior to two beam fringes.

For internal interference, the optical path difference between successive beams depends on both the thickness and the refractive index. On vibration, the change in this path difference is:

6.3 $\delta(2\mu t) = 2t\delta\mu + 2\mu\delta t$ μ being the refractive index.

Considering first an isotropic body, the effect of stress is to make it birefringent.. Hence the fringes split into two components for which the refractive indices are:

6.4 $\mu_1 = K(P+Q) - C(P-Q) + \mu$ (1)

$\mu_2 = K(P+Q) + C(P-Q) + \mu$ (2)

P and Q being the principal stresses and K and C stress-optic coefficients. The stress-optic effect is discussed more fully in Chapter 7. For the type of vibration considered in this work the change of thickness is

6.5 $2hz_2 = h(P+Q) \times \text{Const}$ so that the changes of the path difference between successive beams are

6.6 $\delta(2\mu t)_1 = 2h\left[K'(P+Q) - C(P-Q)\right]$ (1)

$\delta(2\mu t)_2 = 2h\left[K'(P+Q) + C(P-Q)\right]$ (2)

The motion of the fringes may be visualized as a bodily displacement proportional to P+Q (and to the surface displacement) with an additional splitting of the fringe

proportional to $P-Q$. If $P+Q=0$, the fringe is split symmetrically, while if $P-Q=0$, the fringe does not split but is merely displaced. Since the effects due to both the change of thickness and the sum of the principal stresses are additive, the bodily displacement of the fringe will usually be large compared with the splitting. In the case of a vibrating body the general appearance would be similar to that observed by simple interference but the fringes would mostly have a double envelope.

Considering now the particular case of quartz cut normal to the optic axis, certain difficulties arise. When the quartz is stressed, an analysis of the intensity distribution of the broadened fringes is complicated, owing to the combination of rotatory power and birefringence, and has not so far been accomplished. The best approach in the circumstances would have been to observe the behaviour of the fringes formed between the surfaces of a statically stressed bar, similar to that used for the experimental check on the stress-optic effect (Section 14.1). Failing this, the following argument will give some idea of the expected behaviour.

In an unstressed Z-cut plate, each plane polarized element of an incident unpolarized beam suffers a rotation on each passage through the crystal which is annulled whenever

it is reflected in the reverse direction, so that the multiple-beams due to each element are in a condition to interfere in the normal way. If the plate is now subjected to a static isotropic stress, that is, so that $P-Q=0$, in the XY-plane, the mean refractive index alters, but, due to the relation between the stress-optic coefficients in quartz, it does not become birefringent in the Z-direction (see Section 7.4) and so the fringes are unaltered except for a shift proportional to $P+Q$. If now the alternative state is considered, in which $P-Q$ is finite but $P+Q$ is zero, whatever the effect of this stress, the resultant fringes will be symmetrical about their original positions. The most that the effects, not yet known, of elliptic polarization in the crystal could do, would be to spoil the phase conditions and blur the fringes. The general case, in which P and Q have arbitrary values, is a superposition of these two effects. It seems likely, therefore, that the general appearance of the fringe pattern would be somewhat similar to the isotropic case, although the polarization state of the emergent light is uncertain. It will be seen in Chapter 15 that this is, in fact, the case.

CHAPTER 7

THE THEORY OF THE STRESS-OPTIC EFFECT

7.1 The effect of stress on the optical properties of an isotropic medium

Neumann gave the first quantitative explanation of the stress-optic effect in isotropic media and based it on two assumptions, namely:

1) Fresnel's laws hold good for the propagation of light in a homogeneously deformed medium, the principal polarization axes coinciding with the principal axes of strain (and, of course, with those of stress, for an isotropic medium)

2) The principal velocities of light in the strained medium, a,b,c, are linear functions of the principal strains, giving:

7.1 $$a = v + qx_x + py_y + pz_z \quad (1)$$

$$b = v + px_x + qy_y + pz_z \quad (2)$$

$$c = v + px_x + py_y + qz_z \quad (3)$$

where v is the velocity of light in the unstrained medium, p and q are constants characteristic of the medium and x_x etc. are the principal strains. v,p and q are all functions of the light wavelength.

Since stress and strain are linearly dependent and their principal axes coincide for an isotropic medium, the principal velocities may also be expressed in terms of the principal stresses by the same set of equations (7.1) but with different constants p',q', the two pairs of constants p,q and p',q' being connected by relations involving the elastic constants of the medium.

It may easily be shown that the axes of a section of the index ellipsoid defined by the velocities a,b,c are parallel to the secondary principal stresses in the plane of the section (the secondary principal stresses in any plane are the principal stresses resulting when stress components acting normally to the plane are disregarded). Thus the difference between the propagation velocities in any direction at a given point in an isotropic medium is $(p'-q')(P-Q)$, P and Q being the secondary principal stresses in the plane normal to this direction; moreover, the vibration directions of the two waves are parallel to the axes of the section of the ellipsoid and thus to the secondary principal stress directions.

7.2 Isoclinics and isochromats

The intensity transmitted by a lamina of birefringent material between crossed polarizer and analyser and

illuminated by parallel light is:

7.2 $I = I_o \sin 2\alpha \sin^2 \delta/2$ where α is the acute angle between the polarizer axis and a vibration direction in the specimen and δ the phase difference between the two waves emerging from the specimen. The intensity will be zero if $\alpha = 0$ or $\pi/2$, or if $\delta = 2n\pi$. In the general case of a stressed lamina both α and δ vary from point to point and so two systems of dark fringes are seen in the field of view. These join points where a) the polarizer and analyser are parallel to the directions of the principal stresses or b) the phase difference is a whole number of periods. Fringes (a) are known as isoclinics; their configuration alters with the setting of the polarizer and analyser relative to the specimen, but is independent of the wavelength of the incident light. Fringes (b) are known as isochromats or stress fringes, and are independent of the setting of the polarizer and analyser, but dependent upon the wavelength.

It is convenient to be able to examine these fringe systems separately and the stress fringes can be eliminated by using white light and photographing with panchromatic plates (The zero order fringe, for which $\delta = 0$, remains, as this is common to all wavelengths). The isoclinics may be eliminated by using circularly polarized light; a quarter wave plate immediately after the polarizer, with its axes

at 45° to those of the latter, results in circularly polarized light falling on the specimen and, if the phase difference between the waves after the passage through the crystal is a whole number of periods, the emergent light is also circularly polarized. Thus a second quarter wave plate, with axes at 90° to those of the first, produces plane polarized light again, which is stopped by the crossed analyser. Alternatively, the same result may be achieved by setting the second quarter wave plate parallel to the first and the analyser parallel to the polarizer. Since circularly polarized light is incident on the specimen, any effects due to the orientation of the latter are eliminated and the isoclinics entirely removed.

7.3 Effects due to vibration

If the specimen is set into vibration, assuming that the stress-optic effect is instantaneous compared to the frequency of vibration, new stress fringes appear at the regions of maximum stress and move towards the zero order regions, as the stresses are increasing, and conversely as the stresses decrease. This is repeated for each half-cycle, irrespective of the sign of the stresses. Unless stroboscopic illumination is used, it is not possible to see the stress fringes as such but, as in the case of Straubel's interferometric experiments (1933), the intensity has maximum or

minimum values for certain critical amplitudes of vibration. If the phase difference is written as $\delta = B\sin pt$ in eqn 7.2, then the mean transmitted intensity over a period of the vibration is:

7.3 $$I = I_o(1-J_oB)/2$$

This expression has its first maximum for B = 3.832 radians, that is for a peak phase difference of somewhat over half a wavelength. Eqn 7.3 will not hold good in the case of quartz crystals since, as shown later in Fig 7.1, the phase difference is not proportional to the stress and will not, therefore, vary sinusoidally. However, the qualitative results will be the same, and since a diminution of intensity with increasing amplitude of vibration has only once been observed, and then for a thick crystal vibrating very strongly, it is concluded that the first order stress fringe does not normally make an appearance, so that stroboscopic illumination would not be worthwhile. Eichhorn's compensator method (1936) would be difficult to apply in the present work, owing to the variable stress direction; further, since the frequencies used here are 10-30 times as great as those used by Eichhorn, the electrical difficulties involved in making a suitable stroboscope are not easily overcome. Thus for all practical purposes the zero order stress fringes, for which $\delta = 0$ throughout the cycle are the

only ones available for study.

Since the stresses maintain their amplitude and phase relationship relative to one another throughout the cycle, the directions of the principal stresses at any point remain fixed. Thus the isoclinics are entirely unaffected by the vibration. This is true only for isotropic media; in the case of quartz crystals other factors must be considered, and these are discussed in Section 7.5.

7.4 The stress-optic effect in crystals; Pockels' theory

Neumann's theory cannot be applied to crystalline media since, in general, the original principal polarization axes will not be parallel to the principal axes of stress or strain, nor will the axes of stress and strain be parallel to each other. Pockels' theory assumes:

1) Fresnel's laws hold good (as in Neumann's theory)

2) The differences between the original and deformed optic parameters are linear, homogeneous functions of the stress or strain components.

The optic parameters are the six constants required to express the equation of the index ellipsoid when its principal axes do not coincide with the coordinate axes, this being:

7.4 $$a_{11}x^2 + a_{22}y^2 + a_{33}z^2 + 2a_{23}yz + 2a_{31}zx + 2a_{12}xy = 1$$

Thus the stress-optic effect may be expressed by six

equations giving the changes in each optic parameter $(a_{hk} - a^{\circ}_{hk})$, as linear functions of the six components of stress or strain. The two sets of coefficients required are connected by relations involving the elastic properties of the medium. For a particular crystalline symmetry, the array of stress-optic coefficients q_{hk} is similar to that of the elastic constants c_{hk}, except that $q_{hk} \neq q_{kh}$ since the energy considerations requiring $c_{hk} = c_{kh}$ do not apply in the case of the stress-optic coefficients. Hence 36 constants, not 21, are required for a crystal which is devoid of symmetry.

In the case of quartz, if the usual orthogonal axes are taken as axes of coordinates, only 8 independent stress-optic coefficients are required; further a°_{23}, a°_{31} and a°_{12} vanish and $a^{\circ}_{11} = a^{\circ}_{22} = o^2$ and $a_{33} = e^2$, o and e being the ordinary and extraordinary velocities of light in the undeformed crystal.

Thus, in terms of the stress components the optic parameters become:

7.5
$$a_{11} = o^2 + (q_{11}X_x + q_{12}Y_y + q_{13}Z_z + q_{14}Y_z) \quad (1)$$
$$a_{22} = o^2 + (q_{12}X_x + q_{11}Y_y + q_{13}Z_z - q_{14}Y_z) \quad (2)$$
$$a_{33} = e^2 + (q_{31}X_x + q_{31}Y_y + q_{33}Z_z) \quad (3)$$
$$a_{23} = (q_{41}X_x - q_{41}Y_y + q_{44}Y_z) \quad (4)$$
$$a_{31} = (q_{44}Z_x + 2q_{41}X_y) \quad (5)$$
$$a_{12} = (q_{14}Z_x + (q_{11} - q_{12})X_y) \quad (6)$$

The shape and orientation of the deformed index ellipsoid may be found from these parameters; assuming that $a_{11} - a_{11}^{\circ}$ etc. are all small compared with a_{11}° etc and with $a_{11}^{\circ} - a_{22}^{\circ}$ etc, it may easily be shown that the new position of the ellipsoid is attained by rotating the original ellipsoid through small angles about each coordinate axis in turn. The magnitudes of these angles are given by:

7.6 $$\tan 2\varphi_x = 2a_{23}/(a_{22} - a_{33}) \doteq 2a_{23}/(a_{22}^{\circ} - a_{33}^{\circ})$$

φ_y and φ_z are found from similar expressions, the suffixes being changed cyclically. For quartz, since $a_{11}^{\circ} = a_{22}^{\circ}$, φ_z is large and independent of the actual magnitude of the stress. Provided this rotation is made first, however, eqns 7.6 still hold good. Moreover, since $q_{66} = q_{11} - q_{22}$, it is easily shown that for stresses perpendicular to the optic axis $\varphi_z = \theta$, where θ is the angle between the X and Y-axes and the principal stress directions, so that the principal axes of the section of the index ellipsoid by the XY-plane are parallel to the principal axes of stress in this case. It may further be shown that for such stresses the resultant effect of the rotations φ_x and φ_y is that the ellipsoid is turned through a small angle about an axis in the XY-plane making an angle of -2θ with the X-axis. Using Pockels' values for stress-optic coefficients of quartz, this angle is found to be about

1 or 2% of the angle between the optic axes of the now biaxial quartz, for a stress of 1 Kg.mm^{-2}, and will therefore be ignored. The resulting index ellipsoid may be expressed as follows, when the principal stress directions and the original optic axis are taken as axes of coordinates:

7.7 $$x^2(o^2 + q_{11}P + q_{12}Q) + y^2(o^2 + q_{12}P + q_{11}Q) + z^2(e^2 + q_{31}(P+Q)) = 1$$

Thus for the type of stress considered, and for propagation of light along the Z-axis, the quartz behaves very similarly to an isotropic medium as regards the pure stress-optic effect.

7.5 The effect of optical activity

Drude (1905) has shown that the effect of optical activity on the properties of birefringent media is to alter the equation giving the velocity of propagation in any direction from:

7.8 $$2v^2 = a^2 + c^2 + (a^2 - c^2)\cos(g_1 \pm g_2)$$ to:

7.9 $$2v^2 = a^2 + c^2 + (a^2 - c^2)\cos g_1 \cos g_2 \pm \sqrt{(a^2 - c^2)^2 \sin^2 g_1 \sin^2 g_2 + 4\eta^2}$$

Here v is the velocity in the given direction, g_1 and g_2 are the angles between the wave-normal and each optic axis, a,b and c are the principal velocities and η is a parameter depending upon the rotatory power of the medium. Eqns 7.8 and 7.9 are identical when $\eta = 0$. As a result of this theory, a plane polarized wave travels through the medium as a pair of

oppositely-handed elliptically polarized waves, their velocities being given by eqn 7.9; these ellipses have equal axial ratios and lie oppositely, the major axis of one being equal to the minor axis of the other.

An incident plane polarized wave must first be resolved into plane polarized components along the principal axes of the section of the ellipsoid and then each of these is further resolved into a pair of elliptically polarized waves. Drude gives the axial ratio h in the form:

$$7.10 \qquad h + 1/h = \sqrt{(a^2 - c^2)^2 \sin^2 g_1 \sin^2 g_2 + 4\eta^2} \Big/ \eta$$

Considering propagation along the original optic axis of quartz, we have:

$$7.11 \qquad \sin g_1, g_2 = \pm\sqrt{(a^2 - b^2)/(a^2 - c^2)}$$

$$7.12 \qquad \cos g_1 = \cos g_2 = \sqrt{(b^2 - c^2)/(a^2 - c^2)}$$

so that eqns 7.9 and 10 may be written as:

$$7.13 \qquad h + 1/h = 2\sqrt{1 + (a-b)^2/(\eta/a)^2}$$

$$7.14 \qquad v_1 - v_2 = (\eta/a)\sqrt{1 + (a-b)^2/(\eta/a)^2}$$

Preston has considered the general case of an optically active crystal between polarizer and analyser. If the axes of these make angles of α and β respectively with one axis of the section of the ellipsoid by the wave front and, for convenience, the incident light amplitude is taken as $1 + h^2$, then Preston gives for the transmitted light intensity:

7.15 $I = \left[(1+h^2)\cos(\alpha-\beta)\cos\delta/2 - 2h\sin(\alpha-\beta)\sin\delta/2\right]^2$
$+ (1-h^2)^2\cos^2(\alpha+\beta)\sin^2\delta/2$ where δ is the phase difference between the emergent elliptically polarized components. Since both terms in this expression are essentially positive, the intensity can be zero only when they are both zero, thus leading to the conditions:

7.16 $(\beta-\alpha) = \pi/2 + \tan^{-1}\left[\left(2h/(1+h^2)\right)\tan\delta/2\right]$

and either 7.17 $(\alpha+\beta) = \pi/2$, or 7.18 $\delta = 2n\pi$

As $(\beta-\alpha)$ must <u>always</u> be equal to the value given in eqn 7.16 for extinction, the <u>apparent</u> rotation is

7.19 $\rho = \tan^{-1}\left[\left(2h/(1+h^2)\right)\tan\delta/2\right]$

Assuming that the polarizer and analyser have the relative orientation given by eqn 7.16, then extinction occurs when either eqn 7.17 or 7.18 is satisfied, that is, when a) the bisector of the angle between the polarizer and analyser axes is parallel to the bisector of the angle between the axes of the section of the index ellipsoid, the latter axes being parallel to the principal axes of stress in the present case; or b) the phase difference is a whole number of periods, irrespective of the absolute orientation of polarizer and analyser.

Since the apparent rotation varies with the retardation, it will generally not be possible to achieve the condition

necessitated by eqn 7.16 for all points in the field of view simultaneously. It may be achieved automatically, however, by reflecting the light back along its path. In general, this leads to a very complicated expression for the intensity, since a right-handed elliptic wave on incidence is a left-handed wave on reflection; but where the transmitted intensity would have been zero, that is, at just those regions in which we are interested, the light falling on the analyser would necessarily have been plane polarized and so, on reflection, will retrace its path and leave the crystal in the same polarization state as that in which it entered. It may thus be stopped by an analyser whose axis is perpendicular to that of the polarizer.

If a statically stressed quartz lamina is viewed under these conditions, two sets of fringes will be seen. One set joins points where the principal stress directions differ from those of polarizer and analyser by half the apparent rotation at those points; the other set joins points where the phase difference is a whole number of periods (for the single path through the crystal). These two sets correspond to isoclinics and stress fringes with these exceptions: 1) The rotation must be known at any point on the isoclinic to find the principal stress directions.

Since the rotation depends on phase difference the interpretation will be difficult. It will be shown, however, that for the cases encountered in the present work, the apparent rotation hardly varies from the static value and hence the polarizer and analyser settings differ by a constant angle from the stress directions. 2) The fringes correspond to equal increments in the phase difference but this does not depend linearly on the stress, as seen from eqn 7.14. The stress could easily be found, however, by using the graph given later in Fig 7.1. In the present work we are restricted to the zero order fringe, so this question does not arise. It is interesting to note that at points on this zero order fringe the phase difference is finite although the stress difference is zero; since, however, the sections of the index ellipsoids at these points are circular, the incident light is unresolved and darkness prevails.

Turning now to the numerical magnitude of the apparent rotation in quartz, the phase difference between the two elliptic waves is:

7.20 $\delta = (2\pi t/T)(v_1 - v_2)/v_1 v_2 \doteq (2\pi t\eta/a^3 T)\sqrt{1 + (a-b)^2/(\eta/a)^2}$

(from eqn 7.14) where t is the thickness and T the period. The rotation of the unstressed crystal is:

7.21 $\rho_0 = \delta_0/2 = \pi t\eta/a^3 T$ Hence:

7.22 $\delta = 2\varrho_o\sqrt{1+\epsilon^2}$ where $\epsilon = (a-b)/(\eta/a)$

and using eqn 7.13 for $(1+h^2)/h$ we have:

7.23 $\varrho = \tan^{-1}\left[(\tan\varrho_o\sqrt{1+\epsilon^2})/\sqrt{1+\epsilon^2}\right]$

Fig 7.1 shows δ and ϱ plotted against ϵ together with the asymptotes of δ. The two sets of curves are for thicknesses of 0.5 mm and 0.306 mm, the static rotations for $\lambda = 5461\text{Å}$ being 12.7° and 78° respectively. An experimental test of the theory for the thicker crystal is described in Chapter 14. It should be noted that, while ϱ_o and δ are directly proportional to the thickness, ϱ is definitely not. For the smaller value of t the rotation hardly varies from its static value since $(\tan C\varrho_o)/C \to \varrho_o$ as $\varrho_o \to 0$. Thus for thin crystals the rotation may be assumed constant, and equal to the static value for all practical purposes; owing to the flatness of the curve near the origin, the same will be true for thicker crystals, provided the stresses are small enough.

7.6 The electro-optic effect

The linear electro-optic effect, that is, a change of optical properties due to an electric field which reverses sign with the field direction - as opposed to the quadratic, or Kerr effect which does not change sign - is possible with all piezoelectric crystals and with them only (see Cady,1946). There are, in general, 18 electro-optic constants relating

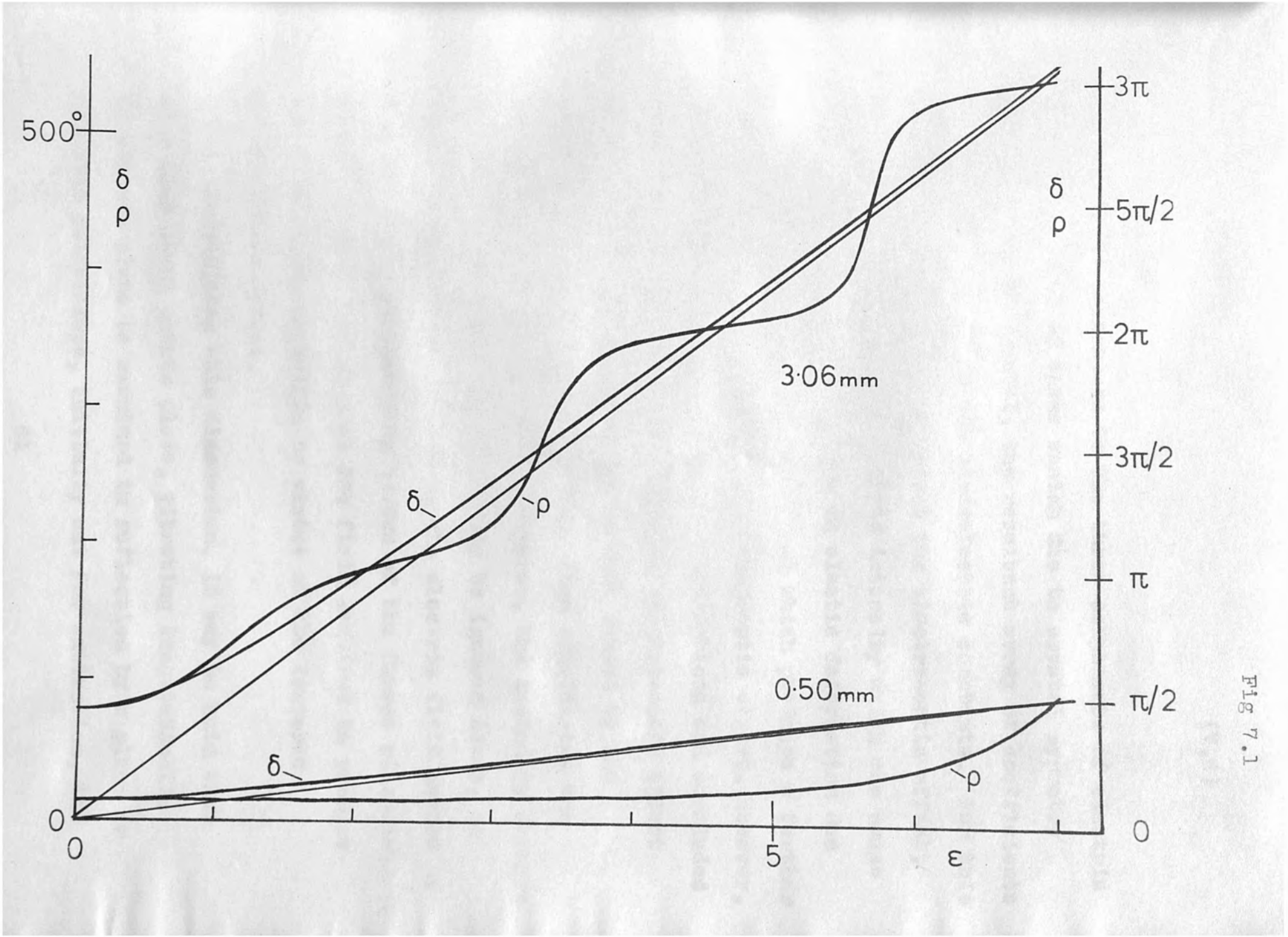

Fig 7.1

the six optic parameters to the three components of electric intensity. Some of these vanish due to crystal symmetry and, for a given crystal, the resultant array of coefficients is the same as that of the piezoelectric constants. For this reason it is difficult to detect the electro-optic effect, since every component of electric intensity which can cause an optical change, also causes an elastic deformation due to the converse piezoelectric effect which produces a further optical change by virtue of the stress-optic effect. However, Pockels (1890) allowed for these complications and concluded that, for quartz, there is a genuine electro-optic effect of the same order of magnitude as that caused by the piezoelectrically induced strain. When considering the optical changes due to stress, however, the secondary changes due to the electro-optic effect may be ignored since, as already mentioned in Chapter 1, the electric field caused by a given stress or strain by virtue of the direct piezoelectric effect is much smaller than the field required to produce the same stress or strain by virtue of the converse piezoelectric effect.

Summarizing this discussion, it may be said that if a thin Z-cut quartz plate, vibrating longitudinally in its own plane be examined in reflection by a plane or circular polariscope, initially set for extinction, the

isoclinic fringes and zero order stress fringes may be observed just as in a statically stressed, isotropic body, except that the isoclinics correspond to principal stress directions differing from the directions of the axes of polarizer and analyser by half the natural rotation in the quartz for the light wavelength in use.

CHAPTER 8

THE MOTION OF POWDER PARTICLES ON A VIBRATING SURFACE

The motion of the particles on a surface vibrating flexurally has already been mentioned in Chapter 2, and is relatively simple. When the flexural motion is combined with a longitudinal motion, the movements of the particles are much more definite, the frictional force between a particle and the surface being of great importance.

Suppose that a particle is on a horizontal surface at a point where the horizontal and vertical displacements are u and w. As we are considering a free vibration of the body, these displacements are in phase. Thus:

8.1 $u = U\sin\omega t$ (1) $w = W\sin\omega t$ (2)

The accelerations are:

8.2 $-U\omega^2\sin\omega t$ (1) and $-W\omega^2\sin\omega t$ (2) respectively.

If the particle is not to slip relative to the surface, then:

8.3 $|U\omega^2\sin\omega t| \leq \mu(g - W\omega^2\sin\omega t)$ μ being the coefficient of friction. Thus slipping occurs if the two curves shown in Fig 8.1 intersect at any time, and continues during the time that they overlap, shown by the shaded region in the figure.

If $U = 0$ then $\omega^2 W \leq g$ for a particle to remain absolutely at rest relative to the surface, this being the necessary

Fig 8.1

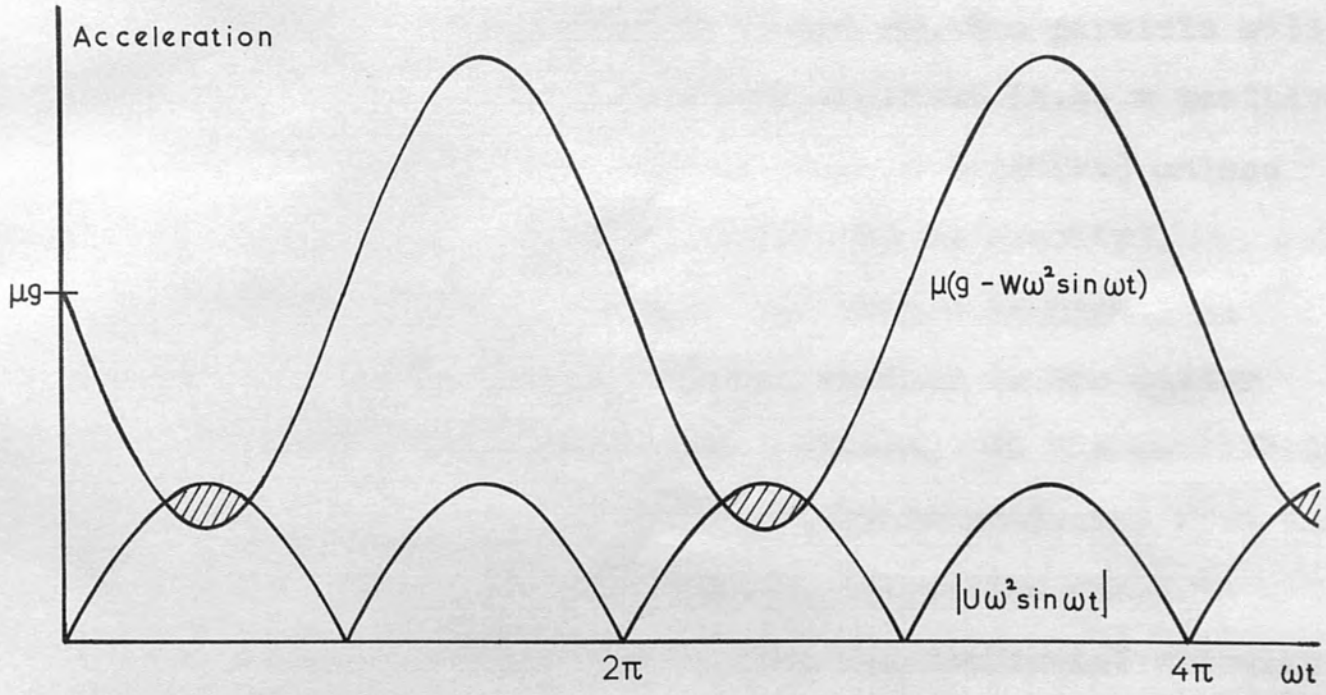

condition in the case of pure flexural modes. In a typical case U or W may be 1000Å and ω may be 10^6 sec^{-1}, giving the acceleration of the surface as 10^7 cm.sec^{-2} or about 10,000g. This is so great that for all practical purposes the particle will only remain completely at rest, relative to the surface, where U = 0 and W = 0. When this is not so, the particle will leave the surface when $-\omega^2 W \sin\omega t$ is negative (i.e. w positive), and will slip when it is positive (i.e. w negative) unless $\mu W \geq |U|$ (neglecting the small effect due to gravity).

If the particle does not slip when w is negative, then it moves horizontally with the surface as the latter moves upwards to its equilibrium position. At the equilibrium position (i.e. u = 0, w = 0) the particle is projected from the surface with horizontal and vertical velocities equal to ωU and ωW respectively. If $\mu W < |U|$, the horizontal velocity of projection would be less than ωU but the subsequent motion would be qualitatively the same. The particle then describes some sort of trajectory and reaches another part of the surface where the process is repeated, ultimately reaching a point where conditions are favourable for it to remain.

For the typical amplitude and frequency mentioned above, the peak velocity of the surface is only 10 cm.sec^{-1}, in spite

of the great acceleration. The terminal velocity of lycopodium spores when falling freely in air is approximately 5cm.sec^{-1}, so that for a vertical projection velocity of 10cm.sec^{-1} the height of the trajectory is approximately 0.22mm and the time of flight 0.014 sec. If the horizontal projection velocity is equal to the vertical, then the horizontal distance travelled by the particle in this time is 0.47 mm. For certain types of vibration, notably the thickness vibrations of X-cut quartz crystals (Wachsmuth and Auer,1928), air currents are set up which may carry the lycopodium powder 50 cms above the surface. However, in the present work such effects have not been observed and the simple projection theory will suffice.

In general, the surface of a vibrating body will be crossed by a set of nodes of the vertical displacement and a set of nodes of the horizontal displacement. Unless a node of either sort is parallel to the horizontal displacement, there is always a component of the latter acting towards it. If the displacements near to a node are such that an upward displacement of the surface is in phase with a horizontal displacement towards the node, then as the surface passes through the equilibrium position in the upward direction the particle is projected towards the node. Near the other

side of the node, since the phase of either the horizontal or the vertical displacement is reversed according as the node is associated with the former or the latter displacement, the direction of projection of a particle is opposite to the previous case, that is, towards the node once more. Thus such a node would collect the powder. Alternatively, the conditions near a node may be such that an upward displacement is in phase with an outward horizontal displacement, in which case the lycopodium would be dispersed.

It should be pointed out that the lycopodium is rarely at rest in these cases, even at those nodes at which the powder accumulates. For, if the node is one of horizontal displacement, the particles are continually projected vertically into the air, while if the node is one of vertical displacement then slipping of the surface beneath the particle occurs for most of the cycle. It will be seen in Chapter 16 that of the two types of node, the latter is usually the more clearly defined. In either case, however, the particles encounter powerful restoring forces if they stray too far from the favoured nodes.

If the vertical displacement is due to a flexure, then the corresponding nodes on opposite surfaces of the body will not both be indicated. This follows since a

given displacement in the horizontal direction corresponds to a displacement normal to the surface which is outwards on one side and inwards on the other, so that if the node on one surface accumulates powder, that on the other surface will disperse it, when the body is turned over; thus the nodal patterns indicated on the two sides will be complementary. If, however, the vertical displacement is due to a longitudinal type of strain, the vertical displacements on opposite surfaces will be symmetrically distributed with respect to the median plane and similar nodes will be indicated on both surfaces. In general, the vertical displacement is a combination of the two types and the nodes will be of symmetrical (i.e. indicated on both surfaces) or asymmetrical type, according as the longitudinal or flexural displacement has the greater magnitude.

The effect of a component of displacement parallel to a node, is to cause creeping of the powder along the node, the motion of the powder being oppositely directed on each side of the node. If the node is precisely parallel to the horizontal displacement, there will be no motion of the powder towards the node and it will hardly be made visible.

Finally, if a node of vertical displacement coincides with one of horizontal displacement, it will hardly be indicated. This follows because if there is any horizontal displacement towards the node, the powder will move towards the node on one side and away on the other, stopping momentarily at the node itself. The node is, in fact, a position of unstable equilibrium for, although it is an absolute node, the slightest jostling by the incoming particles is sufficient to push the particles already there to the other side, where they are swept away. If, on the other hand, the horizontal displacement is parallel to such an absolute node, then particles which stray however slightly from the node are swept along parallel to it, in the same direction whether they stray to one side or the other.

These theoretical conclusions may be summarized by describing a simple method by which the direction of motion of the powder may be determined at any point on a vibrating surface, the horizontal and vertical displacements being known.

The two sets of nodes are drawn on the surface of the body; the surface is thus divided into regions which are bounded on all sides by nodal lines or by the boundary of the surface. Arrows are drawn representing the horizontal

displacements in these regions, for any given instant of the vibratory cycle. If now one of these arrows is regarded as a starting point, the directions of all the others are reversed once for each node of vertical displacement which is crossed in reaching the region in which they are drawn. Then the direction of motion of the powder is given completely, either by the resulting system of arrows, or by the system in which the directions of all these arrows are reversed. The correct system may be decided if the direction of motion is known at any point. For example, at a node of pure longitudinal horizontal displacement, in which the only vertical displacement is due to the cross strain, the powder motion is always towards the node since a compression, that is a horizontal displacement towards the node, results in a dilatation of the plane which is normal to the stress, and hence in an upward vertical displacement.

PART III APPARATUS AND TECHNIQUES.

CHAPTER 9

APPARATUS USED FOR OPTICAL EXAMINATION

9.1 General description

The complete optical arrangement is shown in Fig 9.1, various components being removed according to the method of observation in use. The collimating system consists of the condenser lens C focussing an image of the source A (usually a mercury arc) on the adjustable iris diaphragm D which is situated at the focus of a large, well corrected lens E (focal length 20 cms, aperture f/2.9). B is a Wratten filter used to select the mercury green line, when required, and F is a barrier layer photocell, connected to a spot galvanometer, which may be swung into the light beam to monitor the intensity. G is a front aluminized mirror and H the specimen stage. When observing by reflected light, G is moved to the alternative position G' and used in conjunction with the fully aluminized mirror L and half aluminized mirror J. M and K are pieces of Polaroid sheet in rotatable mounts, used as polarizer and analyser and I is a mica quarter wave plate. The camera has an f/4.5 lens of 12 cms focal length; the microscope coverslip O and lens R focus an auxiliary image of the specimen on the ground glass screen S, which may be observed by means of the eyepiece

Fig 9.1

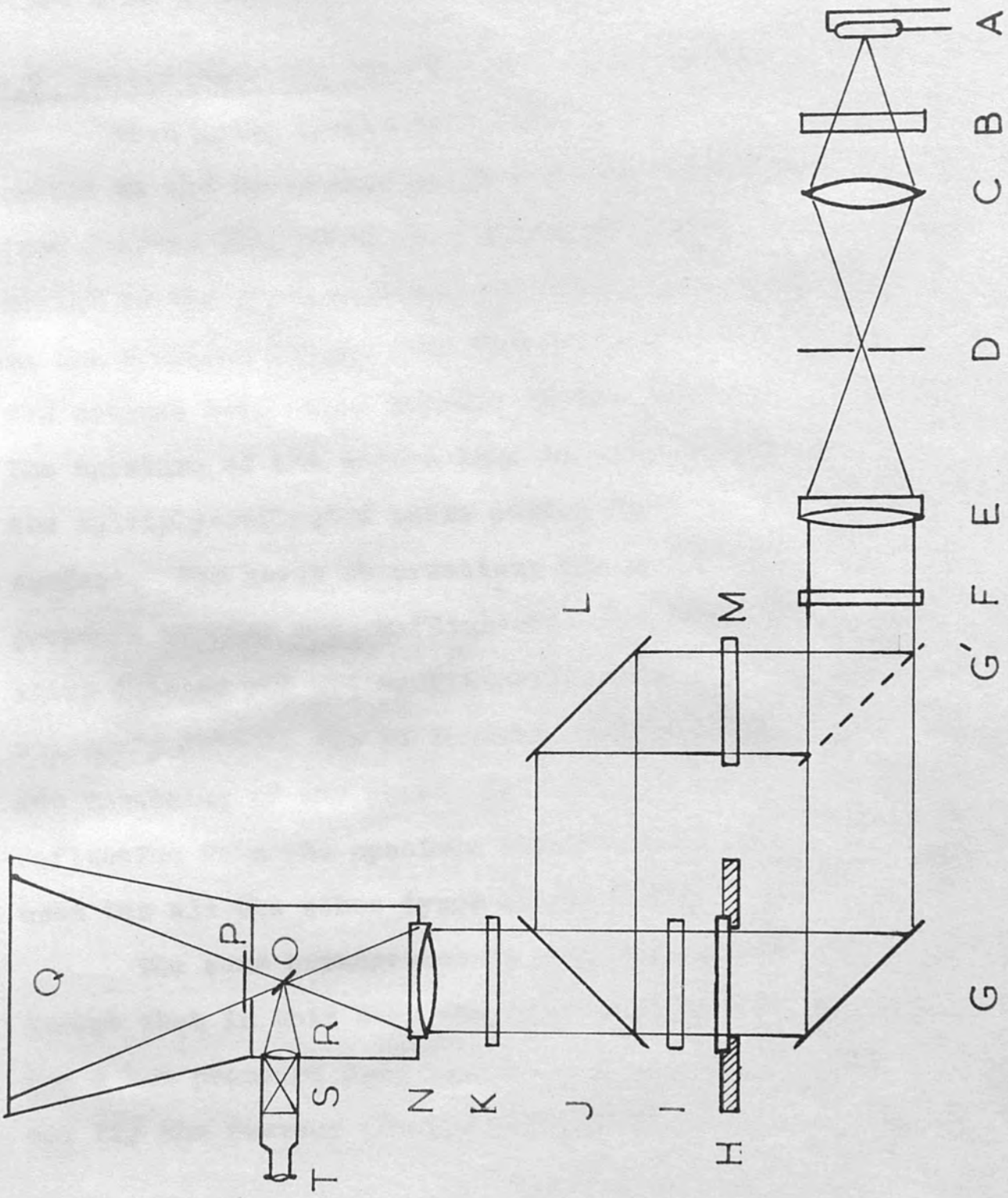

T even while actually exposing the photographic plate Q, since O is placed before the shutter P.

9.2 Interferometric observation

When using simple interferometry, the quartz crystal, coated on the lower surface by a dielectric reflecting layer (see Chapter 11), rests on a glass reference flat, similarly coated on the upper surface, in a suitable electrode jig on the specimen stage. The illumination is from below and the optical components between H and the camera are removed. The aperture of the camera lens is sufficient to collect all the multiply-reflected beams coming from the entire crystal surface. For these observations the source is a high pressure mercury arc, sufficiently monochromatic to produce sharp fringes yet not sufficiently so to show up the secondary fringes due to internal interference. The alignment and focussing of the collimator is carried out by back reflection from the specimen itself, this method also being used for all the other types of observation.

The same arrangement is used for internal interference, except that in this case the crystal is coated on both sides and a low pressure D.C. mercury arc replaces the high pressure one for the reasons given in Chapter 6. At first the crystal

rested on an uncoated glass flat, but in later experiments this was replaced by two stretched hairs, to avoid secondary interference fringes. It was stated in Chapter 6 that the collimation and normality of the incident illumination are critical for this type of interference. The aperture D has to be less than 1 mm for sharp fringes and the jig supporting the crystal rests on three levelling screws. The camera is first focussed on the specimen itself and the plane of localization of the interference fringes can then be made to coincide with the specimen by adjusting the screws until the image of the fringes is as sharp as possible.

9.3 Observation by polarized light

In this case G is moved to G' and the crystal examined by reflection; the crystal is coated on the under surface for this purpose and rests on an uncoated flat. When using plane polarized light, all the optical components are present except the quarter wave plate I. Since L and J would cause the plane polarized light emerging from M to become elliptically polarized, unless the plane of polarization is parallel or perpendicular to the plane of incidence, the orientation of M has to be attended to first. With K removed, M is rotated until the field of view is as bright or as dark as possible, as seen in the eyepiece. The

analyser K is now replaced and rotated for extinction; this is not usually obtained at once, but, by slightly adjusting K and M alternately, the desired condition is easily achieved.

A simple device using a half shade plate is used for marking the vibration direction of the polarized light on the photographs. A sheet of Polaroid was cut by a straight line at a small angle to the axis of vibration of the transmitted light. One piece was turned over and the two pieces mounted side by side between glass plates, the cut edges being adjacent to each other and separated by about $\frac{1}{4}$ mm. When this device is placed at H instead of the specimen, and illuminated from below, the two halves of the field are equally bright when the line of division is parallel or perpendicular to the analyser axis, the setting being quite critical for the latter condition. Having adjusted the half shade plate to the latter condition, if a suitable exposure is made on the same photographic plate as that used to record the stress pattern of the specimen, the analyser remaining undisturbed, the light coming through the gap between the two halves marks the vibration direction of the incident light.

When making observations by circularly polarized light,

a quarter wave plate cannot be placed directly after the polarizer M as the resultant circularly polarized light would be elliptically polarized after reflection at L and J. Hence it is placed at I and, as the light passes through it again after reflection, no second quarter wave plate is needed. Under these conditions the analyser must be set with its axis parallel to that of the polarizer; in fact a single sheet of Polaroid placed directly above I with its axis at 45° to those of I could replace both M and K. It is more convenient, however, to use separate polarizer and analyser. The method of adjustment is first to remove I and set M and K for extinction as before; I is then replaced and rotated until extinction occurs once more, when its axes will be parallel to those of M and K. I is now rotated through 45° and K through 90°; this results in circularly polarized light falling on the crystal. If the crystal is unstressed the light is polarized at 90° to its original direction after being reflected back through the quarter wave plate and is thus not transmitted by the analyser, which is set parallel to the polarizer.

9.4 Observation of lycopodium powder patterns

The lycopodium powder patterns are photographed very simply by using transmitted light, as in the case of

interferometric observation. The mercury arc is replaced by a white Pointolite source to avoid any interference effects.

CHAPTER 10

ELECTRONIC APPARATUS

10.1 Driving Oscillator

The oscillator used for exciting vibrations is a straightforward push-pull type using two 807 tetrodes, the crystal being connected directly across the oscillatory circuit, as shown in Fig 10.1. The frequency range is 20-2000 Kc/s and the maximum output about 800v peak to peak. The somewhat unorthodox feedback circuit is due to the fact that the oscillator was constructed from components at hand. By using fixed grid-bias and adjusting this until oscillations are only just maintained, a low grid current results and the output waveform, as seen by a cathode ray oscillograph, is very good. It is nearly impossible to excite even a very active mode of vibration by a harmonic of the oscillator frequency under these conditions, although this is definitely not the case when the valves are allowed to draw excessive grid current. By disconnecting C_g, the feedback may be increased to maintain oscillations at the higher frequencies.

A pair of telephones can be connected across a small resistance in one cathode lead (not shown in Fig 10.1), so that the 'click' method may be used for the detection of weak modes of vibration. The principle of this method lies

Fig 10.1

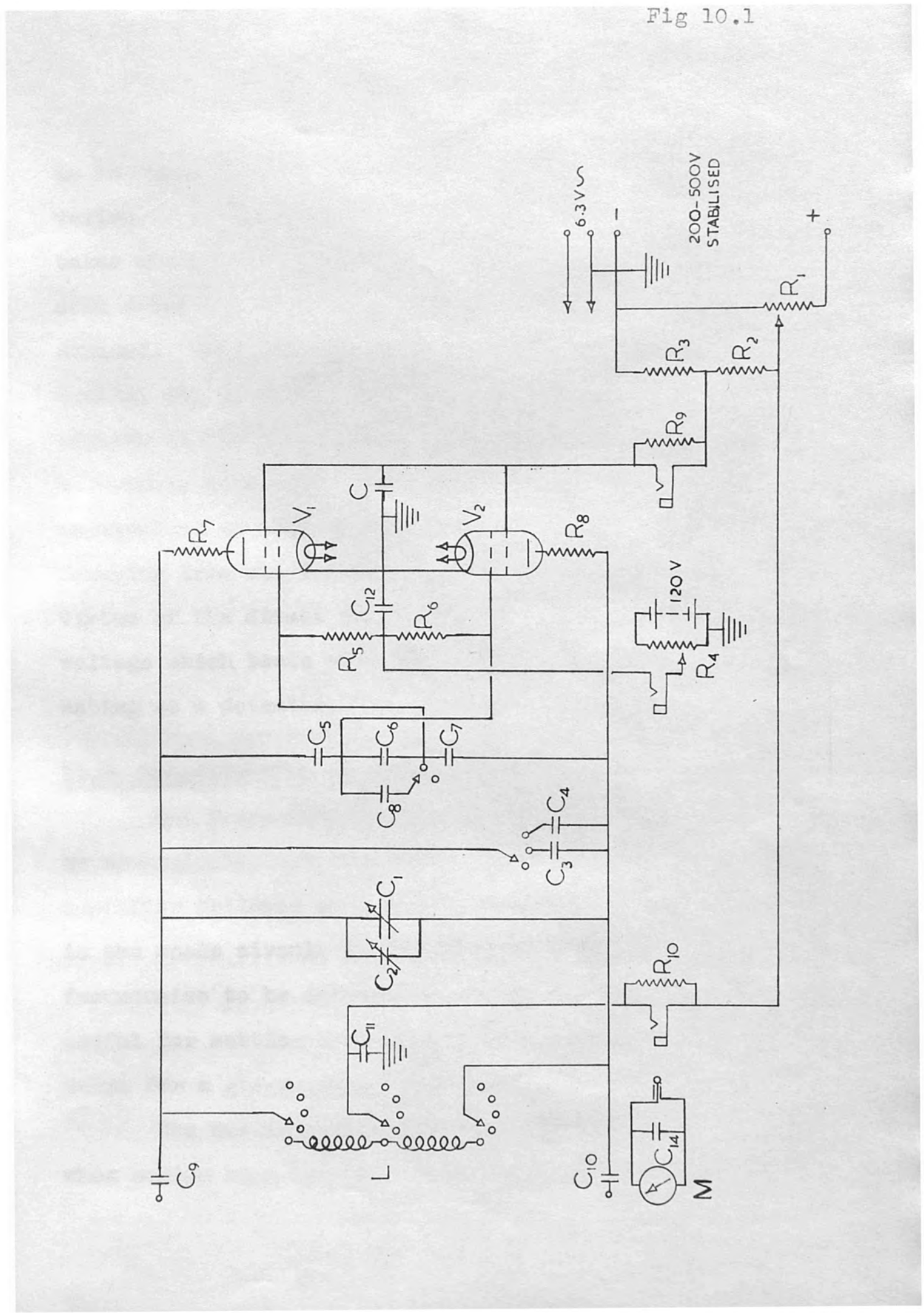
6.3 V ~
-
200-500V
STABILISED
+
R1
R2
R3
R9
R10
R4
120 V
R5
R6
R7
R8
V1
V2
C
C1
C2
C3
C4
C5
C6
C7
C8
C9
C10
C11
C12
C14
L
M

in the fact that if the oscillator frequency is continuously varied, as it approaches that of a vibratory mode, the crystal takes charge of the oscillator frequency and holds it constant, even after the oscillatory circuit has been considerably detuned. When this detuning is sufficient, however, the crystal can no longer control the frequency and the oscillator reverts to its proper frequency, resulting in a click or heterodyne note being heard in the telephones. The explanation of this audible sound is that the exponentially decaying free vibrations of the quartz crystal give rise, by virtue of the direct piezoelectric effect, to an alternating voltage which beats with the oscillator output, the valve acting as a detector.

10.2 Determination of the frequency

The frequencies are found approximately by using an ex-Admiralty G57 wavemeter. This consists of a tuned amplifier followed by a triode detector with a micro-ammeter in the anode circuit to indicate resonance. It enables the frequencies to be determined to about 0.5% or better and is useful for setting the oscillator frequency to the expected value for a given mode of vibration.

The preliminary use of this wavemeter is essential when making more accurate frequency determinations with an

ex-American Signal Corps heterodyne frequency meter, type BC-221-AF. In this instrument the beat notes between a harmonic of the internal oscillator and the frequency to be ascertained are used to tune the frequency meter to a submultiple of the latter frequency. This frequency must be known quite closely beforehand, as otherwise considerable confusion arises from the multitude of combinations of harmonics of the two frequencies. The frequency of the heterodyne oscillator can be checked against a built in crystal oscillator, thus allowing frequency determinations to be made to much better than 0.1%, which is more than adequate for the present experiments. The use of this frequency meter is even more valuable than the 'click' method for the detection of weak modes of vibration. The small frequency jump occurring when a crystal resonance is passed through, represents a much larger change of pitch of the heterodyne beat note; if the latter is arranged to be very low, by suitably adjusting the heterodyne oscillator frequency, the extremely small change of frequency associated with very weak modes of vibration can be detected.

CHAPTER 11

PREPARATION OF SPECIMENS AND EXPERIMENTAL PROCEDURE

11.1 Polishing of specimens

All the crystals used in this work were supplied by the Post Office Research Station and were cut normal to the optic axis to a tolerance of ±5' of arc, at most. They were all nominally 1" in diameter and of various thicknesses between 0.5 and 3.0 mm. As supplied, they had the usual etched finish of high quality quartz vibrators used for frequency control or other electrical applications.

A few of the crystals were polished commercially but the majority were polished by the author, using conventional techniques. Every effort was made to grind the surface evenly, prior to polishing, but inevitably the polished surfaces were not parallel to the original ones. In fact, they could not both be so in the case of a 2 mm crystal which was specially prepared for observation by internal interference, as a definite angle had to be introduced between the surfaces to achieve the requisite fringe dispersion. This crystal was ground in the usual way with successively finer grades of aloxite grinding powder, and while using the finest grade the appropriate wedge angle was introduced, the thickness being checked with a micrometer. It was then fully polished

on one side and sufficiently polished on the second for the observation of two-beam internal interference fringes, in reflection. After two or three regrindings of the second side, followed by rough polishing each time, the dispersion was seen to be suitable and the final polishing was carried out.

It is desirable that the surfaces should be as flat as possible, not only because the resultant initially straight fringes are easier to interpret when they are broadened by the vibrations of the crystal but, more important, because the dispersion is then constant over the whole crystal, and equal fringe broadenings represent equal amplitudes of vibration. The flatness is more important for internal interference than for simple interference. Invariably the crystal surfaces were slightly convex after polishing; if both surfaces have the same degree of convexity then, since the refractive index of quartz is approximately 1.5, the variation of optical thickness of the crystal is 3 times the deviation of either surface from flatness. Hence the comparatively thick crystal already mentioned was used for the internal interference experiments, since it was not found possible to achieve a high degree of flatness for thin crystals, owing to the distortion occurring when cementing

them to metal discs for ease of handling during polishing.

11.2 Reflective coatings

For the reason mentioned in Chapter 6, evaporated, dielectric multilayers were used as reflective coatings. These consisted of alternate quarter wave layers of zinc sulphide and cryolite deposited on the surface under observation, the first and last layers being zinc sulphide. These layers are more troublesome to deposit than evaporated silver layers, since the reflectivity, being due to reinforcement of the light reflected from successive layers, depends critically on their thickness.

A small vacuum coating plant was used, with separate, boat-shaped filaments for evaporating the two substances; the layer thickness was estimated by watching the reflection of an opal electric bulb in a glass monitor plate at near normal incidence. As the layer thickness increases, the reflected light goes through a characteristic series of colour changes, this sequence being different for the two types of layer, since for a cryolite layer there is *no* additional phase change of π at the cryolite-glass interface. The crystals or reference flats to be coated were mounted in a horizontal plane above the filaments, as near as possible to the

monitor glass; this could be exposed to the filaments in successive strips, one for each layer deposited, by a movable shutter.

For maximum reflectivity in the mercury green region, the characteristic colour of a zinc sulphide layer on glass goes through bluish-white to white at the quarter wave thickness, followed by yellow, these changes being quite easy to observe. The colour of a cryolite layer on glass goes through yellow to magenta at the quarter wave thickness, followed by blue; since a single quarter wave layer of cryolite on glass forms an anti-reflection coating, these changes are more difficult to observe and most of the errors in the reflectivity of the finished coating are probably due to incorrect thickness of the cryolite layers. As previously mentioned, the theoretical reflectivity of a 5-layer coating, as used on all the specimens in this work, is 87%, for mercury green light.

The Z-cut quartz bar used for the static bending experiments described in Chapter 14, was coated on one Z-face with an opaque layer of evaporated silver, as the conductivity was not objectionable in this case.

11.3 Experimental procedure

The crystal under observation was mounted on a clear

or coated glass flat in a jig which could be provided with various electrode systems, this being shown in Fig 11.1 with the six-electrode system in position. For the observation of internal interference, the glass flat was replaced by two hairs in later experiments, as mentioned in Chapter 9. In the case of the symmetrical modes (Types A and B) six electrodes were used; the orientation of the crystal relative to the electrodes for maximum excitation was found by trial, and was substantially different for the two types. In the case of type C modes, a two electrode system gave the strongest excitation; at first the electrodes were diametrically opposed (as shown in Fig 11.1) but it was found later that very weak type C modes were excited more strongly by two electrodes placed very close together on the circumference of the crystal so as to give an intense, localized field. The electrodes used for the C modes could be rotated relative to the crystal, without disturbing it, to select the most suitable orientation, this being different for each individual mode.

The first experiments carried out used the simple interferometric method of observation. The fringes were watched carefully while slowly varying the oscillator frequency about the calculated value for a particular mode

Fig 11.1

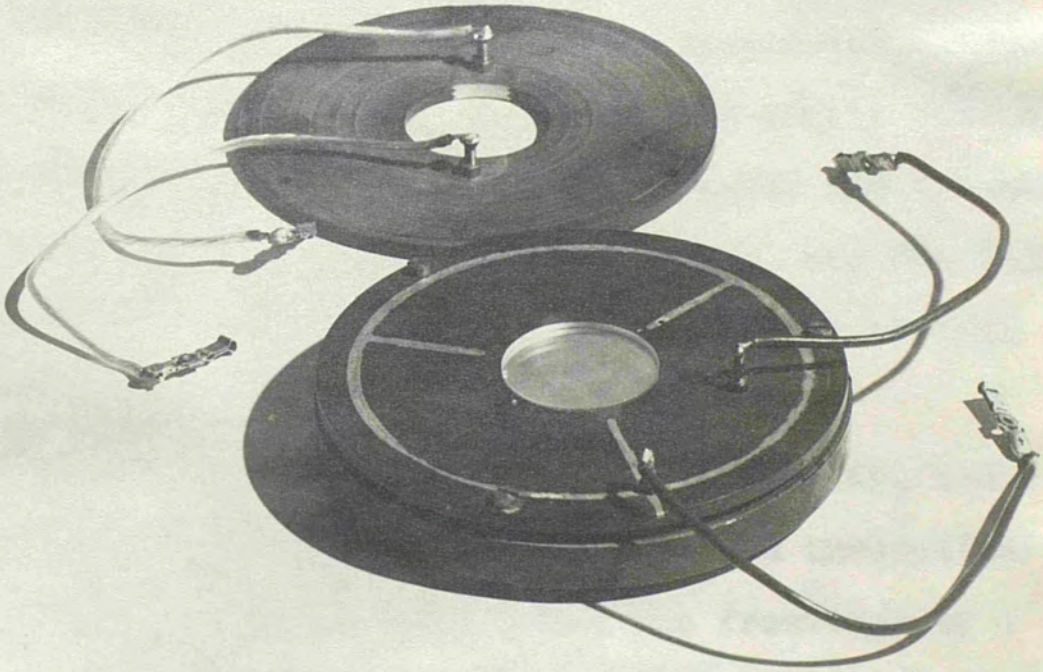

of vibration. In the case of type A and B modes the characteristic nodal patterns (very different from the theoretical ones) were soon recognized, and 'landmarks' in the frequency spectrum were thus established. While searching for weak modes with full oscillator output, the frequencies of the more easily excited modes had to be avoided, but, in spite of all precautions, many crystals were shattered by inadvertently passing through such frequencies. Apart from the modes under investigation and the easily recognized flexural modes (having any number of circular and diametral nodes), there is a multitude of other modes, and for this reason the type C modes could not be identified by this method of observation.

When observing by polarized light, however, there was very good agreement between the observed and theoretical patterns, and so, having established the frequency of a type C mode, it could then be observed by interference. Moreover, the polarized light method is very sensitive, since the brief flashes of light seen as a mode is passed through, are more easily detected than the momentary broadening of the interference fringes. For this reason, the weakest modes were usually set into vibration while observing by polarized light, and the optical system then altered to that required for interference without

disturbing the crystal. As it was more convenient to make such preliminary polarized light observations in transmission, to avoid moving the mirror G (Fig 9.1), a polarizer was held temporarily under the specimen for this purpose.

In the case of observations by internal interference there was no doubt as to the mode of vibration, the theoretical predictions being quite well fulfilled. For the reasons mentioned in the previous paragraph, however, it was still desirable to set the crystal into vibration while observing it by polarized light.

Before making lycopodium powder observations, the crystal was thoroughly degreased in acetone. Vibrations were then started, while observing by polarized light, and the powder was sprinkled on uniformly. This was achieved by drawing a piece of cotton wool, dipped in the dried powder, across a piece of stretched lens tissue held about 5-10 cms above the crystal. The photography of the resulting patterns was extremely simple, as it could be carried out after the crystal had stopped vibrating. Since the lycopodium patterns were formed on the upper surface of the crystal, whereas the simple interference patterns were viewed <u>through</u> the crystal, on the lower surface, some of the photographic plates corresponding to a given side of the crystal had to be placed

emulsion side up during printing, to secure correct registration of corresponding features of the two types of pattern.

PART IV NUMERICAL CALCULATIONS AND EXPERIMENTAL RESULTS.

12.1 Type A and B modes (n=0).

CHAPTER 12

CALCULATION AND MEASUREMENT OF THE FREQUENCIES OF VIBRATION

All the experimentally observed frequencies listed here are for a quartz disc of diameter 2.54 ± 0.005cm and thickness 0.85 ± 0.01 mm. The disc was truly circular within ±0.005cm. The other discs used for the work described in the next few chapters had the same diameter within the limits given and were circular to the same degree of accuracy. The various vibratory modes for which the frequencies are given were identified by polarized light observation, since this method is most sensitive and the observed patterns are in very good agreement with theory.

12.1 Type A and B modes (n=0).

The frequency equation for type A modes (eqn 5.17) may be re-arranged as:

12.1 $$J_1(ka) - kaJ_0(ka)/(1-\sigma) = 0$$

where $k = 2\pi\sqrt{\rho(1-\sigma^2)/E} \times f$, f being the frequency of vibration. For quartz $\rho = 2.65 gm.cm^{-3}$, $E = 1/s_{11} = 78.8 \times 10^{10}$ dyne cm^{-2} and $\sigma = -s_{12}/s_{11} = 0.133$. These values are taken from Cady (1946) and are based on static measurements; he considers that the value of s_{11} is probably correct to better than 1% but that s_{12} is less reliable. Hence:

12.2 $$f = 87.57k \text{ Kc/s}$$ where (ka) is a root of

eqn 12.1. This function is plotted in Fig 12.1 and the roots, which were interpolated from eqn 12.1 by simple proportion, are given in Table 12.1 together with the calculated and observed frequencies for the disc already mentioned. The fractional excesses of the calculated frequencies over the observed frequencies, shown in the last column, are given in parts per thousand.

For type B modes, eqn 5.18 reduces to:

12.3 $$J_2(k_1 a) = 0, \quad \text{where } k_1 = 2\pi\sqrt{2\rho(1+\sigma)/E} \times f$$

Using the numerical values given above:

12.4 $$f = 57.65 k_1 \text{ Kc/s}.$$

Eqn 12.3 is plotted in Fig 12.2 and Table 12.2 gives the roots and frequencies as before.

12.2 Type C modes (n > 0)

For graphical solution, eqns 5.16 are most conveniently arranged in the form:

12.5 $$\left(\frac{A}{B}\right)_1 = \frac{n(1-\sigma)\left[(k_1 a)J_{n-1}(k_1 a) - (n+1)J_n(k_1 a)\right]}{(1-\sigma)(ka)J_{n-1}(ka) + \left[(ka)^2 - n(n+1)(1-\sigma)\right]J_n(ka)} \quad (1)$$

$$\left(\frac{A}{B}\right)_2 = \frac{2(k_1 a)J_{n-1}(k_1 a) + \left[(k_1 a)^2 - 2n(n+1)\right]J_n(k_1 a)}{2n\left[(ka)J_{n-1}(ka) - (n+1)J_n(ka)\right]} \quad (2)$$

These two values A/B are plotted against (ka) in Figs 12.3 and 4 for the two cases n = 1 and n = 2. The values of (ka) and (A/B) corresponding to a given mode are given

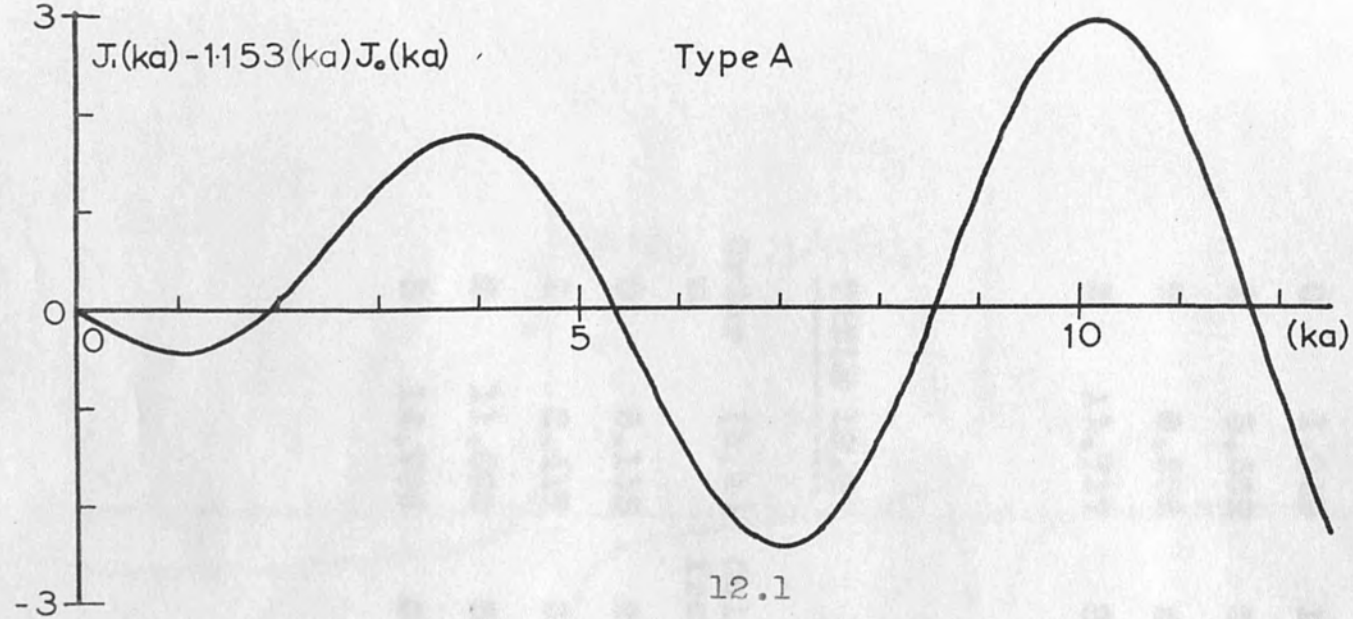

12.1

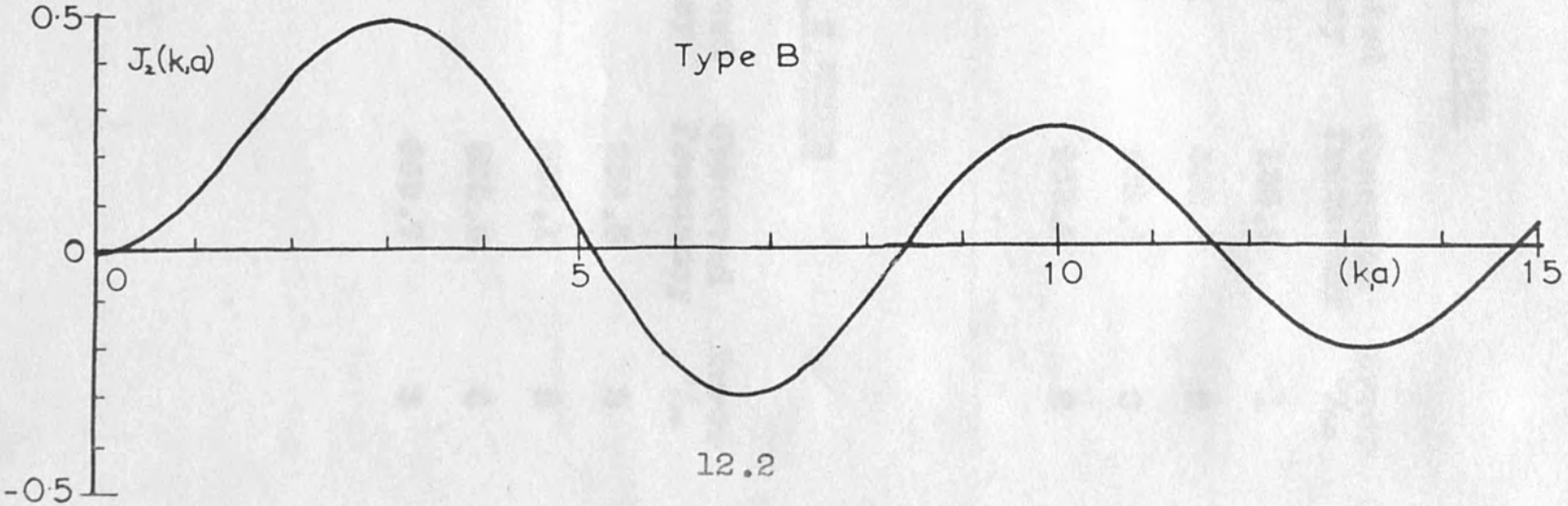

12.2

Fig 12.1-2

TABLE 12.1 TYPE A MODES

Order m	(ka)	Calculated frequency	Observed frequency	Error °/oo
0	1.939	133.7	133.8	-1
1	5.362	369.7	368.8	2
2	8.552	589.7	589.6	0
3	11.717	807.9	805.9	2

TABLE 12.2 TYPE B MODES

Order m	(k,a)	Calculated frequency	Observed frequency	Error °/oo
0	5.135	233.1	232.5	3
1	8.417	382.0	380.1	5
2	11.620	527.4	525.5	4
3	14.796	671.6	669.7	3

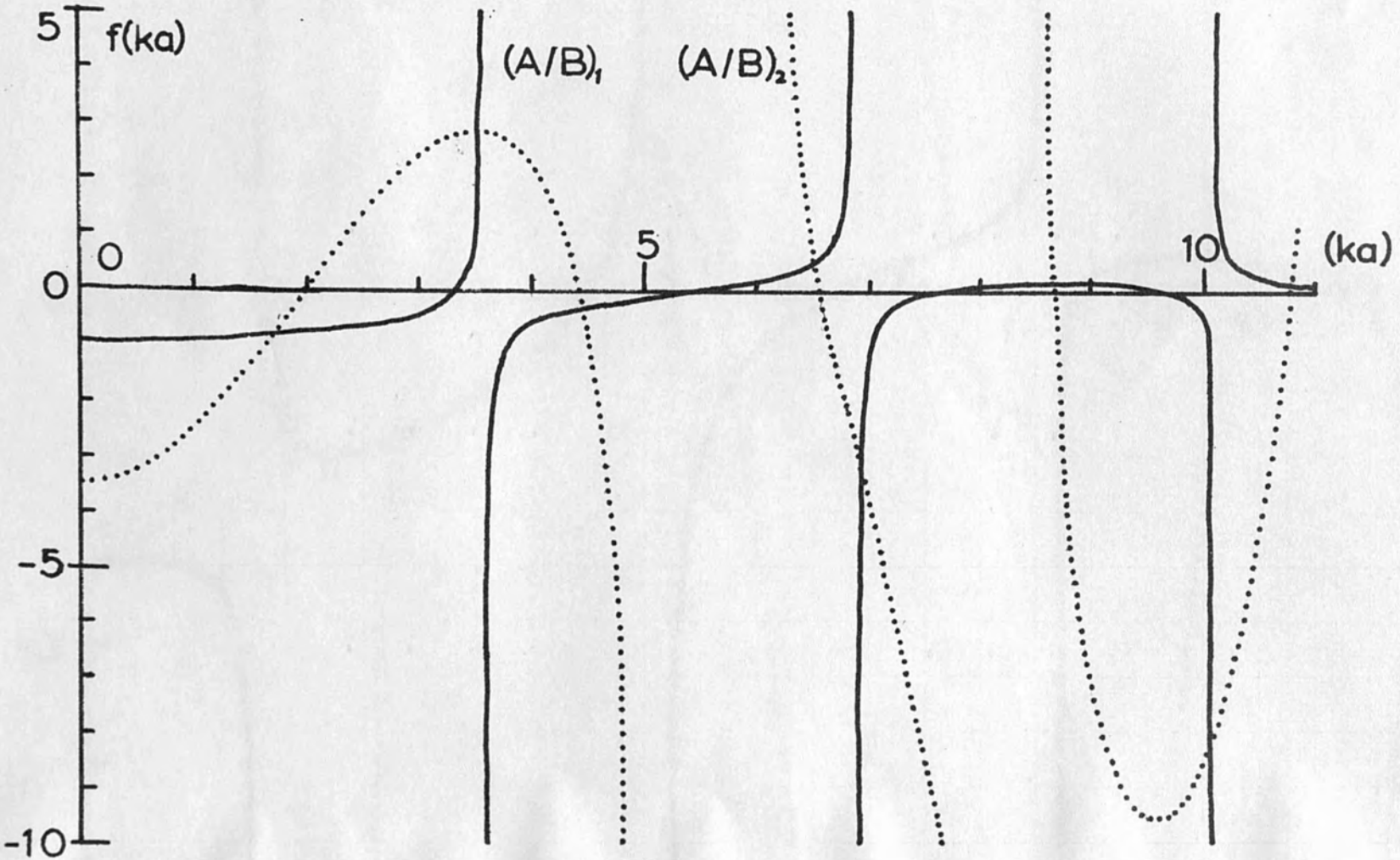

Type C n=1

Fig 12.3

Fig 12.4

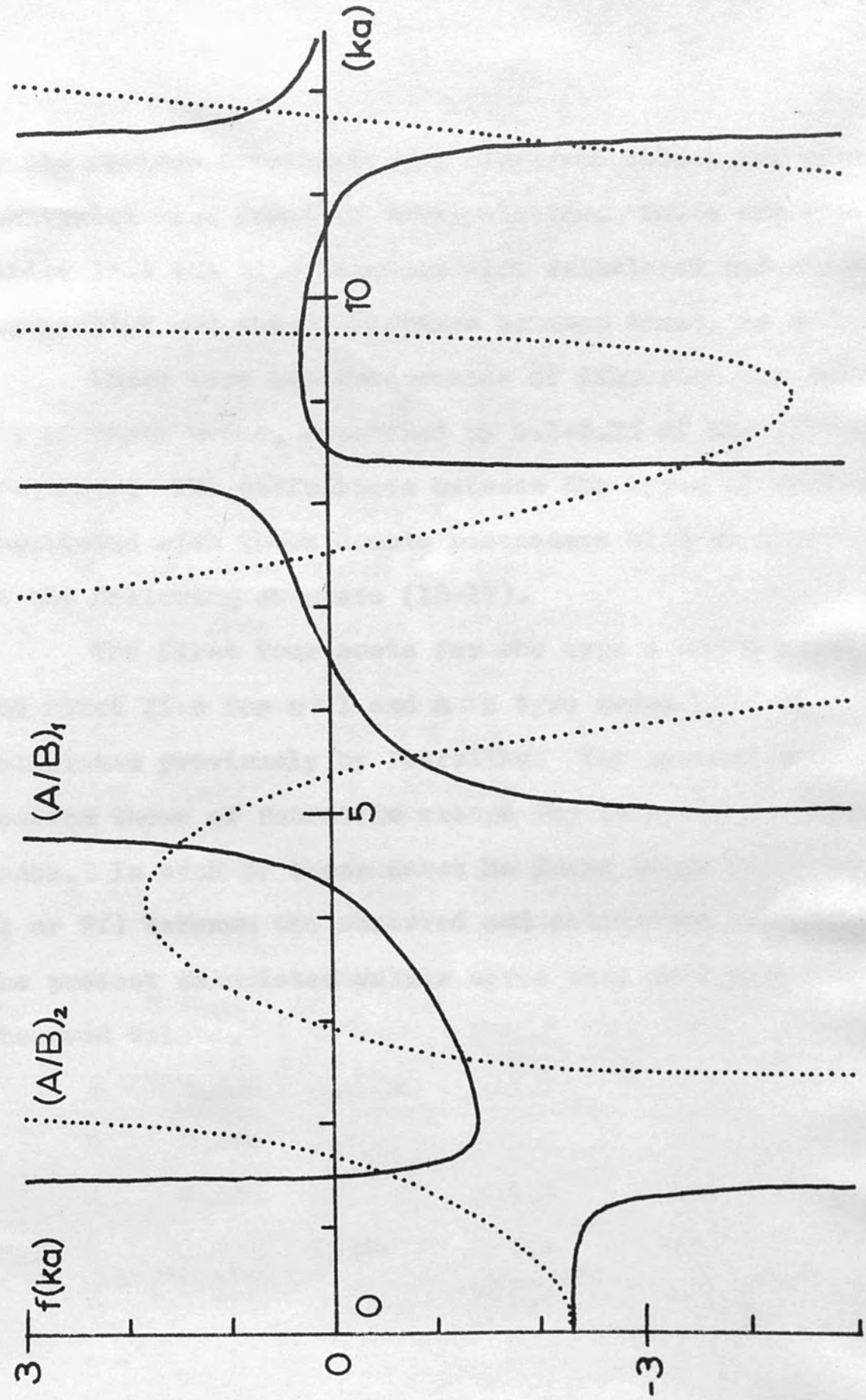

by the various intersections. Accurate values for these quantities were found by interpolation. These are given in Tables 12.3 and 12.4 together with calculated and observed frequencies and the differences between these, as before.

There were two frequencies of vibration for nearly all of these modes, separated by 0.1-0.2% of the vibration frequency. The differences between the types of vibration associated with these double resonances will be discussed in the following chapters (13-17).

The first four roots for the type A and B modes and the first five for n = 1 and n = 2 type modes have been calculated previously by Petrzilka. The present calculations confirm those of Petrzilka except for three of the type C modes. In each of these cases he found large discrepancies (1 or 2%) between the observed and calculated frequencies. The present calculated values agree very well with his observed values.

TABLE 12.3 TYPE C MODES n = 1

Order m	(ka)	A/B	Calculated frequency	Observed frequency	Error ‰
0	1.713	0.8127	118.1	117.6	5
				117.8	3
1	3.537	2.848	243.9	243.4	2
				243.7	1
2	4.452	0.3517	307.0	305.2	6
				305.6	5
3	6.512	0.4696	449.0	447.3	4
				-	-
4	6.936	3.305	478.2	476.7	3
				477.0	3
5	8.668	0.1267	597.7	595.2	4
				595.8	3
6	10.080	7.981	695.0	694.0	1
				-	-
7	10.769	0.1579	742.5	741.1	2
				-	-

TABLE 12.4 TYPES C MODES n = 2

Order m	(ka)	A/B	Calculated frequency	Observed frequency	Error ‰
0	1.542	0.4480	106.3	105.6	7
				105.7	6
1	2.643	1.263	182.2	181.4	4
				181.9	2
2	4.712	1.500	324.9	324.3	2
				324.5	1
3	5.547	0.7944	382.5	380.8	4
				-	-
4	7.463	0.4158	514.6	512.4	4
				513.0	3
5	8.339	3.506	575.0	573.7	2
				573.8	2
6	9.647	0.2370	665.2	663.3	3
				664.2	2
7	11.462	2.182	790.3	790.0	0
				-	-
8	11.826	0.6708	815.4	814.4	1
				-	-

CHAPTER 13

CALCULATION OF THE NORMAL DISPLACEMENT AND EXPERIMENTAL RESULTS

The normal displacement is, in general, more simply expressed mathematically than either the longitudinal displacement or the stress system. Further, since the interferometric method of observation indicates the normal displacement only, the observed patterns should be readily interpretable.

Since the strains are constant throughout the thickness of the crystal, the normal displacement relative to the median plane is $w = hz_z$. From eqn 5.2(4):

13.1 $z_z = -\sigma(x_x + y_y)/(1-\sigma) = -\sigma\Delta/(1-\sigma)$. Thus:

13.2 $w = \text{Const} \times J_n(kr)\cos n\theta$ from eqn 5.13(1).

The causes of the discrepancies between the displacements given by the above theory and the experimentally observed displacements will be discussed empirically in this chapter, although since performing the experiments it has been found possible to explain them on a firm mathematical basis; the theory of this explanation will be given in Chapter 17.

The optical arrangement used for these experiments was that described in Chapter 9 for multiple-beam interference

in transmission. The crystals were all 2.54cm in diameter but of various thicknesses.

13.1 Symmetrical modes (n=0)

a) Type A. Here the displacement is given by:

13.3 $w = A'J_o(kr)$ The profile of the surface between centre and circumference is given by that part of the graph of $J_o(kr)$ lying between 0 and (ka), the root of the frequency equation for the mode concerned. The profiles of the first four modes are shown in Fig 13.1(a) and Table 13.1 gives the radii of the nodal circles as fractions of the disc radius.

The experimental patterns for these modes are in all cases more complex than predicted. None show circular symmetry and most show trigonal symmetry about the axis of the disc. Figs 13.2-5 and 13.6-9 show the modes A.0-3 for a 1.0 mm and 2.0 mm crystal respectively. (Note that the nodal regions show up most clearly when the photographs are viewed obliquely in a direction perpendicular to the interference fringes). All of these patterns show trigonal symmetry. The larger number of 'circular' nodes in the case of the thinner crystal is very noticeable. This suggests that the observed motion may be predominantly flexural. None of the observed nodes crosses the centre of the crystal; the theory requires maximum displacement here.

Fig 13.1(a)-(c)

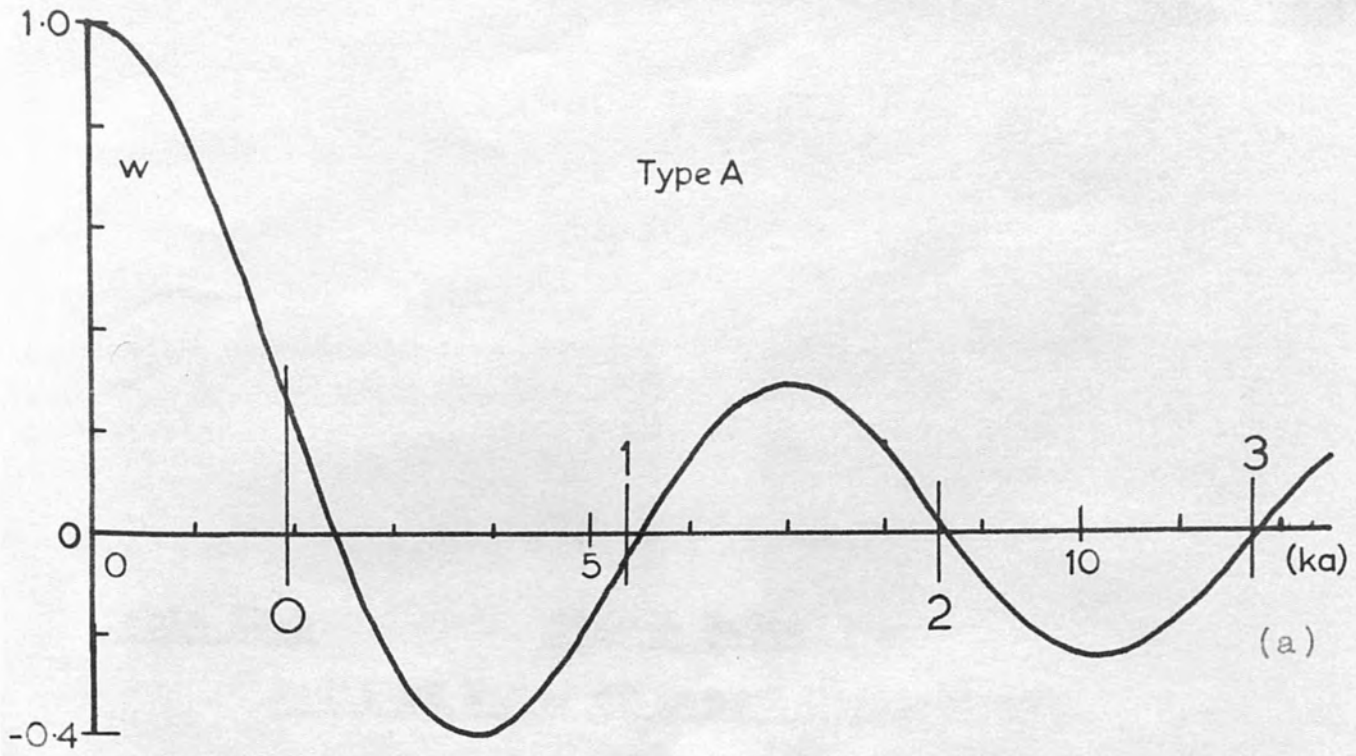
1·0
w
Type A
0
-0·4
0
5
10
(ka)
1
2
3
(a)

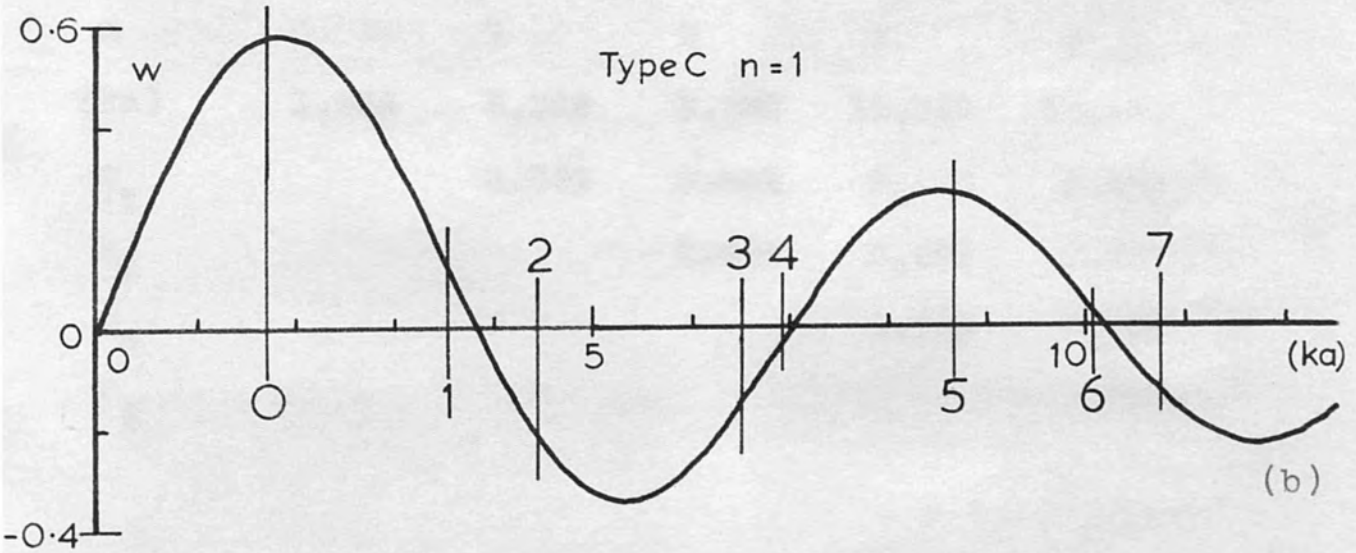
0·6
w
Type C n = 1
0
-0·4
0
5
10
(ka)
1
2
3
4
5
6
7
(b)

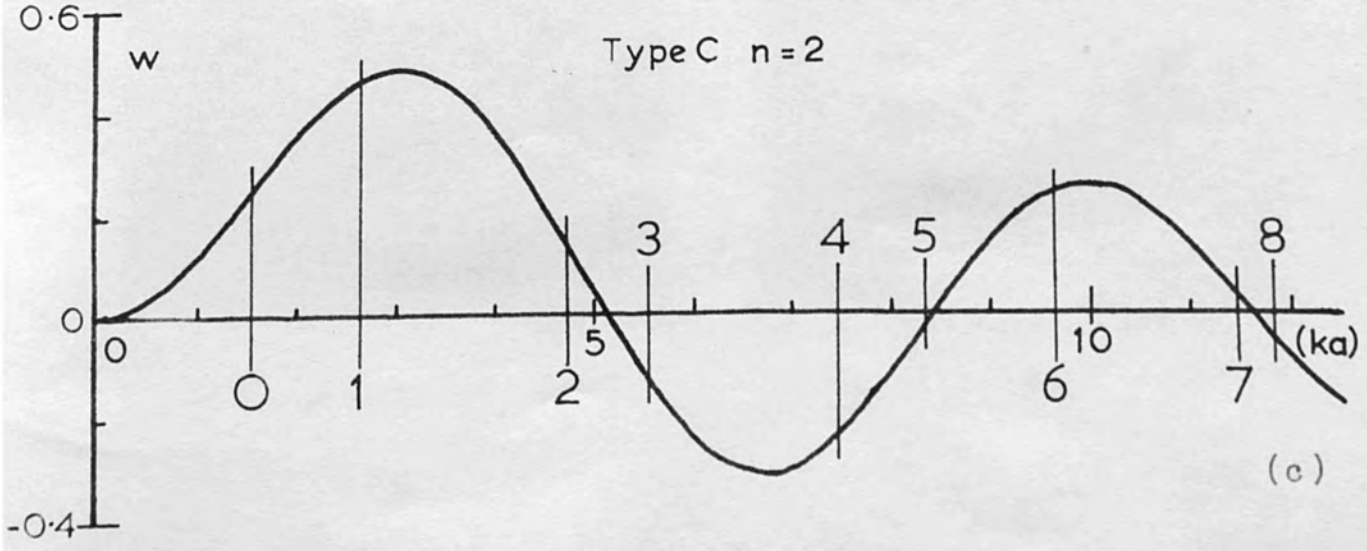
0·6
w
Type C n = 2
0
-0·4
0
5
10
(ka)
1
2
3
4
5
6
7
8
(c)

Table 13.1 Type A Modes

Radii of Nodes of Normal Displacement

m	0	1	2	3	4
(ka)	1.939	5.362	8.552	11.717	14.873
r_1		0.449	0.281	0.205	0.162
r_2			0.645	0.471	0.371
r_3				0.739	0.582
r_4					0.793

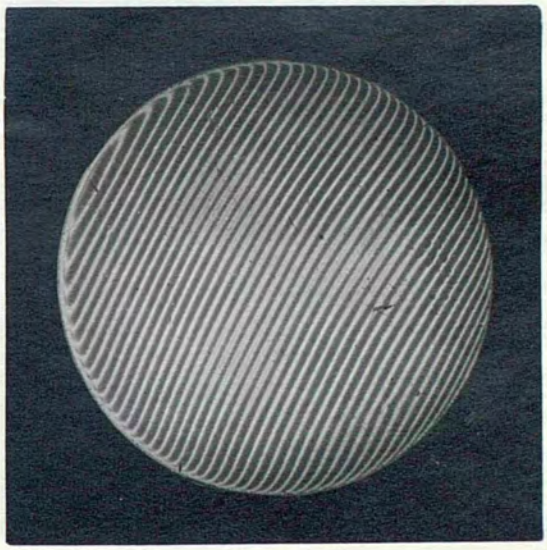

13.2

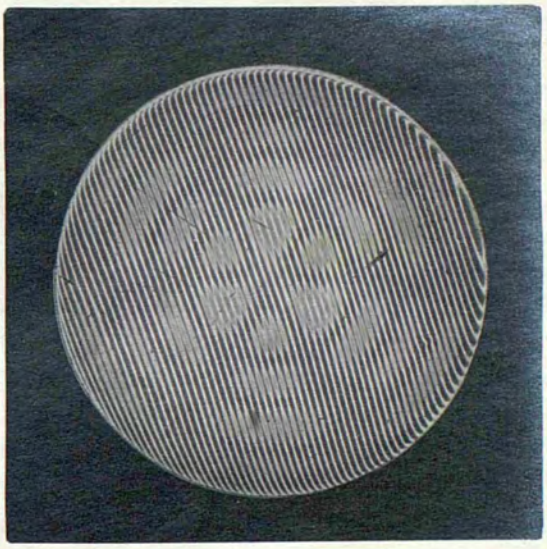

13.3

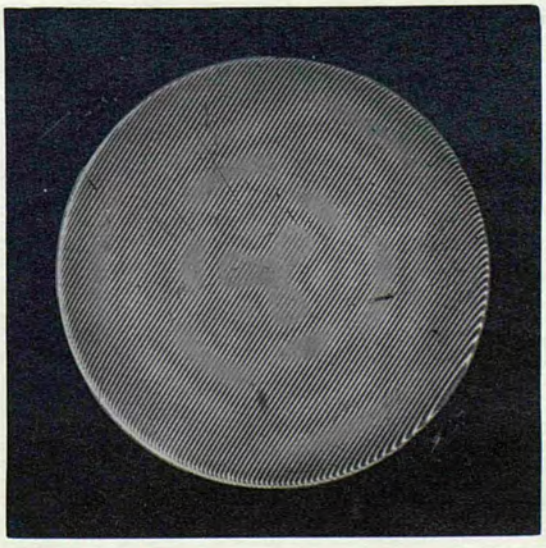

13.4

13.5

A modes, side 2

13.6

13.7

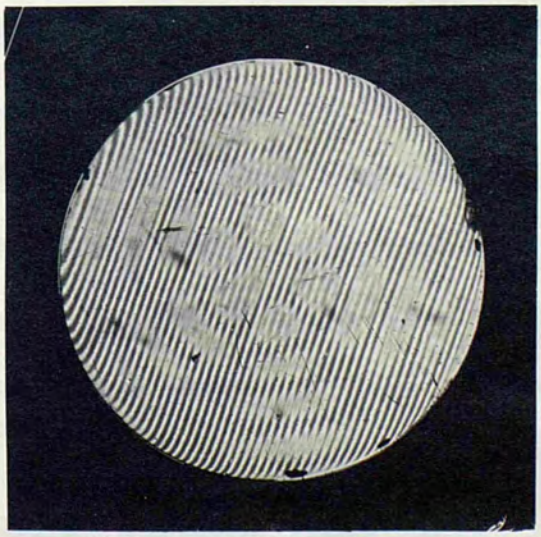

13.8

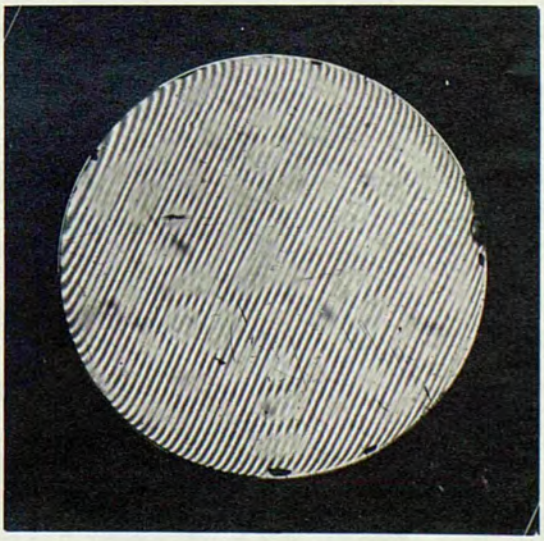

13.9

Certain of the nodal features are complementary on the two sides of the crystal, and if the two nodal patterns are superposed, a pattern with six-fold symmetry results. This holds good for all the patterns mentioned so far and is most strikingly demonstrated by the A.1 mode of the 2.0 mm crystal. Figs 13.10 and 13.11 show the patterns on the other side of this crystal for the A.1 and A.2 modes. These have been reversed in printing so that they are both viewed from the same side of the crystal as are Figs 13.7 and 13.8.

Although all the patterns for the 1.0 and 2.0 mm crystals show trigonal symmetry, this is not always the case. The trigonal symmetry is presumably favoured by the crystal structure of the quartz, but if an A mode has a frequency which is very close indeed to some other mode, then the latter will almost certainly combine with it. To illustrate this point, Figs 13.12 and 13.13 show the interferometric patterns on the two sides of a 3.0 mm crystal for the A.0 mode, both seen from the same side of the crystal. These patterns have digonal symmetry about the axis of the disc. The amplitude is very small at the centre, indicating that the coupled mode is very strong compared with the A mode.

It is simple to deduce the qualitative nature of the nodal pattern resulting from the superposition of two vibratory

A modes, side 1

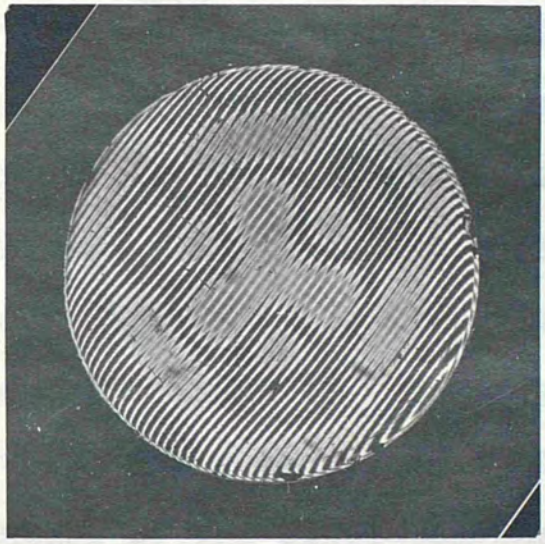

13.10

13.11

A.0 mode, 3 mm crystal

Side 1

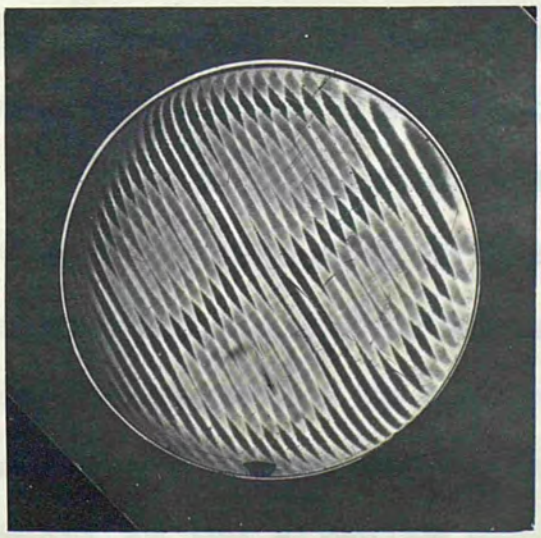

13.12

Side 2

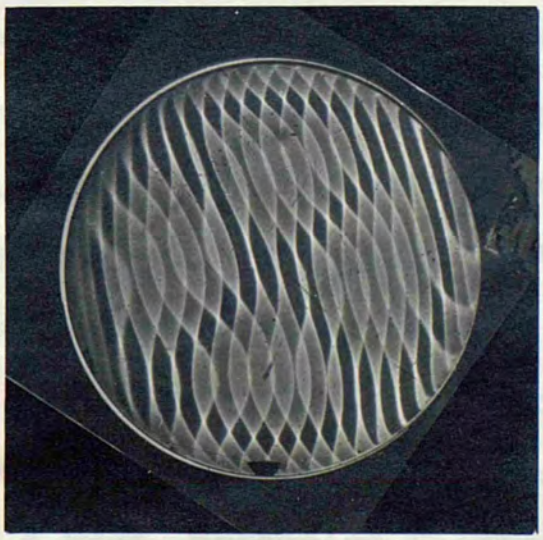

13.13

modes. If, for example, a positive normal displacement is superposed on a region of a vibrating surface which is crossed by a node of the existing normal displacement, then provided the additional displacement is not too large, the node will be moved to a new position in that region which formerly had a negative displacement, such that the former negative displacement equals the superposed positive displacement. To find the nodal pattern resulting from the superposition of two modes, each with its own set of nodes, these two sets are first drawn on the crystal surface. The signs of the displacements, at a particular phase of the vibratory cycle, due to each mode are then marked in each of the regions so formed; these regions are of two types for which the displacements due to each mode are of like or unlike sign. Clearly the resulting nodes must lie entirely in regions of the second type and will indicate points where the displacements due to the two modes are equal and opposite.

Considering now the A.1 mode of the 2.0 mm crystal, the observed normal displacement may be synthesized by the superposition of the theoretical normal displacement on the displacement due to a flexural mode having three diametral and two circular nodes, but the latter do not have the same radii as the circular nodes of a pure, uncoupled flexure. Figs 13.14 and 13.15 show the pure flexural modes with three

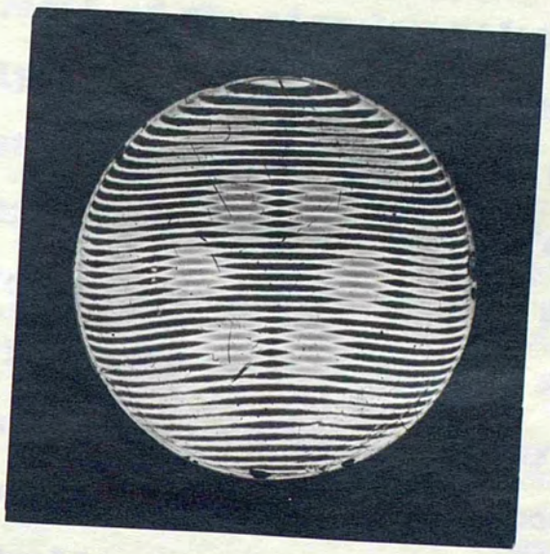

13.14

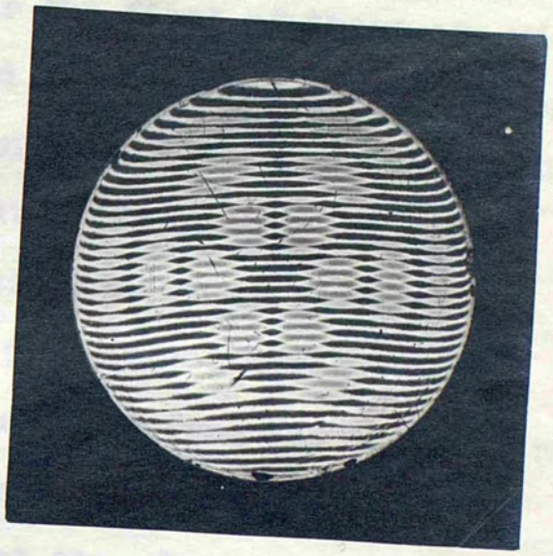

13.15

Radii of flexural nodes 0·52, 0·79a
Radius of type A node 0·449a

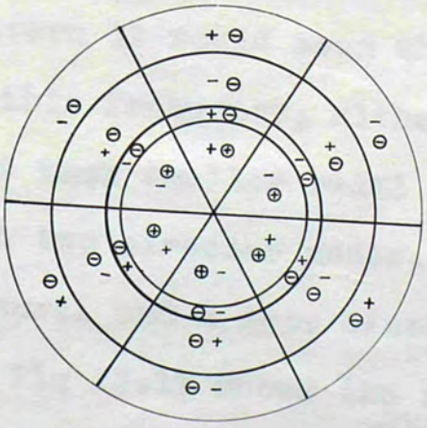

Type A displacements shown thus :- ⊖

13.16

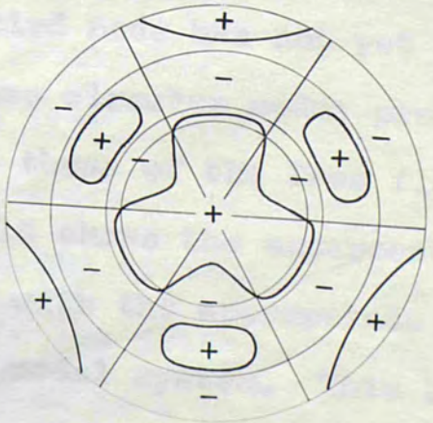

13.17

diametral nodes and two and three circular nodes occurring at frequencies of 273.0 and 417.6 Kc/s respectively. The radii of the circular nodes for the first of these are within 1% of Kirchoff's values, quoted by Petrzilka (1932), in spite of the comparatively large thickness of the crystal and the different value of Poisson's ratio (Kirchoff's theory is for $\sigma = \frac{1}{4}$). Now if it were possible to force flexural vibrations of this type at any frequency between the two just given, as the frequency increased from the lower value one would expect the two nodal circles to contract, and finally a new one would appear at the circumference and move in to the required radius at the higher resonant frequency.

Thus the flexure coupled to the A.1 mode, frequency 368.4 Kc/s, has circular nodes somewhere in between those of the two flexures shown, and from the observed resultant pattern it would seem that the third node has not yet appeared at this frequency, although the two circular nodes present have much smaller radii than have those of the free flexure with two circular nodes. Fig 13.16 shows the superposed flexural and A type displacements with the appropriate signs and Fig 13.17 shows the resultant nodal system. This type of coupling explains most of the observed type A modes with the exception of the one already mentioned; it is probable

that this mode is also coupled to a flexure with three diameters but as the coincident flexure with two diameters has such a large amplitude it is difficult to decide if this is so.

b) Type B. Here $\Delta = 0 = w$ everywhere, so that there should be no normal displacement whatever. Experimentally this is far from the case and strong patterns could be excited at all the appropriate frequencies. These are shown in Figs 13.18-21 and 13.22-25 for 1.0 and 2.0 mm crystals respectively. These patterns, which must be entirely due to coupled modes, all show three nodal diameters and a number of circular nodes, the number increasing with mode order. Once again the thinner crystal shows more nodes than the thicker one. For the 1.0 mm crystal the patterns are more regular than those for the type A modes and have the appearance of perfect flexures. The patterns on the reverse side of the crystal appear to be identical.

For the 2.0 mm crystal the displacements again seem to be flexural but the patterns are not so perfect, particularly B.1, Fig 13.23. As the pattern on the reverse side of this crystal appeared to be identical to the latter pattern, it is possible that the observed pattern is a combination of two flexures, one with three nodal diameters and one with

Fig 13.18-21

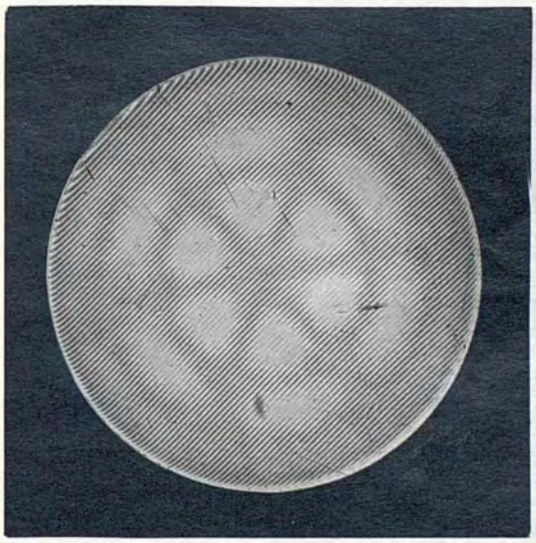

13.18

13.19

13.20

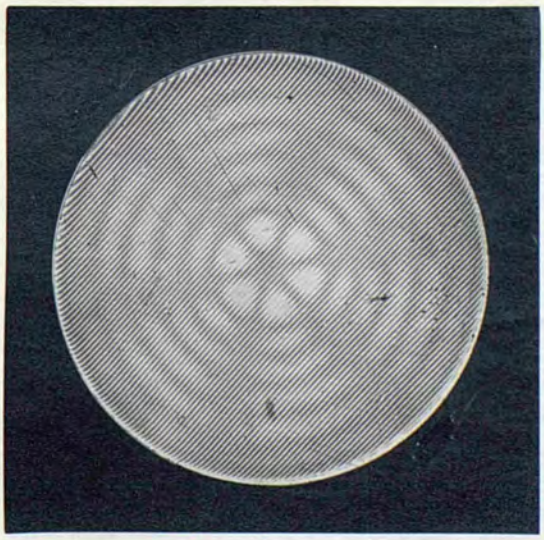

13.21

13.22

13.23

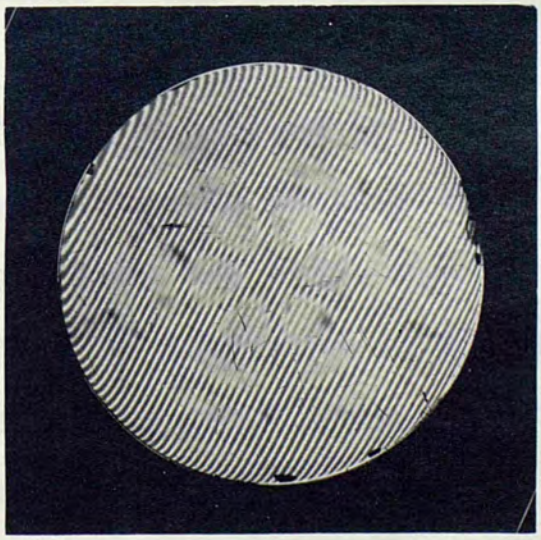

13.24

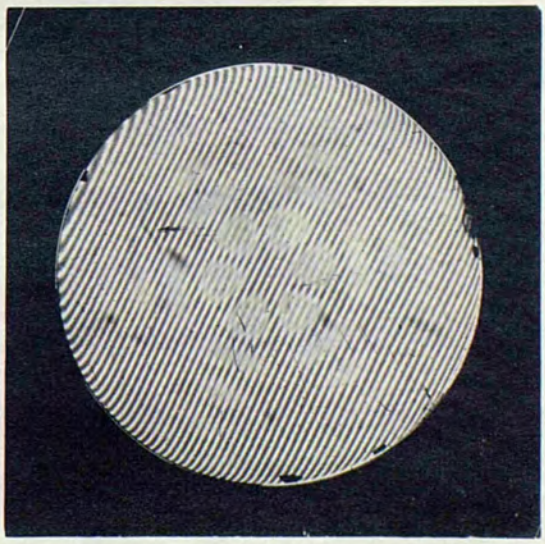

13.25

only one diameter. The frequency of this mode is nearly the same as that of the n=2, m=3 mode and it will he shown in Section 13.2(b) that n=2 modes are often coupled to flexures with one diametral node. The nodal radii for the B.0 mode of the 2.0 mm crystal, which is the only one that can be checked against Kirchoff's theory, are substantially larger than the theoretical values.

13.2 Type C modes

a) n=1 modes. Here the normal displacement is:

13.4 $$w = CJ_1(kr)\cos\theta$$

There are thus a diametral node plus a number of circular nodes. Fig.13.1(b), after page 91, shows the profile of the surface for the first 8 modes and Table 13.2 gives the nodal radii as fractions of the disc radius.

For all these modes two frequencies of vibration were found, separated by a few hundred cycles per second, as mentioned in Chapter 12. The observed interferometric patterns are different for the two frequencies, but, as will be described in Chapter 14, the stress patterns are the same apart from a reorientation relative to the crystal. If, however, there were a coupled mode which takes up a different orientation relative to the primary mode in the two cases, the combined normal displacements would be quite

Table 13.2

Type C, n = 1 Modes

Radii of the Circular Nodes of the Normal Displacement

m	0	1	2	3	4	5	6	7
(ka)	1.713	3.537	4.452	6.512	6.936	8.668	10.080	10.769
r_1	0	0	0	0	0	0	0	0
r_2			0.861	0.588	0.552	0.442	0.380	0.356
r_3						0.809	0.686	0.651
r_4								0.945

Table 13.2

different in the two cases.These modes were usually fairly weak and a 2.0mm crystal was used to get sufficient amplitude for a clear indication of the nodal system.

Figs 13.26-29 show the patterns on the two sides of the crystal (as viewed form the same side) for the m=0 and m=1 modes.Figs 13.30 and 13.31 show the alternative patterns at slightly different frequencies on the first side only.

Qualitatively,this type of pattern may be explained by assuming the presence of a coupled flexural mode having two diametral nodes.It is found,however,that detailed correspondence is not achieved unless the circular nodes of the flexure are distorted.Figs13.32 and 13.33 show how such a distorted flexure can combine to give the observed resultant displacement of Fig 13.30.The flexural mode itself is the resultant of two flexures,one having two diametral and one circular node and the other,of smaller amplitude,having four diametral nodes only. By rotating these flexures through 45° and $22\frac{1}{2}^{\circ}$ respectively, relative to the type C mode,the alternative patterns of Figs 13.26 and 13.28 may be accounted for.For some n=1 modes,such as the m=3 mode,Fig13.34,the flexure with four diametral nodes is obviously stronger than that with two;in every case however,the presence of both flexures is necessary to account for the observed displacement.

b) n=2 modes.Here the normal displacement is:

13.5 $$w = C'J_2(kr)\cos 2\theta$$

n = 1 modes

m = 0 117.9 Kc/s

Side 1

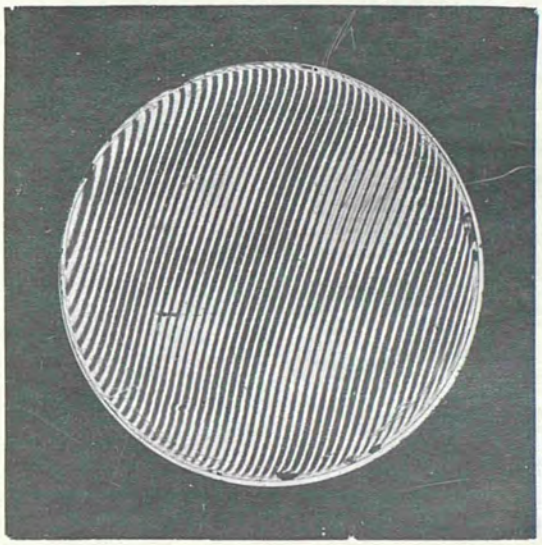

13.26

m = 1 243.6 Kc/s

Side 1

13.27

Side 2

13.28

Side 2

13.29

n = 1 modes

m = 0 117.7 Kc/s m = 1 243.7 Kc/s

Side 1

13.30

Side 1

13.31

The flexural mode is the resultant of a flexure with 4 diametral nodes, and another with 2 diametral nodes and a circular node, radius 0·82a appx. The type C mode has a single diametral node.

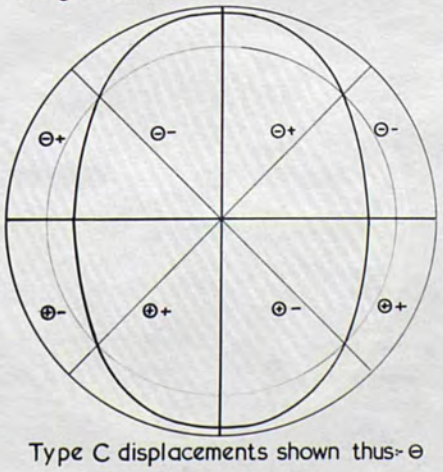

Type C displacements shown thus- ⊖

13.32

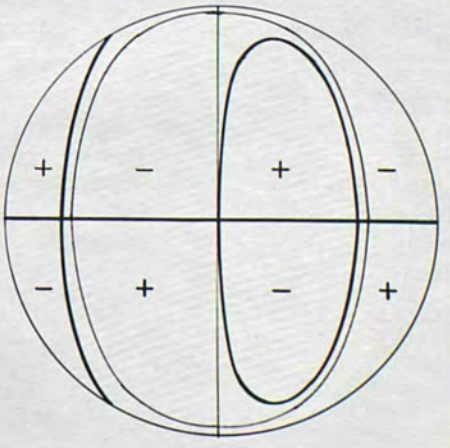

13.33

n = 1, m = 3 mode

Side 2

13.34

n = 2, m = 0; 105.8 Kc/s

Side 1

13.35

Side 2

13.36

There are thus two diametral nodes plus a number of circular nodes. The profiles of the surface for the first 9 modes are shown in Fig 13.1(c), after page 91, and Table 13.3 gives the nodal radii as fractions of the disc radius.

Once more there were two frequencies of vibration for each mode, and the corresponding interference patterns are different from each other. Further, the patterns on the two sides of the crystal at a given frequency are complementary. Figs 13.35-38 show the patterns on the two sides of the crystal for the m = 0 and m = 1 modes. Figs 13.39 and 13.40 show the alternative patterns for these modes, on one side only.

These patterns are very much complicated by coupled modes and it is not possible to explain them by the assumption of a single coupled flexure. However, all the patterns shown can be synthesized from the primary mode together with two flexural modes, one having a solitary diametral node and the other having five diametral nodes; for example, the patterns for the m = 0 mode, Figs 13.35,13.36 and 13.39 can be produced by a combination of the primary motion with suitably orientated flexures having one circular and one diametral node, and no circular and five diametral nodes respectively.

Table 13.3

Type C, n = 2 Modes

Radii of the Circular Nodes of the Normal Displacement

m	0	1	2	3	4	5	6	7	8
(ka)	1.542	2.644	4.712	5.547	7.463	8.339	9.647	11.462	11.826
r_1	0	0	0	0	0	0	0	0	0
r_2				0.926	0.688	0.616	0.532	0.448	0.434
r_3							0.873	0.734	0.712
r_4									0.983

Table 13.3

n = 2, m = 1 mode; 181.9 Kc/s

Side 2

13.37

Side 1

13.38

n = 2 modes

m = 0 105.6 Kc/s

Side 1

13.39

m = 1 181.7 Kc/s

Side 1

13.40

The reasons for the various particular types of flexure being coupled to specific types of longitudinal mode will be discussed theoretically in Chapter 17.

CHAPTER 14

CALCULATION OF STRESS PATTERNS AND EXPERIMENTAL RESULTS

14.1 Experimental test of the stress-optic effect in quartz

Before describing the experiments on the modes of vibration, an account will be given of an experimental test of the conclusions reached at the end of Chapter 7 with regard to the effect of optical activity on the stress-optic effect in quartz.

Fig 14.1 shows the jig used to subject a Z-cut quartz bar (thickness 3.06 mm) to uniform bending in the XY-plane. The thrust applied to the bending jaws by the thumbscrew acts via a phosphor bronze strip mounted between similar jaws, the bending of the strip being proportional to this thrust. The bending of the strip was previously calibrated in terms of thrust by mounting the jig in a vertical plane and replacing the thrust from the screw by the thrust from known weights. The actual bending stresses in the bar were calculated directly from the thrust, knowing the dimensions of the bar and bending jaws.

The optical arrangement was that described in Chapter 9 for using plane polarized light in reflection. Reflection took place at the silvered lower surface of the bar, the jig being mounted horizontally and adjusted so

Fig 14.1

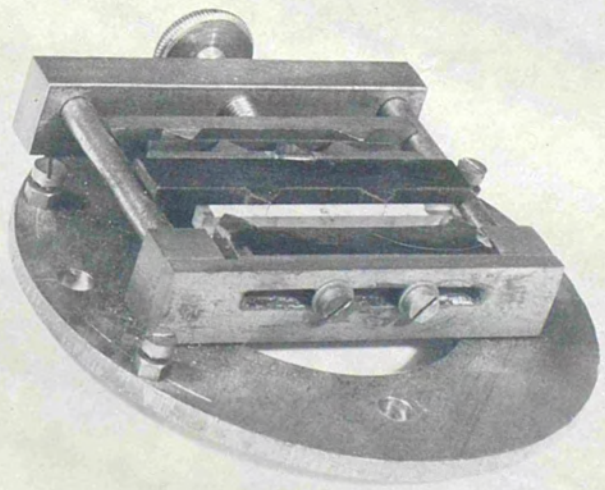

that the Z-faces of the bar were normal to the incident monochromatic light.

On applying a small stress by means of the thumb screw, the field brightened at the edges of the bar. At a slightly higher stress, the central black band could be split into three by rotating the bar relative to the polarizer and analyser, the separation depending upon the actual angle turned through. When the stress had been increased sufficiently, the first order stress fringes appeared at the extreme edges of the bar. The stress was increased slightly until these were clear of the edges and then the series of photographs shown in Figs 14.2-7 was taken; the applied stress is the same for each but the jig was gradually turned relative to the polarizer and analyser axes. The dark line across each photograph gives the direction of the polarizer axis and was marked by the method described in Chapter 9.

It will be noticed that the zero and first order fringes, at the centre and edges of the bar respectively, retain their position throughout the series, and also that the split "isoclinic" is approximately symmetrical, although one side of the bar is in compression and the other in tension. If the bar were isotropic, there would be a solitary isoclinic fringe blacking out the whole bar (or at least the whole of the region over which the stress was sensibly parallel to

Fig 14.2-7

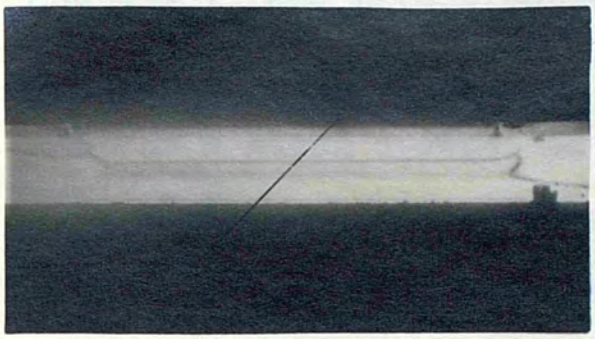

14.2

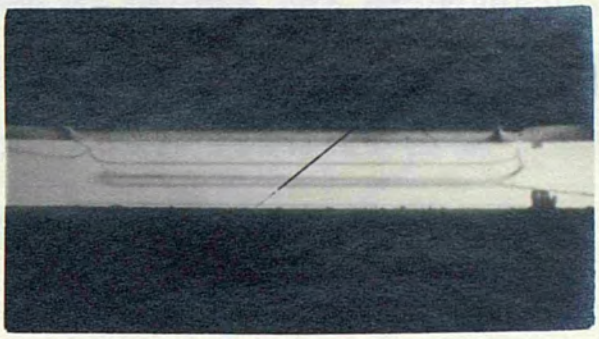

14.3

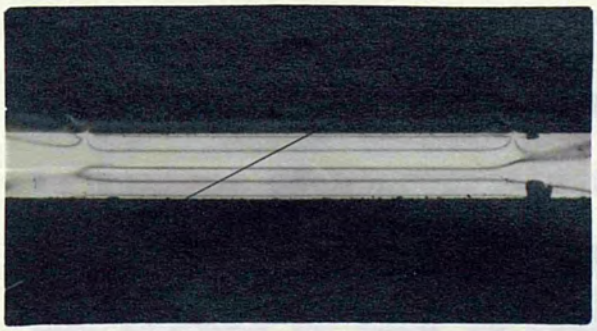

14.4

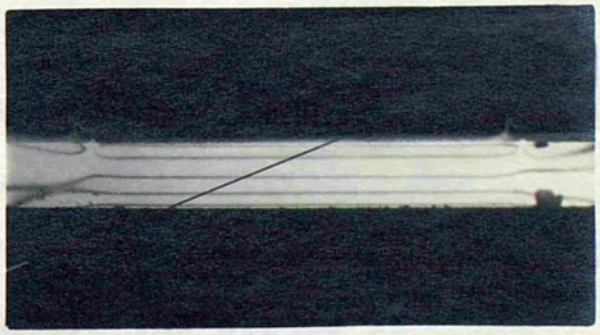

14.5

14.6

14.7

the axis). This would occur when the bar was parallel to the polarizer or analyser axis. But, as explained in Chapter 7, the effective rotation of quartz for propagation along the optic axis depends on the stresses in the XY-plane, and for a given stress, darkness is only attained when there is a certain relation between polarizer orientation and principal stress directions.

Now the stress in a uniformly bent bar increases linearly from zero at the neutral axis to a maximum at the edge; for a given applied stress the "isoclinic" fringe consists of two lines parallel to the neutral axis and, as the orientation of the bar is altered, these lines move to regions of appropriate stress. Alternatively, for a given orientation, variation of the applied stress causes the fringes to move to regions where the stress is the same as previously. Although in these experiments the absolute stress is not known accurately, due to the rudimentary nature of the bending jig, a graph of rotation against relative stress may be plotted, knowing that the stress is a linear function of the distance from the neutral axis.

Fig 14.8 shows part of the theoretical curve of Fig 7.1 and the circles show the experimental points.

Fig 14.8

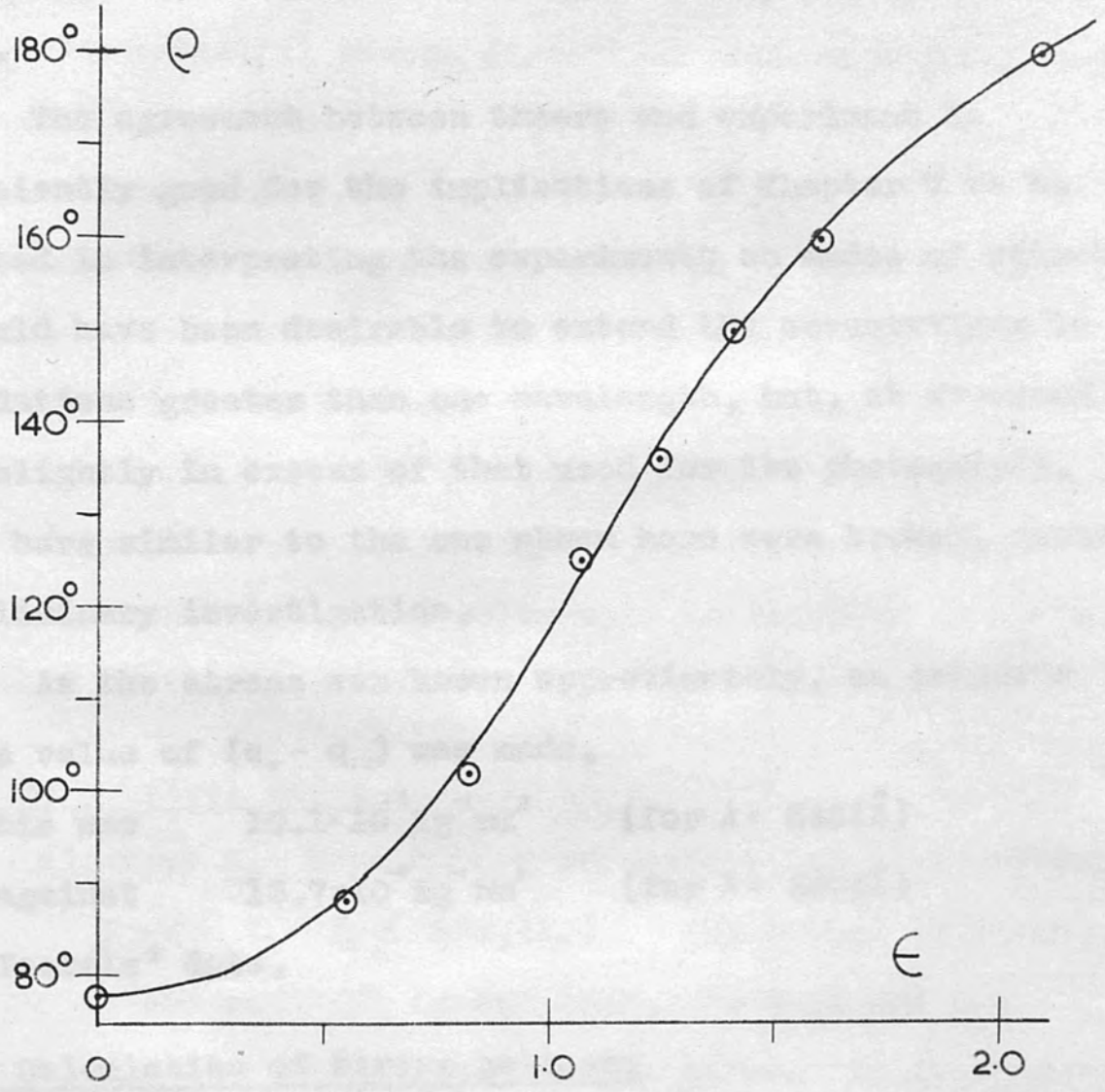

The point for which $\varphi = 180^\circ$ is based upon the first order stress fringe and this has been set on the theoretical curve; all the other points have correct abscissae relative to this point.

The agreement between theory and experiment is sufficiently good for the implications of Chapter 7 to be accepted in interpreting the experiments on modes of vibration. It would have been desirable to extend the observations to retardations greater than one wavelength, but, at stresses very slightly in excess of that used for the photographs, three bars similar to the one shown here were broken, during a preliminary investigation.

As the stress was known approximately, an estimate of the value of $(q_{11} - q_{12})$ was made.

This was 10.1×10^{-6} Kg^{-1} mm^2 (for $\lambda = 5461$Å)

as against 13.7×10^{-6} Kg^{-1} mm^2 (for $\lambda = 5893$Å)

from Pockels' data.

14.2 Calculation of stress patterns

The principal stress difference in the XY-plane is connected with the stress resultants T_r, T_θ and $S_{r\theta}$ by the relation:

14.1 $$2h(P-Q) = \sqrt{(T_r - T_\theta)^2 + 4S_{r\theta}^2}$$

Thus the zero order stress fringe, for which this difference is zero, joins points satisfying the conditions:

14.2 $(T_r - T_\theta) = 0$ (1) and $S_{r\theta} = 0$

The principal stress directions make an angle φ with those of T_r, T_θ where:

14.3 $\tan 2\varphi = 2S_{r\theta}/(T_r - T_\theta)$

Since the stress resultants are referred to axes parallel and perpendicular to the radius at any point, the angle between the principal stress directions and the fixed directions $\theta = 0, \theta = \pi/2$ is $\psi = (\varphi + \theta)$. The isoclinic fringes, observed by plane polarized light, join points for which ψ has a constant value; this value will be referred to as the parameter of the isoclinic.

14.3 Symmetrical modes (n = 0)

a) Type A. Here $S_{r\theta} = 0$ everywhere, so that

14.4 $P - Q = T_r - T_\theta = A'J_2(kr)$ (Note that A' is not the same as the constant in eqn 13.3. In this and the following chapters, A',B' and C' will be used indiscriminately as unknown arbitrary constants whereas A and B have the special significance of Chapter 5 and the ratio A/B assumes a definite value for each particular mode). The variation of the principal stress difference between the centre and circumference of the disc is shown in Fig 14.9(a) for the

Figs 14.9(a)-(b)

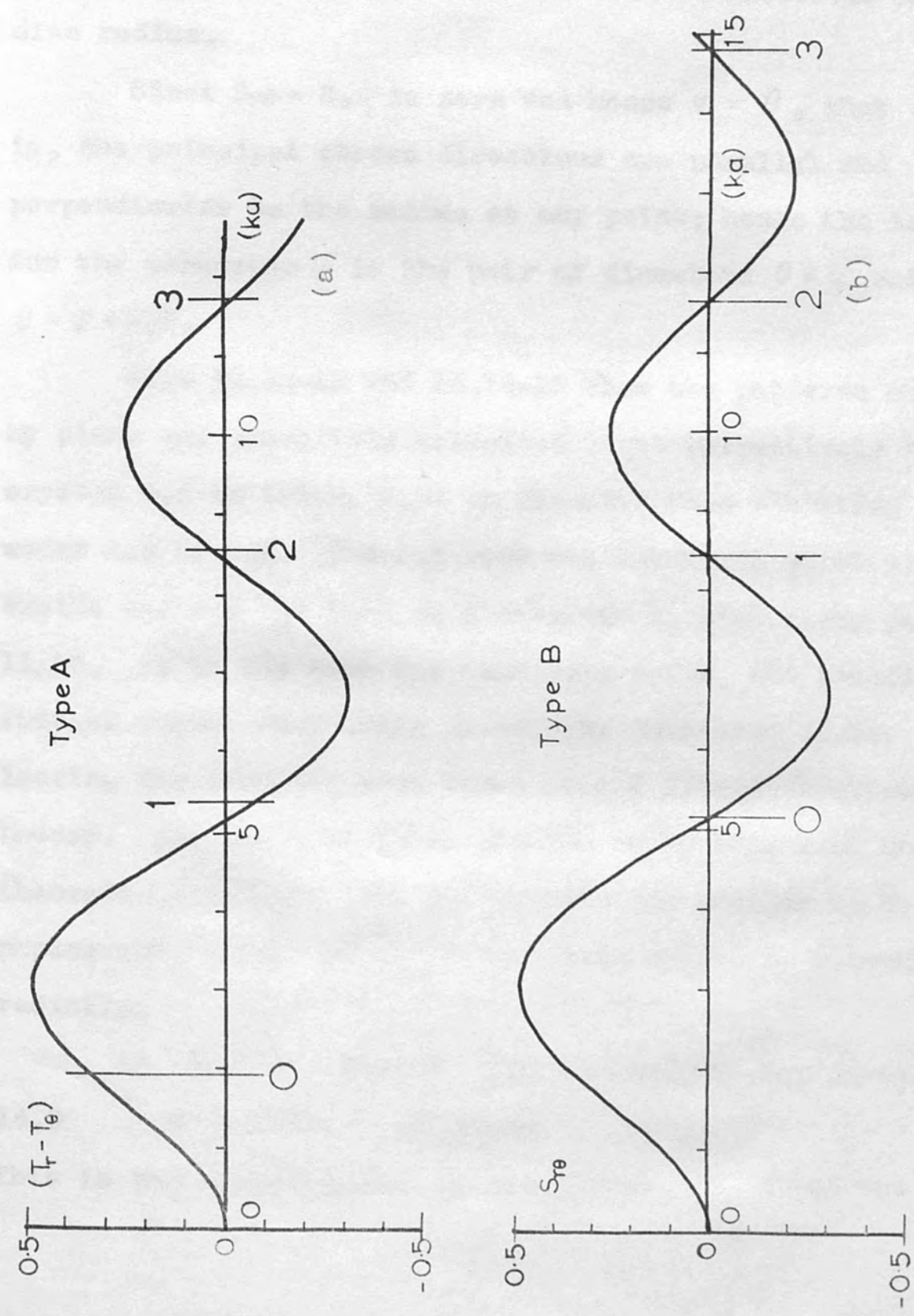
Type A
$(T_r - T_\theta)$
0·5
0
-0·5
0
5
1
10
2
3
(ka)
(a)
Type B
$S_{r\theta}$
0·5
0
-0·5
0
5
1
10
2
15
3
(ka)
(b)

first four modes and the radii of the circular zero order stress fringes are given in Table 14.1 as fractions of the disc radius.

Since $S_{r\theta} = 0$, φ is zero and hence $\psi = \theta$, that is, the principal stress directions are parallel and perpendicular to the radius at any point; hence the isoclinic for the parameter ψ is the pair of diameters $\theta = \psi$ and $\theta = \psi + \pi/2$.

Figs 14.10-13 and 14.14-16 show the patterns observed by plane and circularly polarized light respectively for a crystal 0.5 mm thick, 2.54 cm diameter, when vibrating in the modes A.0 to A.3. The A.0 mode was extremely difficult to excite and was too weak to photograph by circularly polarized light. As is the case for isotropic media, the isoclinic fringes vanish when using circularly polarized light, leaving the circular zero order stress fringes required by theory. The radii of these circles agree well with the theoretical values. The photographs are similar to Bergmann's photographs (1949) of thick isotropic cylinders vibrating radially.

b) Type B. Here $(T_r - T_\theta) = 0$ everywhere, giving:

14.5 $$P - Q = 2S_{r\theta} = B' J_2(k_1 r)$$

This is the same function as for type A but, since the values

Table 14.1 Type A Modes

Radii of Zero Order Stress Fringes

m	0	1	2	3	4
(ka)	1.939	5.362	8.552	11.717	14.873
r_1	0	0	0	0	0
r_2		0.958	0.600	0.438	0.345
r_3			0.984	0.718	0.566
r_4				0.992	0.781
r_5					0.995

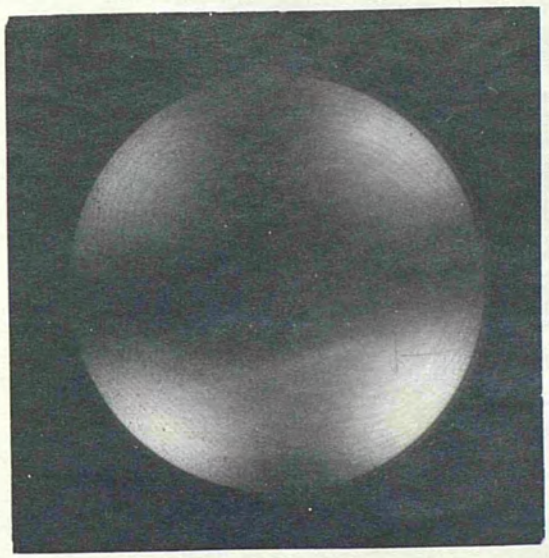

14.10

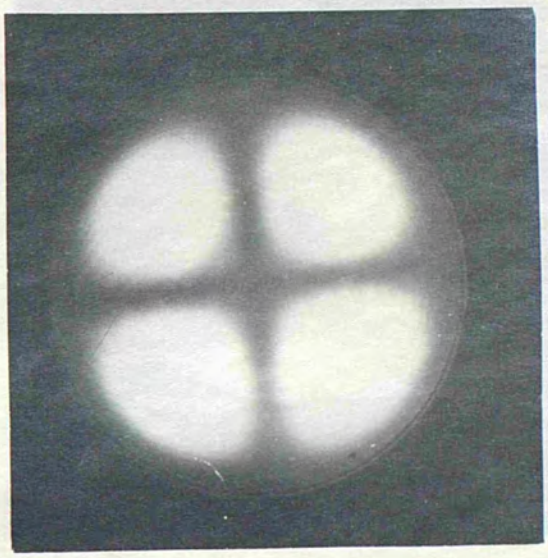

14.11

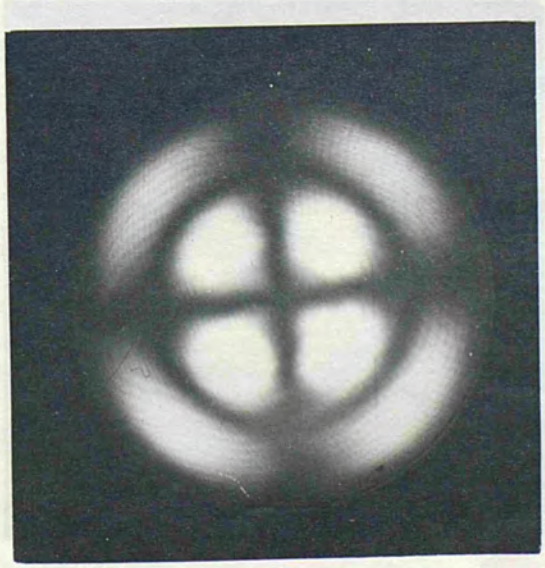

14.12

14.13

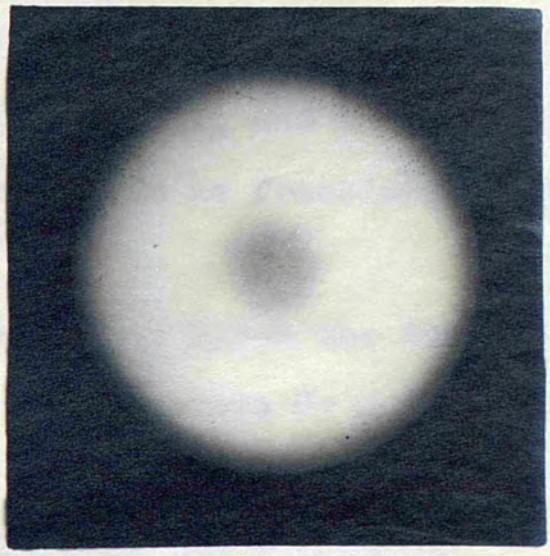

14.14

14.15

14.16

of $(k_t a)$ are derived from a different frequency equation the radii of the zero order stress fringes are different from those for the corresponding type A modes; in particular, there is always a dark fringe at $r = a$. The variation of $P - Q$ with r is shown in Fig 14.9(b), after page 104, and the radii of the zero order stress fringes are given as fractions of the disc radius in Table 14.2.

Since $(T_r - T_\theta)$ is zero, $\varphi = \pi/4$; hence the isoclinic for the parameter ψ is the pair of diameters $\theta = \psi + \pi/4$ and $\theta = \psi + 3\pi/4$.

Figs 14.17-20 and 14.21-24 show the appearance of type B modes when illuminated by plane and circularly polarized light respectively; these are again for the 0.5 mm crystal. The agreement between experimental and theoretical values of the radii of the circles is again good.

14.4 Disturbing influences

a) Effect of optical activity. It will be noticed that in both the sets of photographs taken by plane polarized light, the isoclinic cross is twisted slightly anti-clockwise away from the theoretical position (the polarizer and analyser axes are approximately vertical and horizontal in the photographs). The quartz crystal used for these experiments was right-handed, that is, it rotated the light vector anti-

Table 14.2 Type B Modes

Radii of Zero Order Stress Fringes

m	0	1	2	3	4
$(k_i a)$	5.135	8.417	11.620	14.796	17.960
r_1	0	0	0	0	0
r_2	1.0	0.610	0.442	0.347	0.286
r_3		1.0	0.724	0.569	0.469
r_4			1.0	0.785	0.647
r_5				1.0	0.824
r_6					1.0

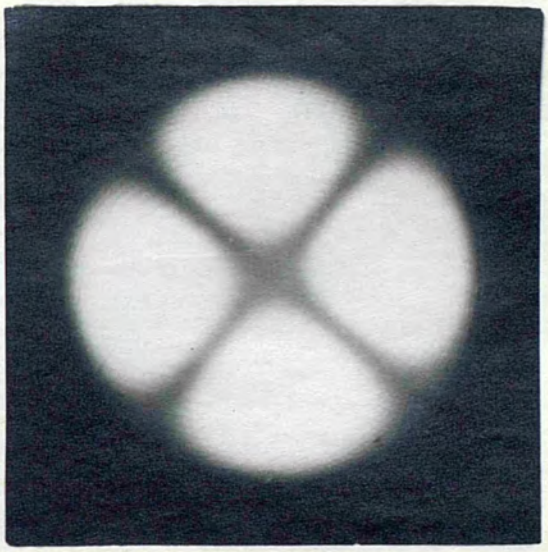

14.17

14.18

14.19

14.20

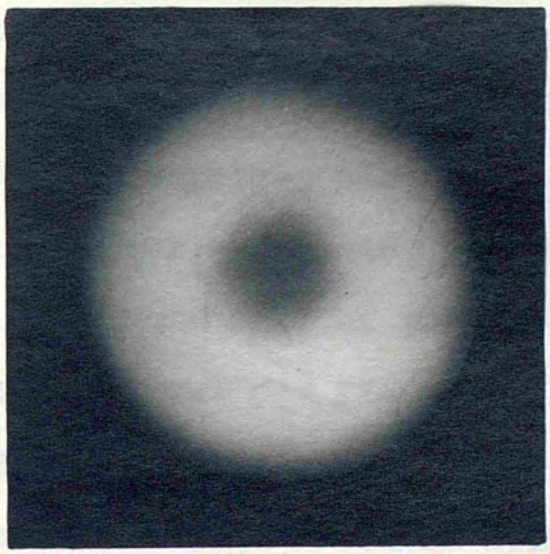

14.21

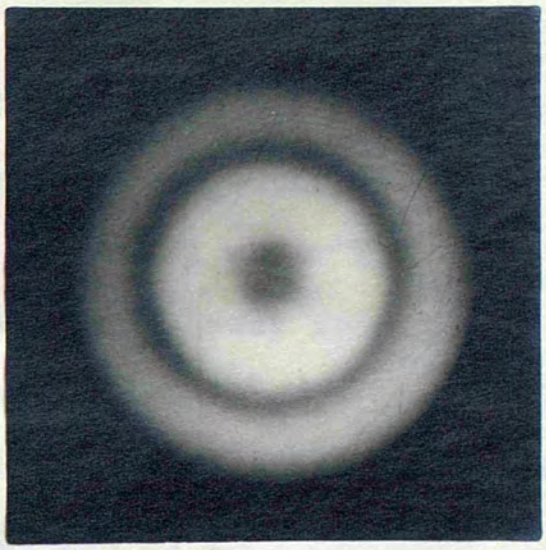

14.22

14.23

14.24

clockwise when looking in the direction of propagation of the light.

To illustrate this point further, Figs 14.25 and 14.26 show the A.1 and B.1 modes for a 0.5 mm left-handed crystal and Figs 14.27 and 14.28 show the A.1 and B.2 modes for a 2.0 mm crystal, also left-handed, the direction of the polarizer axis being marked in the usual way. The misorientations of the isoclinic cross, away from the theoretical positions, are about 7° and 26° for the 0.5 and 2.0 mm crystals respectively, the optical rotations of these crystals for λ = 5461Å being 13° and 51°.

The theoretical prediction of Chapter 7, namely that the observed isoclinic is that corresponding to principal stress directions differing by half the optical rotation of the crystal from the directions of the axes of polarizer and analyser, is thus substantiated.

b) Effect of thickness. Considering now the effect of the crystal's not being extremely thin, it will already have been noticed that the B.2 mode of the 2.0 mm crystal, Fig 14.28, is not perfect. The types A and B modes were examined for a 3 mm crystal and irregularities were very pronounced, often rendering the patterns unrecognizable.

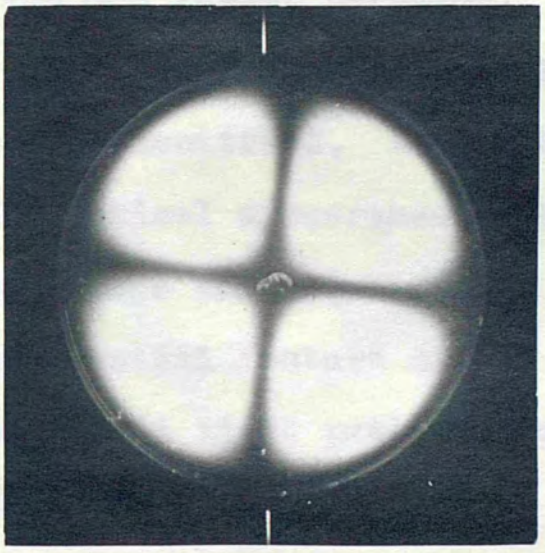

14.25

14.26

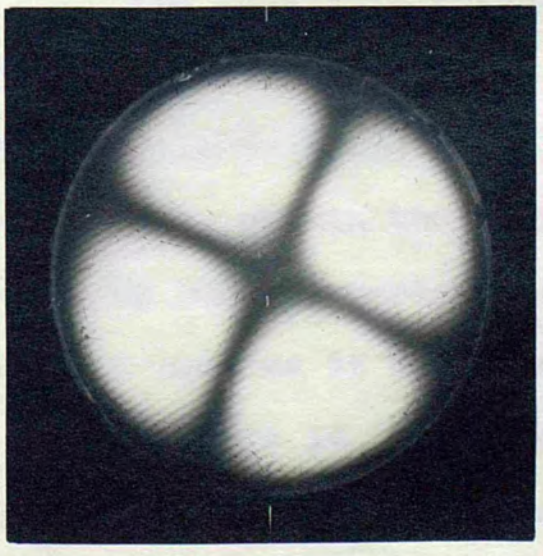

14.27

14.28

Figs 14.29-32 show the A.2 and B.2 modes by plane and circularly polarized light; both modes are recognizable from the latter patterns. Of the other type A modes, A.0 and A.1 were recognizable but A.3 was too badly distorted to be identified. Although departing greatly from the theoretical appearance, the patterns for the B modes were much more regular than for the A modes. In particular, the central feature of Fig 14.30 re-appears in all the plane polarized light patterns, while the central spot of the circularly polarized light pattern is in each case three branched as in Fig 14.32. The zero order stress fringes are no longer circular or even continuous. This discontinuity of the zero order stress fringe is the rule for the vast majority of possible vibration modes.

The isoclinic fringes do not retain their shape when the parameter ψ is varied, since the stress system no longer has circular symmetry. In Fig 14.30 the conditions were adjusted to obtain the most symmetrical pattern possible, so as to make comparison easier; this was not possible for the A.2 mode as it was so distorted.

In Figs 14.33-36 the B.1 mode is shown for various isoclinic parameters, the polarizer axis being marked in the usual manner. For a stress distribution with no symmetry

14.29

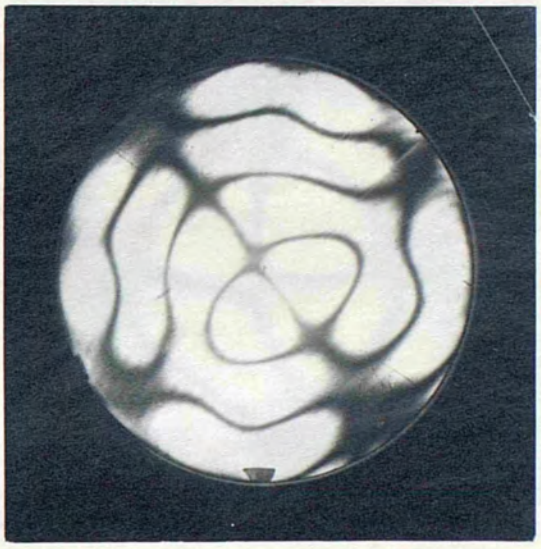

14.30

14.31

14.32

14.33

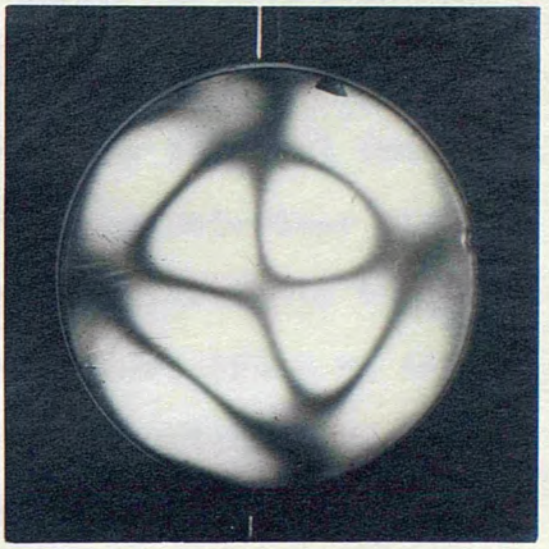

14.34

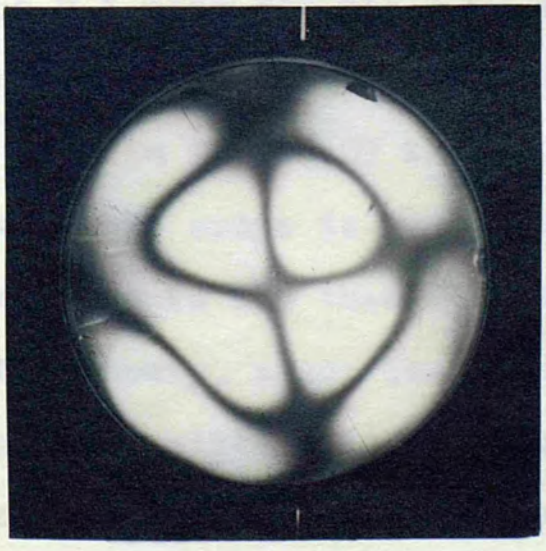

14.35

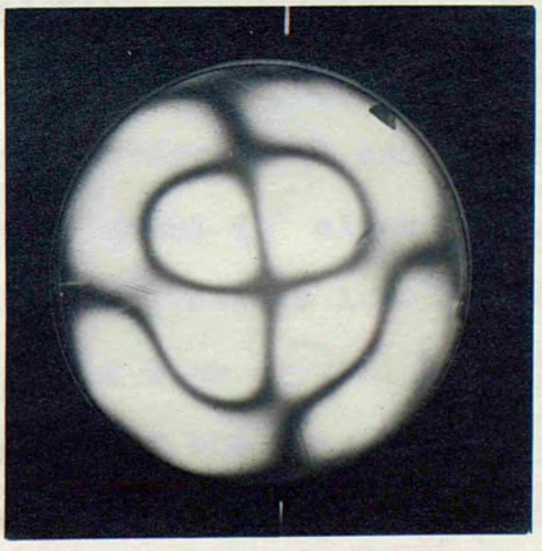

14.36

about an axis normal to the plane of stress, a given isoclinic pattern is repeated when the parameter ψ increases by 90°. In the present case an increase of 30° in ψ results in a given pattern being repeated, but turned through 120° relative to the crystal. Fig 14.36 is the same as 14.33 but turned through 120° anti-clockwise, while the polarizer axis has turned just over 30° anti-clockwise relative to the crystal. (The position of the crystal may be identified by the chip at the edge). Thus the stress distribution shows three-fold symmetry and this is doubtless influenced by the trigonal symmetry of the crystal.

c) Effect of large amplitude. In all the photographs shown so far, the excitation was deliberately small, to avoid changes in the effective rotatory power. Figs 14.37-40 show the B.1 mode for the 3 mm crystal with progressively increasing strength of excitation.

In Fig 14.37 the amplitude is very small and the isoclinic cross is misorientated by about 40° clockwise relative to the theoretical position. This is in accordance with theory, since the rotation for a 3 mm crystal is 78°. As the amplitude is increased, parts of the isoclinic cross move in a direction corresponding to increased rotatory power, the displacement depending on the magnitude of the

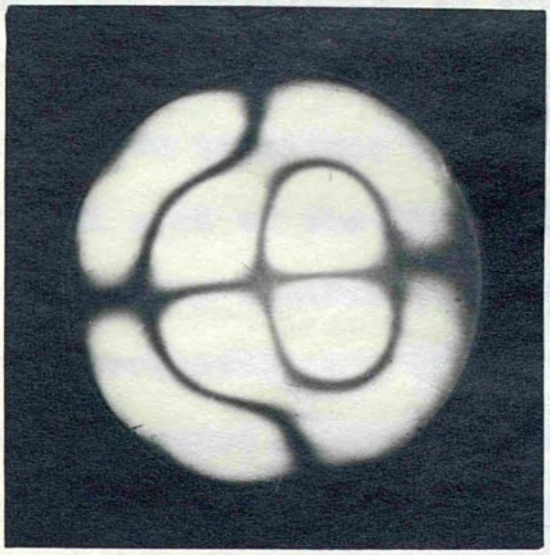

14.37

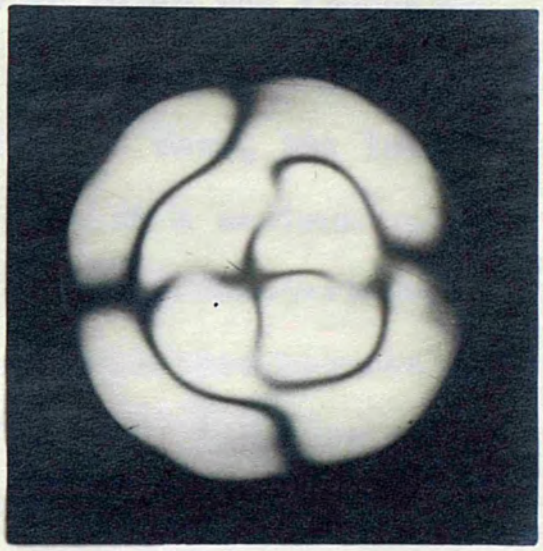

14.38

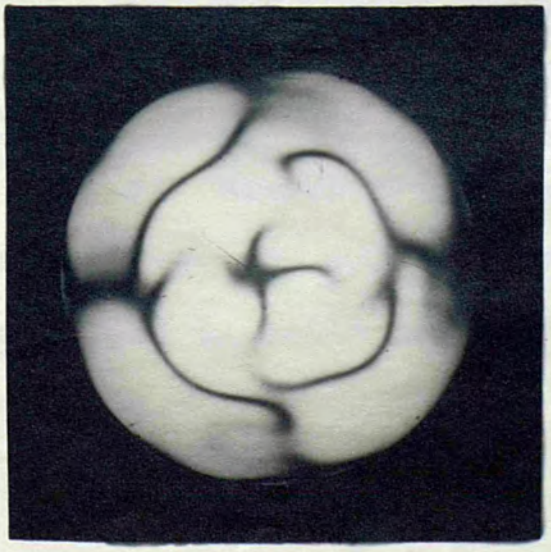

14.39

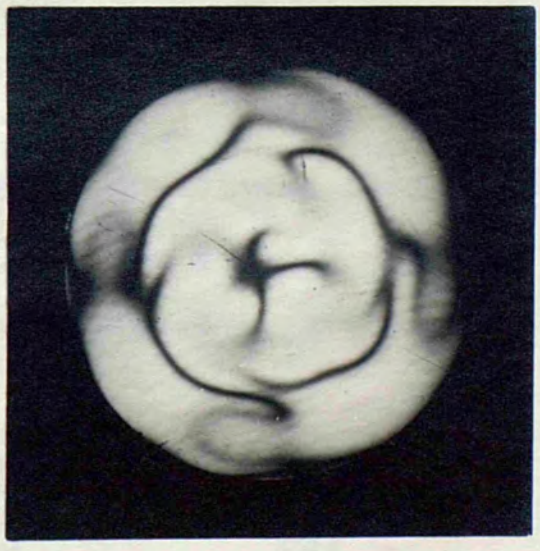

14.40

stress at a given point. It is perhaps surprising that the displaced 'isoclinic' is so clearly defined, for it is actually oscillating to and fro at twice the frequency of vibration. The reason is that in the extreme position the displaced isoclinic is momentarily at rest, the intensity of the rest of the field being then at a maximum and momentarily constant; thus the system effectively acts as its own stroboscope and the non-linear relation between stress and birefringence enhances this effect. In the case of the 0.5 mm crystal there was no sign whatever of the stress being sufficient to cause increased rotation; this was also true for the 1.0 mm crystal except at dangerously large amplitudes. Thus for thin crystals we may examine the more complex modes without fear of the patterns being affected by anything other than the stress distribution.

14.5 Type C modes

a) Numerical calculation of the stress fringes and isoclinics. By substituting the values U and V given by eqns 5.14 in the equations for the stress resultants, eqns 5.10, we find:

14.6 $$(T_r - T_\theta) = (T_r - T_\theta)'\cos(n\theta) \qquad (1)$$

$$S_{r\theta} = S'_{r\theta} \sin(n\theta) \qquad (2)$$

where $(T_r - T_\theta)'$ and $S'_{r\theta}$ are functions of r only. The actual

functions are too long and cumbersome for inclusion here. Thus $(T_r - T_\theta)$ is zero along certain circles and diameters and so also is $S_{r\theta}$. Since the two sets of diameters alternate and the two sets of circles do not generally coincide, the zero order stress fringe is given by the intersection of the diameters of each set with the circles of the other set and is thus a series of discrete points.

For the isoclinics:

14.7 $$\tan 2\varphi = 2S_{r\theta}/(T_r - T_\theta) = \tan(n\theta) \times 2S'_{r\theta}/(T_r - T_\theta)'$$

This may be re-arranged in the form

14.8 $$2S'_{r\theta}/(T_r - T_\theta)' = \tan(2\psi - 2\theta)/\tan(n\theta)$$

The method of calculation was to evaluate the right-hand side of eqn 14.8 for various values of θ and a particular value of ψ. Then, from a graph of the left-hand side against r, the value of r for each value of θ could be found. Each point so fixed was a point on the isoclinic for the chosen value of ψ. If ψ is replaced by $\pi/n - \psi$ and θ is replaced by $\pi/n - \theta$, the value of the right-hand side of eqn 14.8 is unaltered. Thus the isoclinic pattern for the parameter $\pi/n - \psi$ is the same as that for ψ reflected in the plane $\theta = \pi/2n$.

The calculations were extremely long and laborious even with the aid of a Brunsviga calculating machine, for

the expressions involved were such that no approximations could be made at any stage. For this reason the calculations were restricted to two modes for n = 1 and two for n = 2.

b) n = 1 modes. Using the appropriate values of (ka) and A/B, taken from Table 12.3, graphs of $(T_r - T_\theta)'$ and $2S'_{r\theta}$ were plotted against r and are shown in Figs 14.41 and 14.43 for the m = 4 and m = 5 modes respectively, while Figs 14.42 and 14.44 show the ratio of these quantities. Values of $\tan(2\psi - 2\theta)/\tan\theta$ were calculated and could be used for both modes; since this expression is unaltered by substituting $(\theta + \pi)$ for θ, only half of each pattern had to be calculated. Figs 14.45-48 and 14.53-56 show the theoretical appearance of the isoclinics for various values of ψ between 0° and 45°. The isoclinics for $\psi = 45^\circ$ to 90° are the same as those for $\psi = 45^\circ$ to 0° reflected in the plane $\theta = 90^\circ$. In each case the zero order stress fringe or isotropic points are marked on the 0° isoclinic.

As might have been expected from the almost random nature of the roots to the frequency equation, the isoclinic fringes form a very complicated pattern, and although there are some characteristic features which recur as m increases, there is no regular series as for type A and B modes.

Figs 14.49-52 and 14.57-59 show the observed isoclinics

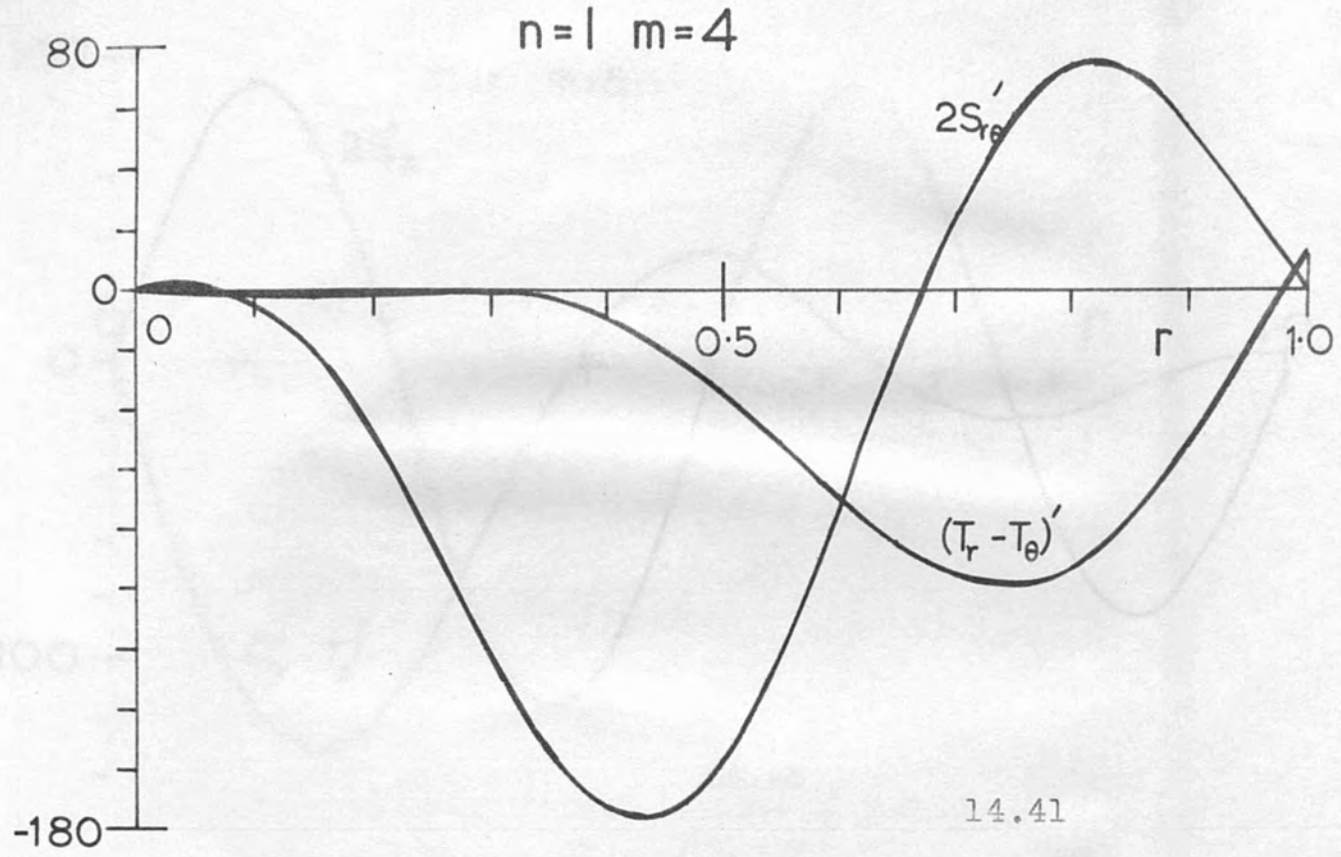
n=1 m=4
80
0
-180
0
0·5
1·0
r
$2S'_{r\theta}$
$(T_r - T_\theta)'$

14.41

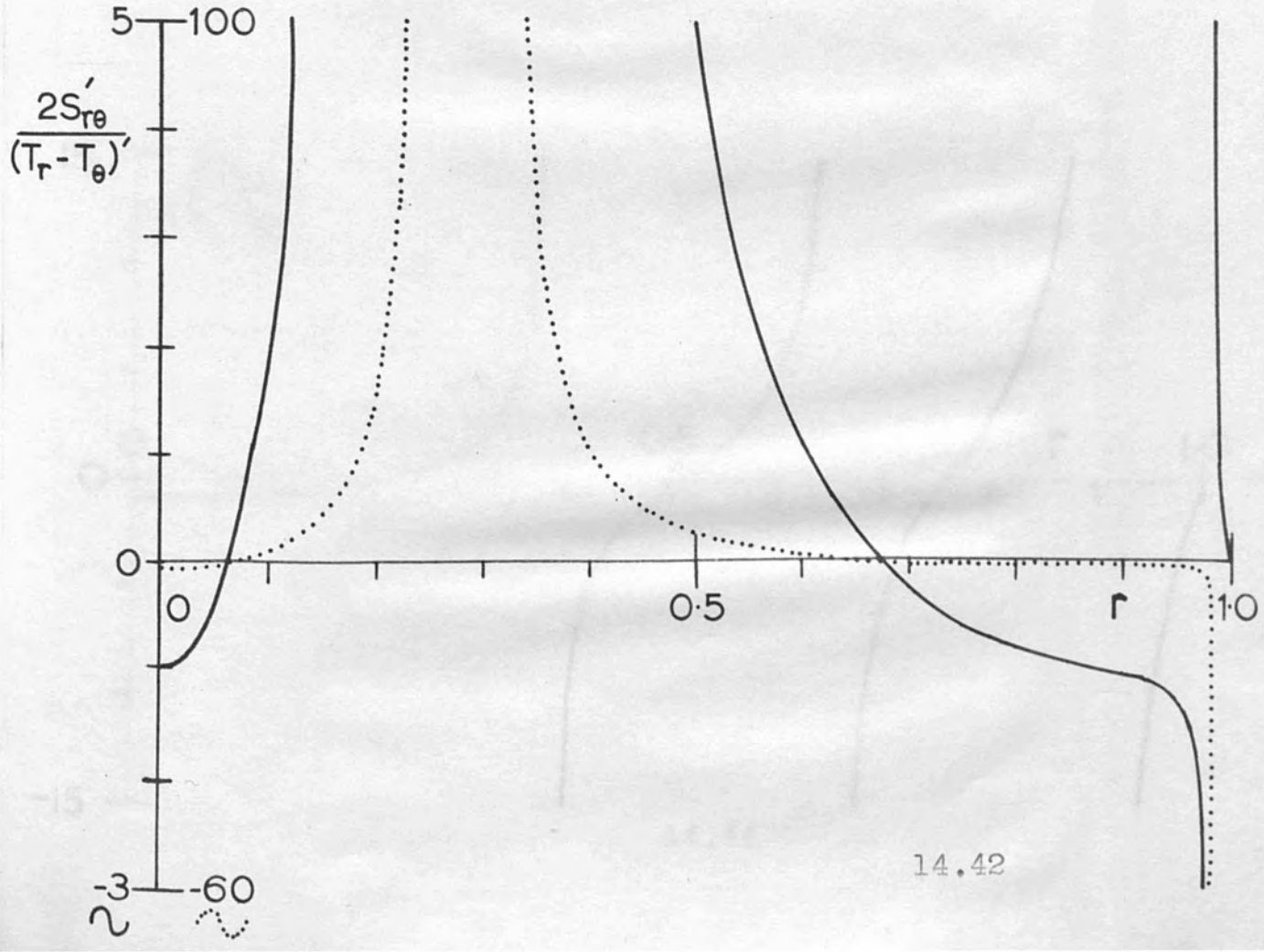
5
100
$\frac{2S'_{r\theta}}{(T_r - T_\theta)'}$
0
-3
-60
0
0·5
1·0
r

14.42

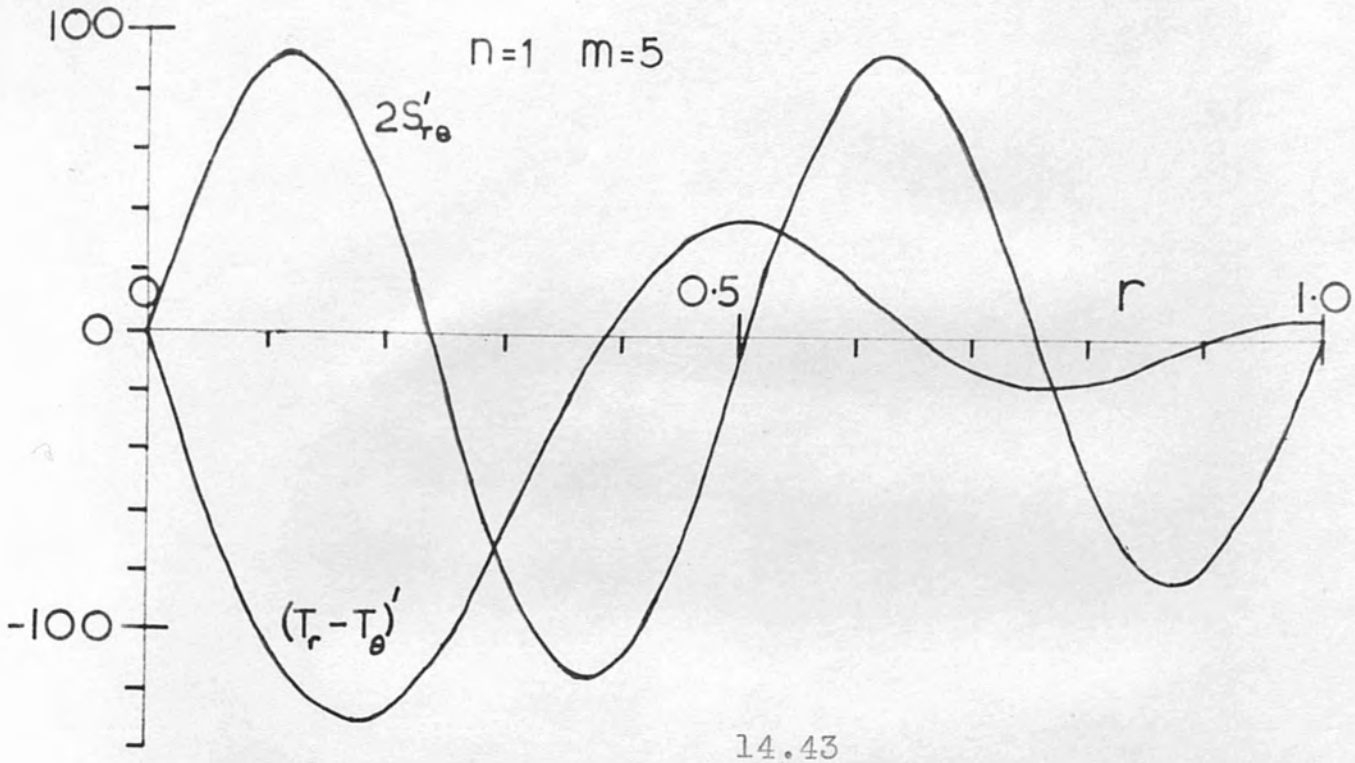
100
0
-100
n=1 m=5
$2S'_{r\theta}$
$(T_r - T_\theta)'$
0·5
r
1·0

14.43

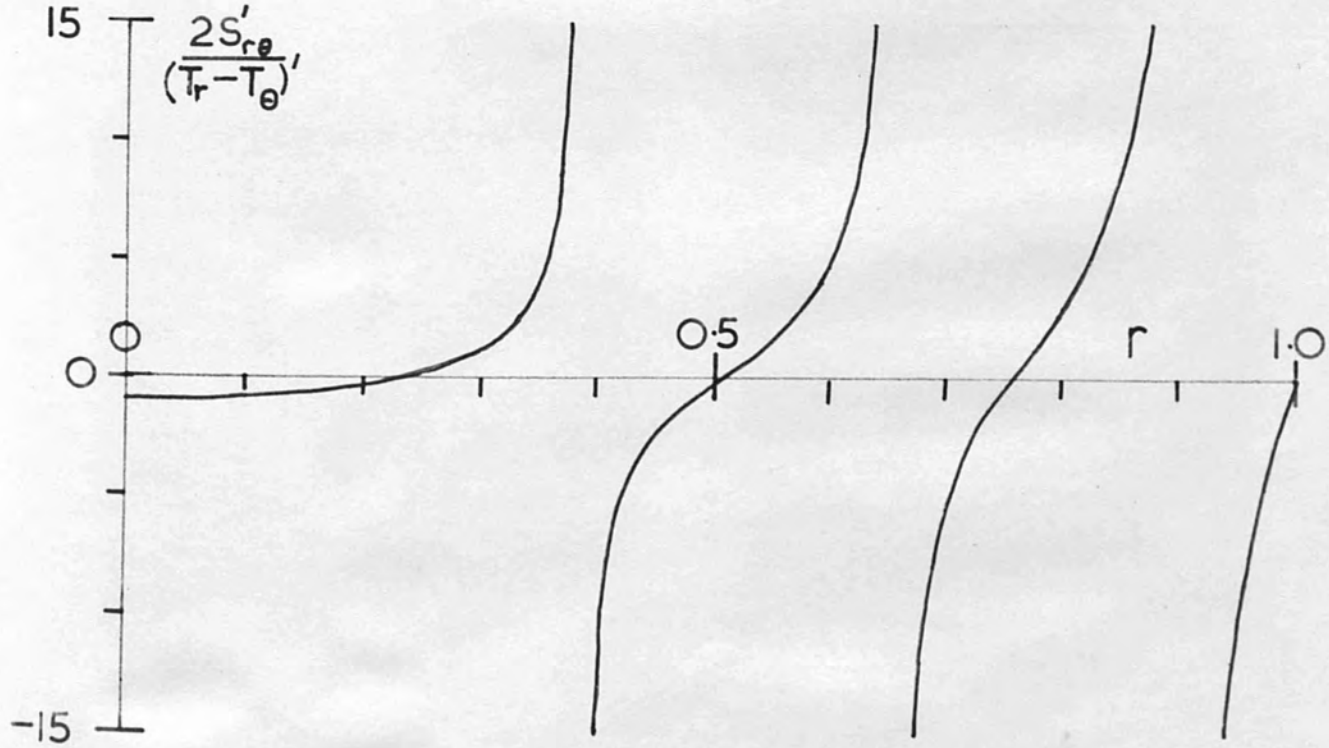
15
0
-15
$\frac{2S'_{r\theta}}{(T_r - T_\theta)'}$
0·5
r
1·0

14.44

Figs 14.45-48

(overleaf)

n = 1 m = 4

ψ = 0°

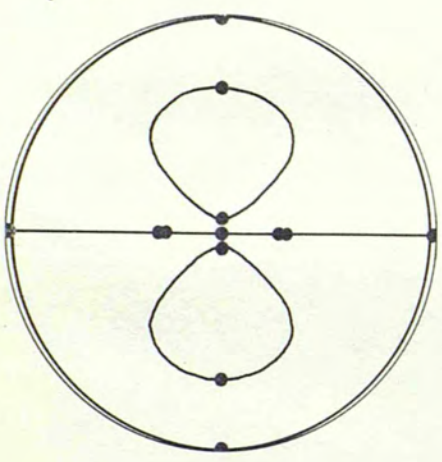

14.45

ψ = 20°

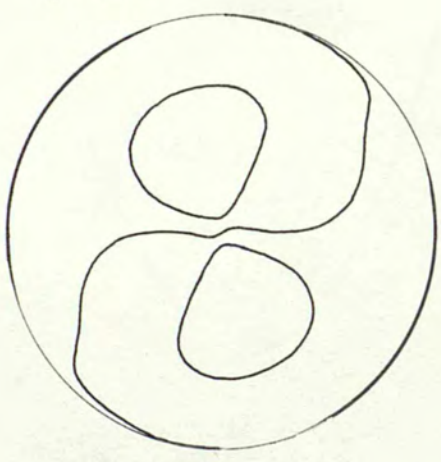

14.46

ψ = 35°

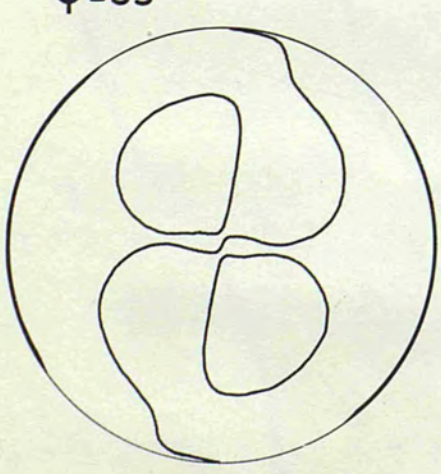

14.47

ψ = 45°

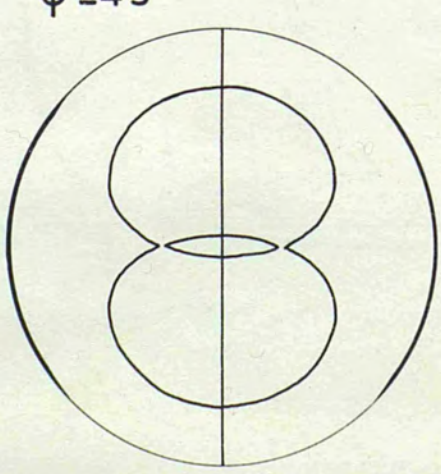

14.48

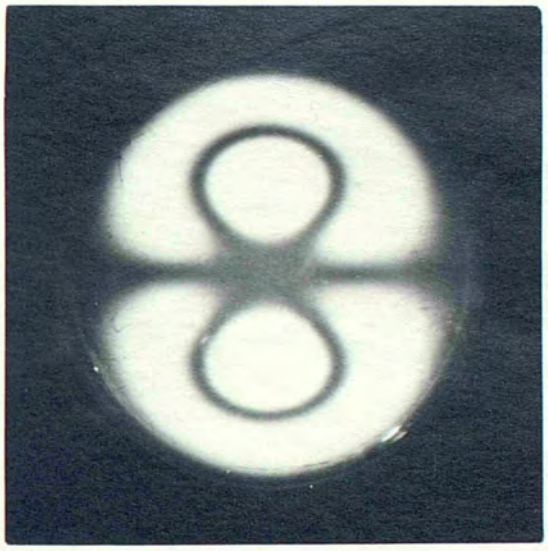

14.49

14.50

14.51

14.52

n=1 m=5

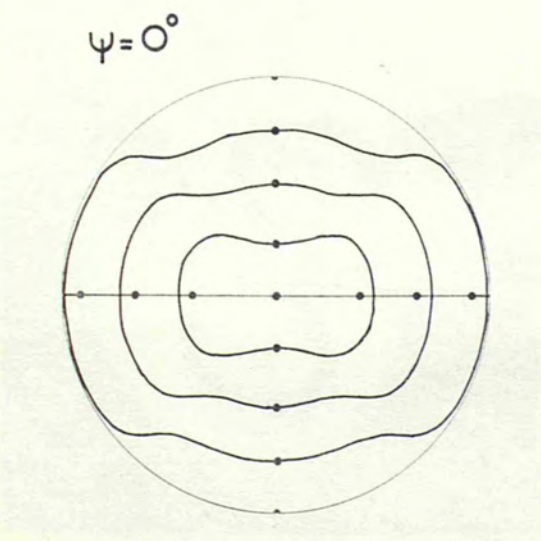

14.53

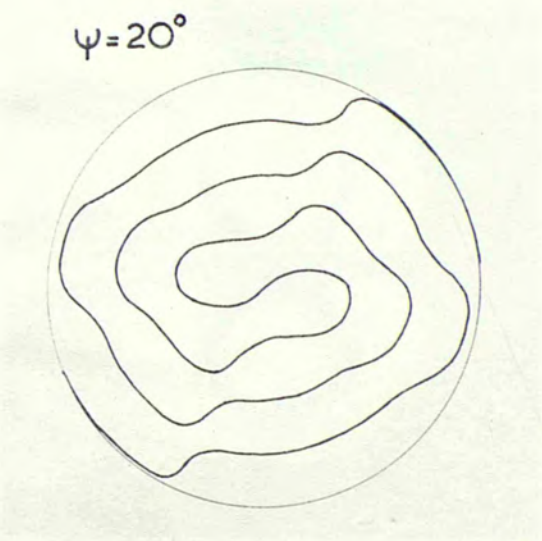

14.54

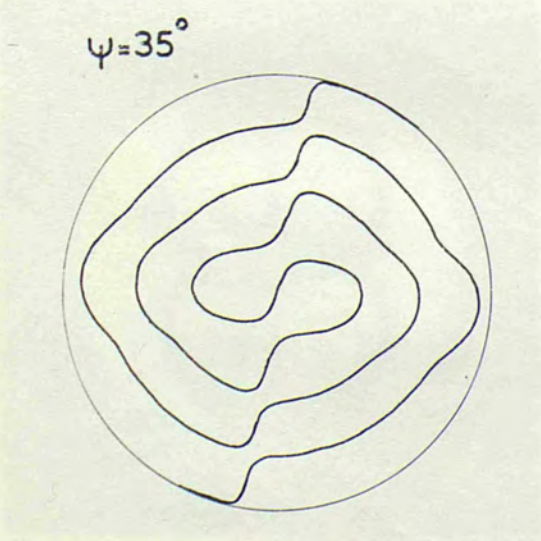

14.55

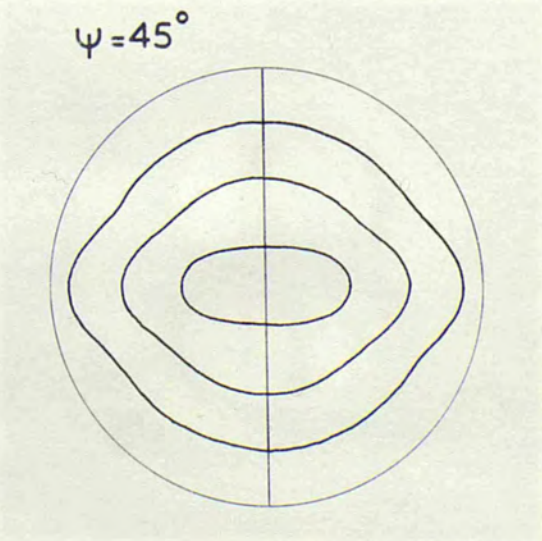

14.56

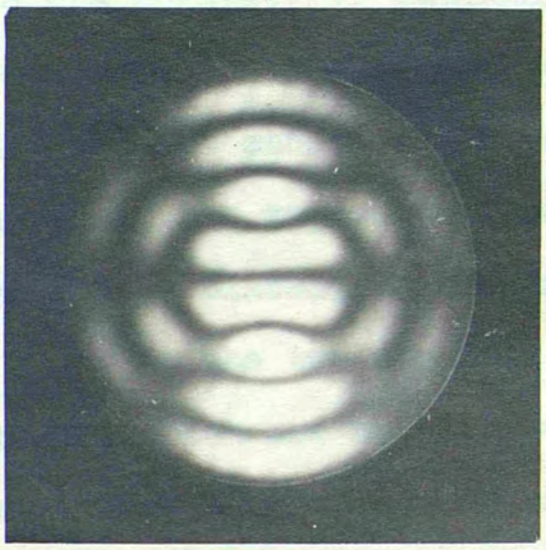

14.57

14.58

14.59

for the two modes. No precise measurement of the parameter Ψ was made and the photographs are arranged to correspond to the theoretical isoclinics which they most nearly represent. The m = 4 mode was examined using a 0.85 mm crystal and all the others shown after this were examined for a 1.0 mm crystal; the exposures were often as long as an hour, even with fast plates, as the intensities were so low.

At the two possible frequencies of vibration for these modes, which are not allowed for by the theory but have been mentioned in Chapters 12 and 13, the isoclinics for any value of Ψ were identical in form but turned through 90° relative to their previous positions. This implies that the whole vibratory system with its attendant stresses and strains turns through 90° also. Rayleigh (1894) has shown that if an isotropic disc vibrates in a mode having n-fold symmetry about its axis, then if the disc is perfect there is nothing to fix the orientation of the vibratory system; if, however, there is some imperfection which defines a singular direction in the disc, then there are two stable orientations of the vibratory system relative to this direction differing by $\pi/2n$. This is in accordance with the present observations, except that since the trigonal symmetry of the quartz probably provides the necessary 'imperfection' it

might be argued that there are three singular directions and hence six stable orientations; however, the influence of the single pair of exciting electrodes probably fixes one of the three possible directions in this case.

The isotropic points seen by circularly polarized light seemed to agree with the configurations shown in Figs 14.45 and 14.53. They were usually very diffuse, however, since their visibility depends on the rate of change of the principal stress difference in their neighbourhood and this is often small over a considerable region; moreover, their distribution is often very erratic, as seen from Fig 14.45, and it is impossible to resolve them when they are very close together. For these reasons they add very little information to that yielded by the isoclinic patterns and their separate photography was not undertaken.

Although the isoclinics for other n = 1 modes were not calculated, an experimental test showed that, of the first 8 modes, most were similar to the m = 5 mode and the others to m = 4. No theoretical reason for the difference between these modes can be given; it is dependent on the random nature of the values of A/B and a different value of Poisson's ratio could alter the type of pattern appropriate to a given order of m.

c) $n = 2$ modes. The values of $(T_r - T_\theta)'$, $S'_{r\theta}$ and their ratio were calculated as before and are shown in Figs 14.60-63, for the $m = 1$ and $m = 5$ modes. The isoclinics have tetragonal symmetry about the axis of the disc and planes of symmetry at $\theta = (\psi/2 + \pi/8)$ and $(\psi/2 + 3\pi/8)$. For values of ψ between 45° and 90° the patterns are the same as those for ψ between 45° and 0° reflected in the plane $\theta = 45°$.

The isoclinics are rather more complicated than for $n = 1$ and in some regions alter rapidly for very small changes in ψ. For this reason a large number has to be calculated to give an overall picture of the stress directions. Since, however, the polarized light system is insensitive to changes of a degree or two in the stress directions, it is impossible to show these subtle changes in the isoclinic pattern experimentally. Regions where the stress directions differ only slightly from the isoclinic direction appear uniformly dark.

Figs 14.64-76 and 14.77-89 show the theoretical and experimental isoclinics for $m = 1$ and $m = 5$. The isotropic points are shown on the calculated 0° isoclinic. These modes were much more easily excited than the $n = 1$ modes. As in the case of $n = 1$ modes there were two orientations for

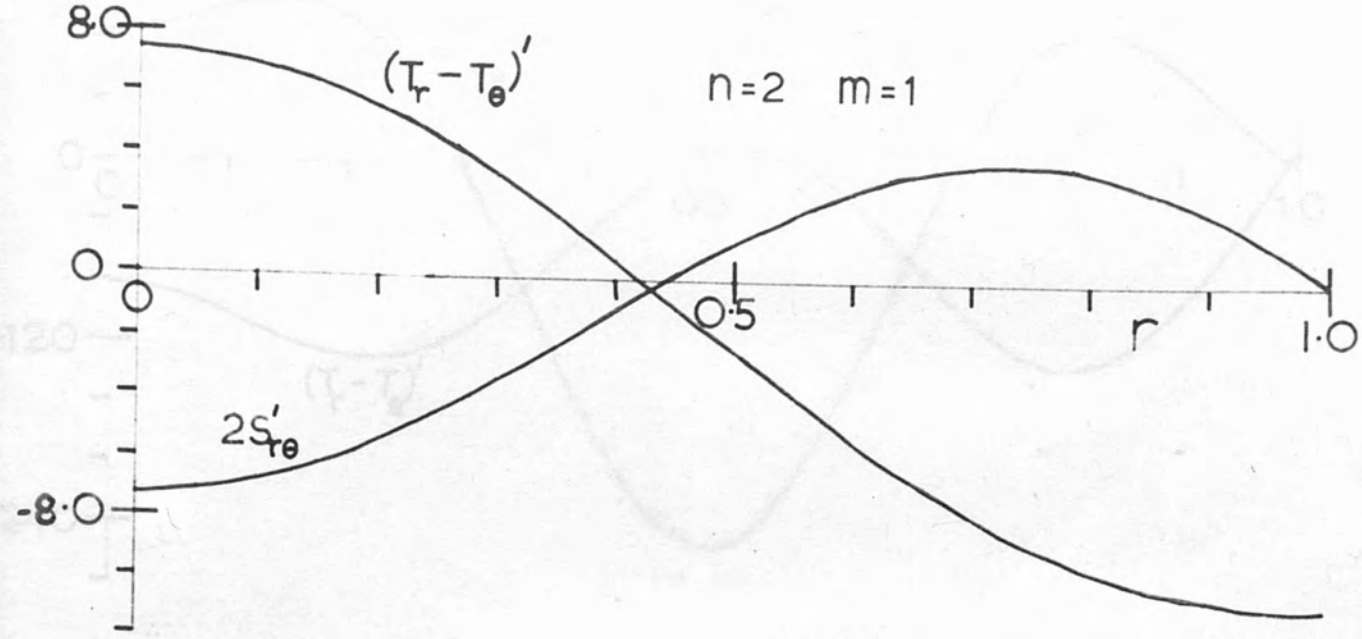
8·0
$(T_r - T_\theta)'$
n=2 m=1
0
0
0·5
r
1·0
$2S'_{r\theta}$
-8·0

14.60

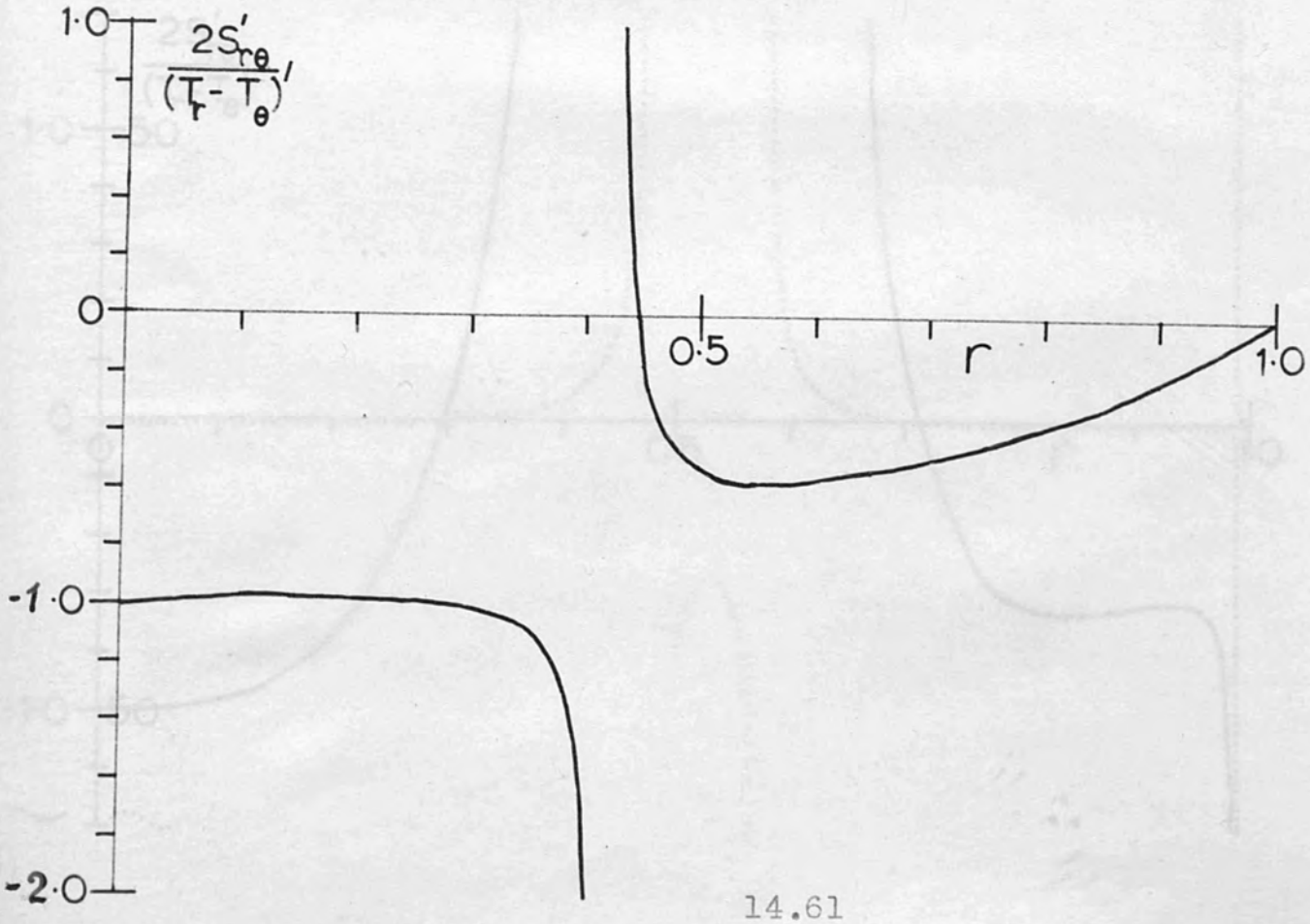
1·0
$\frac{2S'_{r\theta}}{(T_r - T_\theta)'}$
0
0·5
r
1·0
-1·0
-2·0

14.61

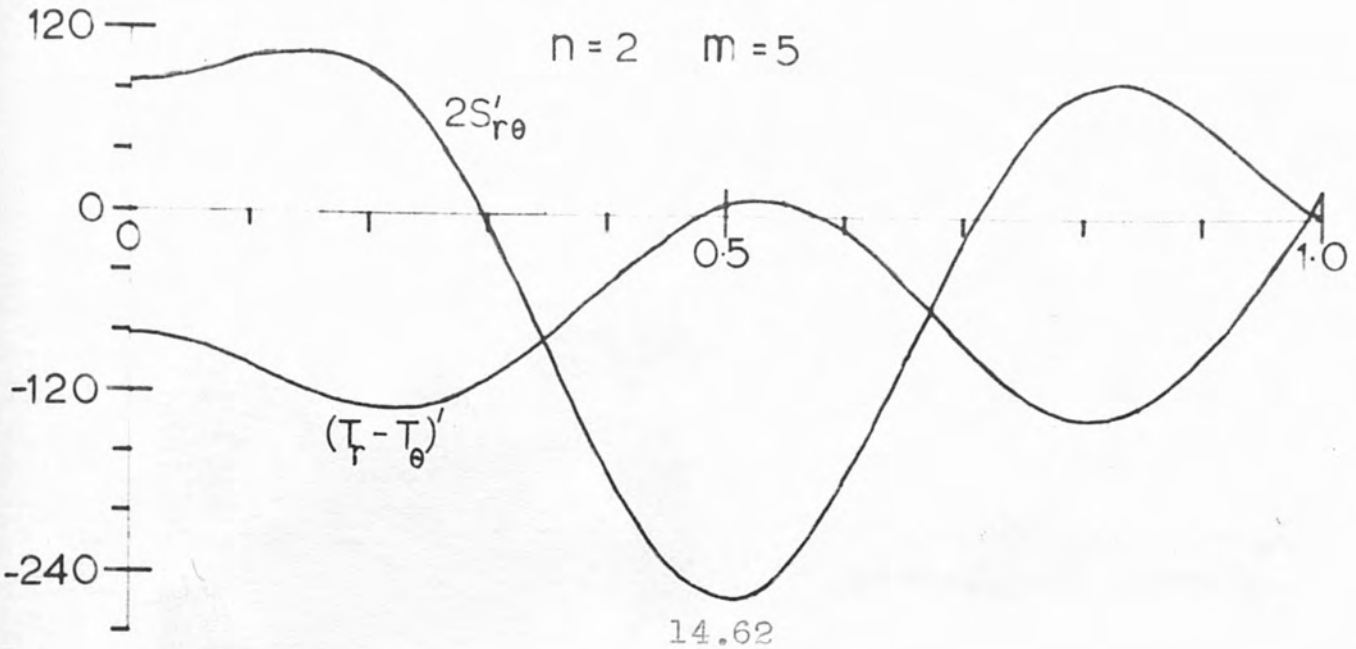
120
0
-120
-240
n = 2 m = 5
$2S'_{r\theta}$
$(T_r - T_\theta)'$
0
0·5
1·0

14.62

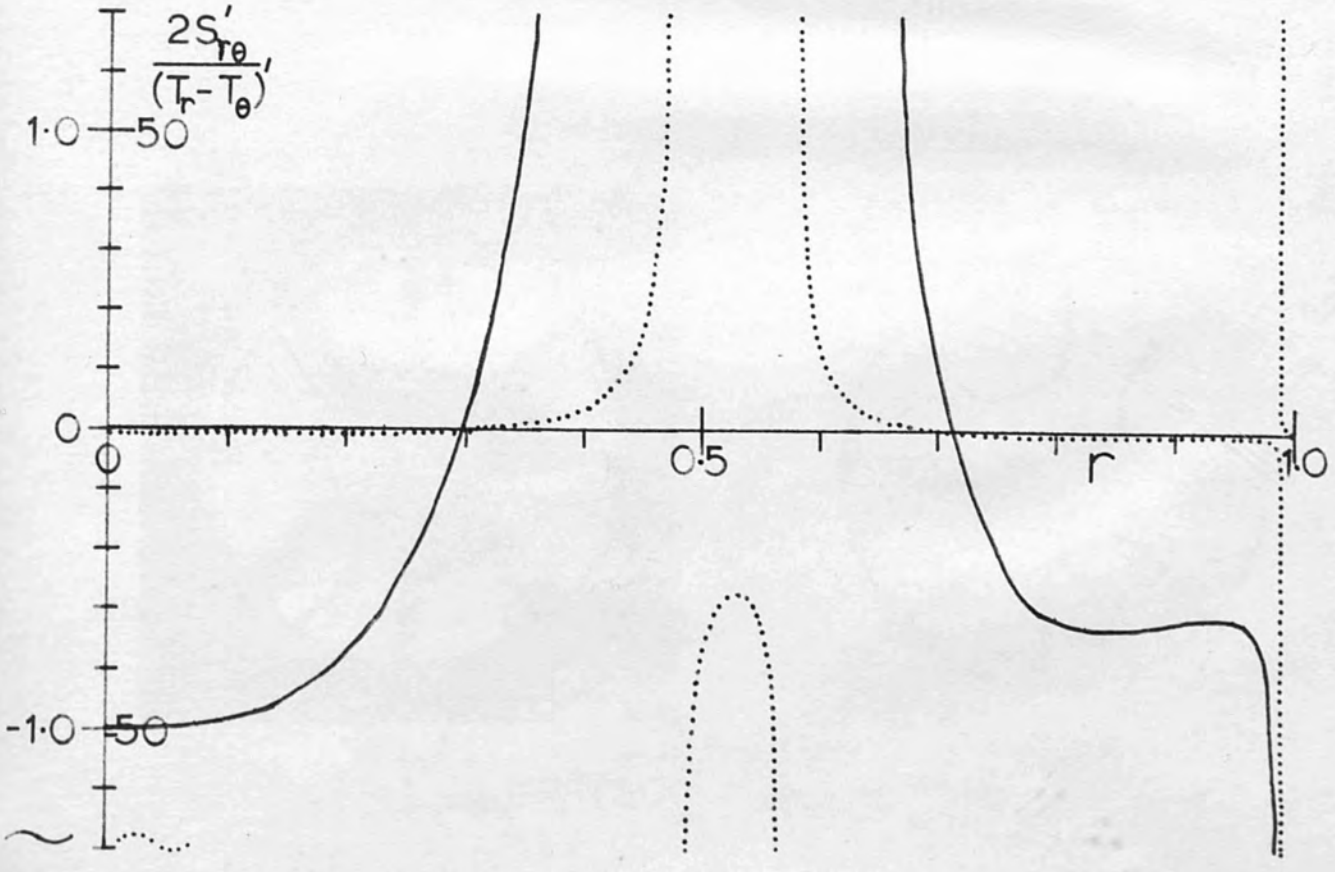
$\frac{2S'_{r\theta}}{(T_r - T_\theta)'}$
1·0
50
0
-1·0
-50
0
0·5
r
1·0

14.63

Figs 14.64-67

(overleaf)

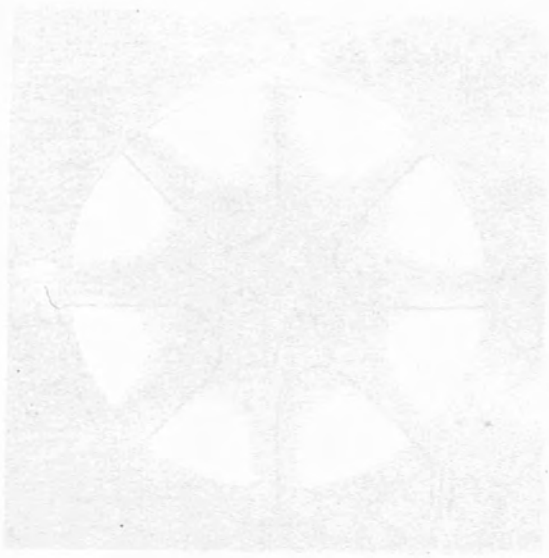

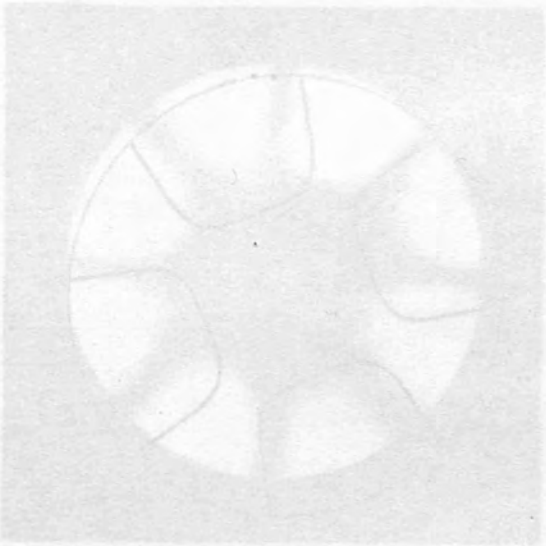

n=2 m=1

$\psi = 0°$

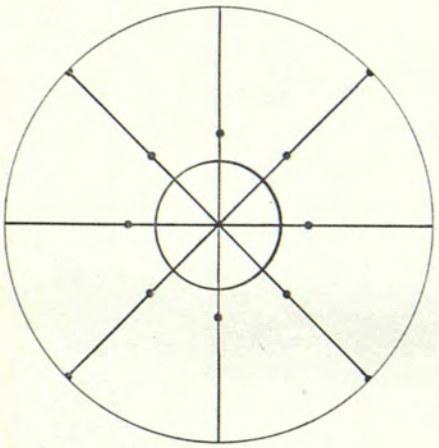

14.64

$\psi = 0°20'$

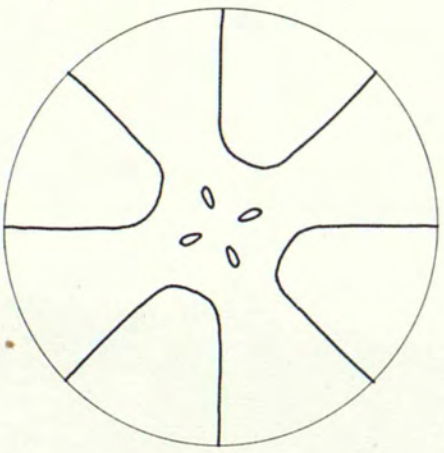

14.65

$\psi = 2°30'$

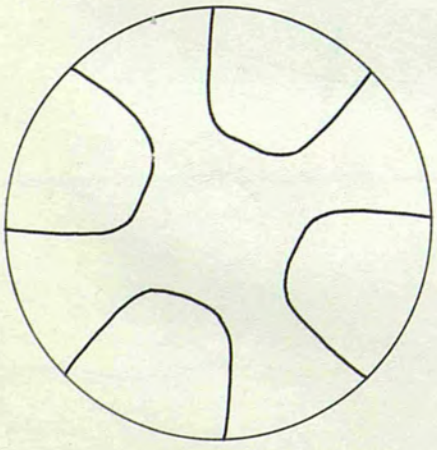

14.66

$\psi = 5°$

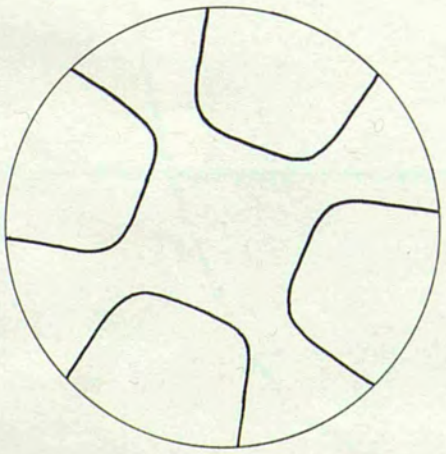

14.67

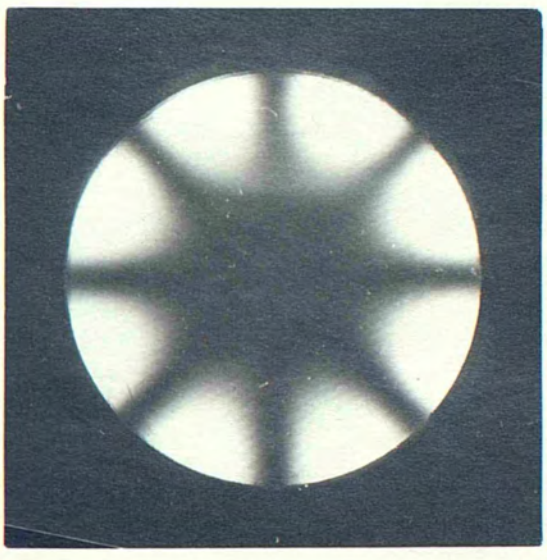

14.68

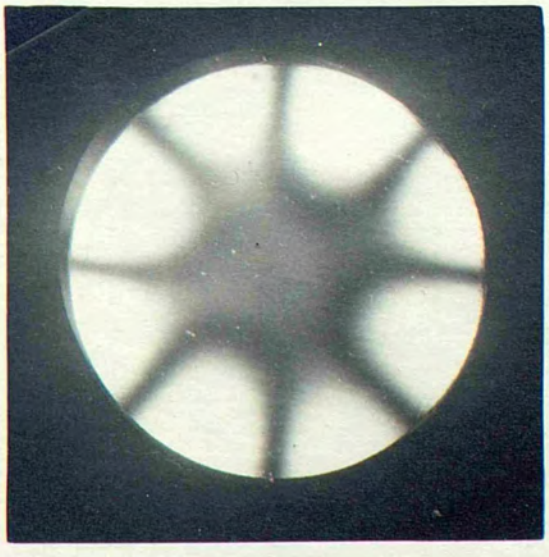

14.69

Figs 14.70-73

(overleaf)

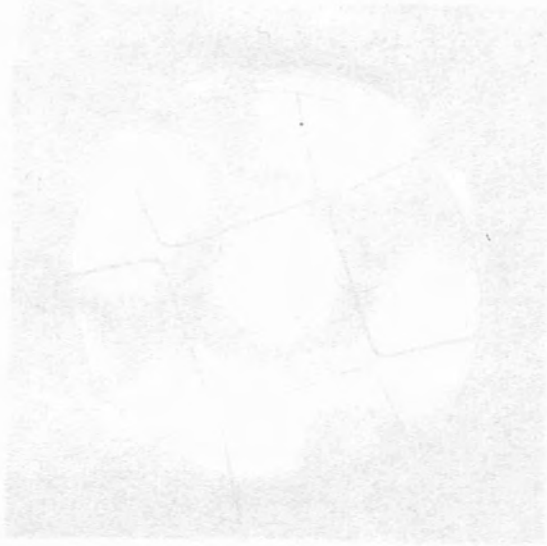

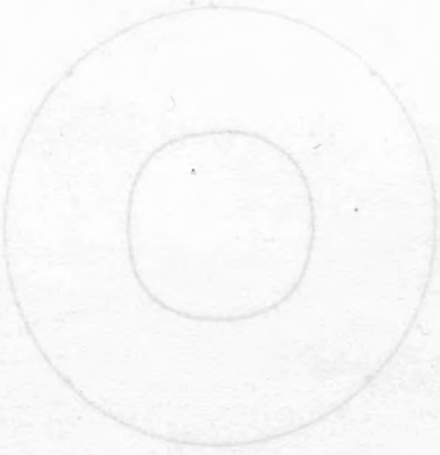

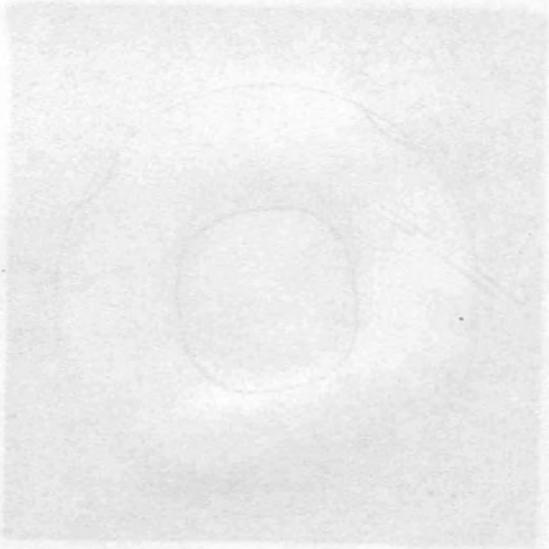

n=2 m=1

$\psi = 7°30'$

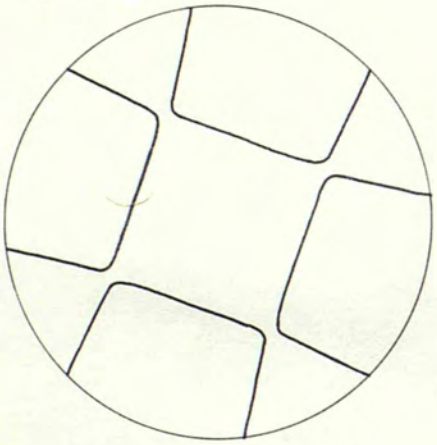

14.70

$\psi = 10°$

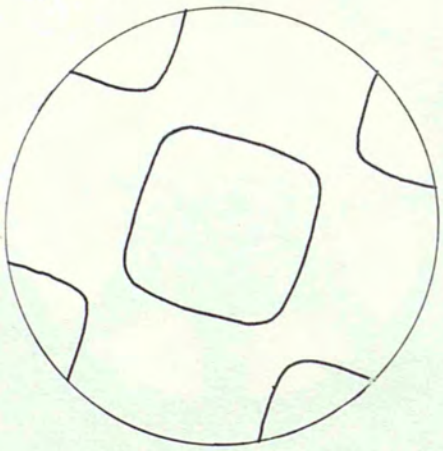

14.71

$\psi = 25°$

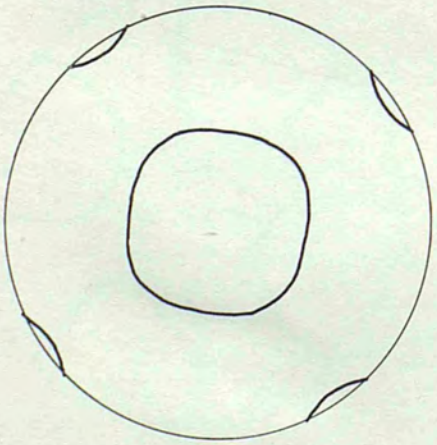

14.72

$\psi = 45°$

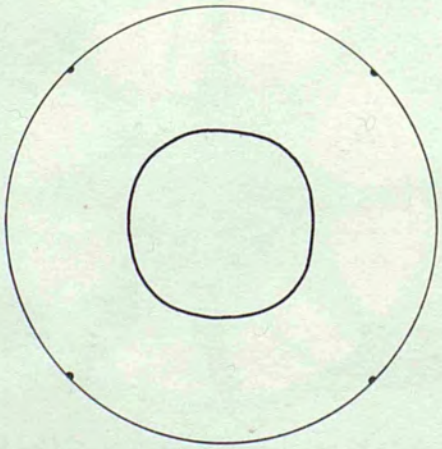

14.73

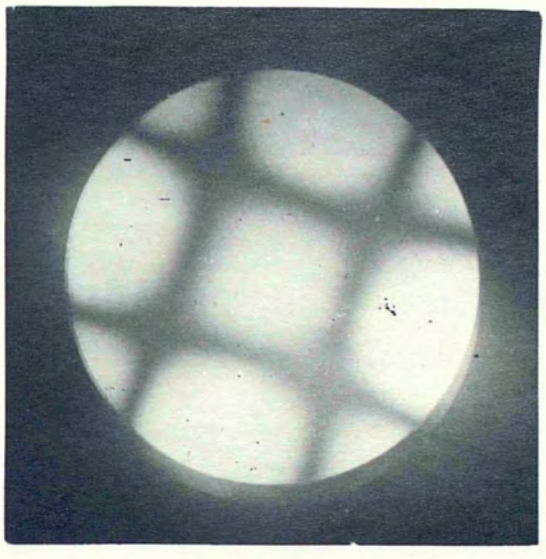

14.74

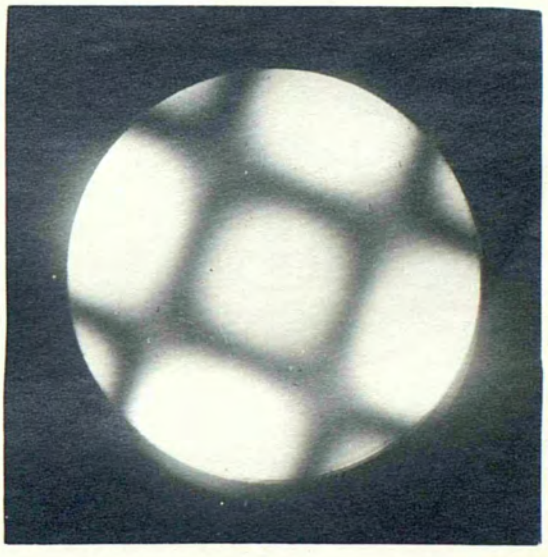

14.75

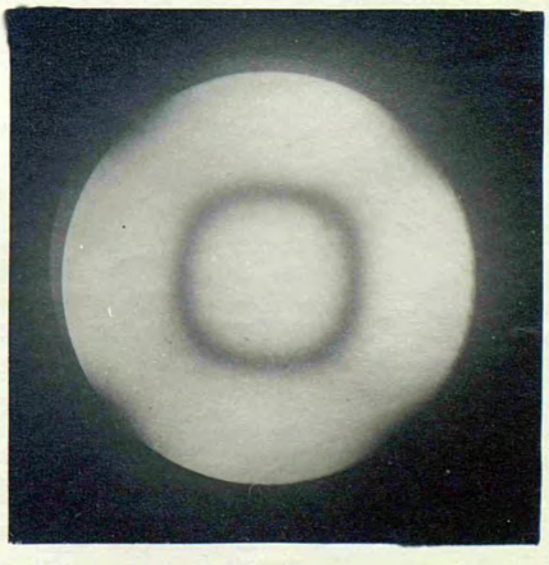

14.76

Figs 14.77-80

(overleaf)

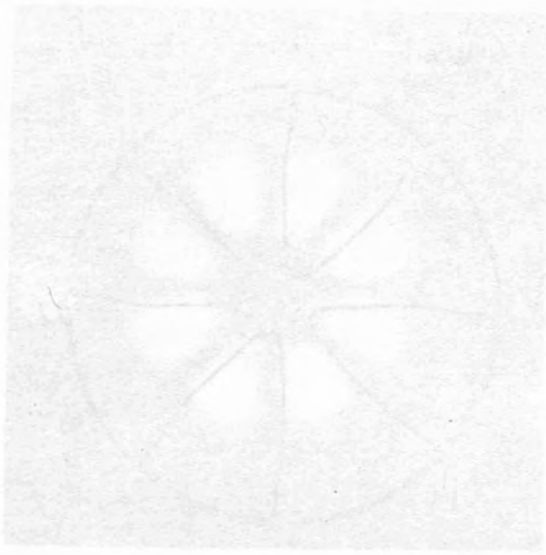

n = 2 m = 5

$\psi = 0°$

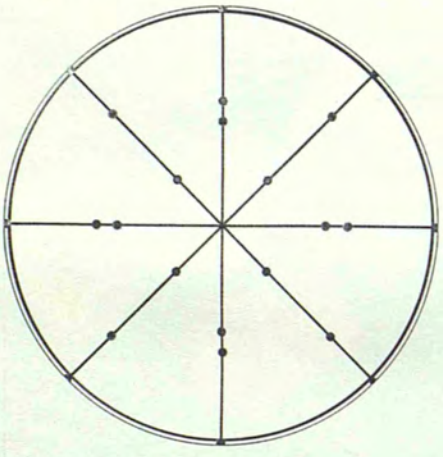

14.77

$\psi = 1°$

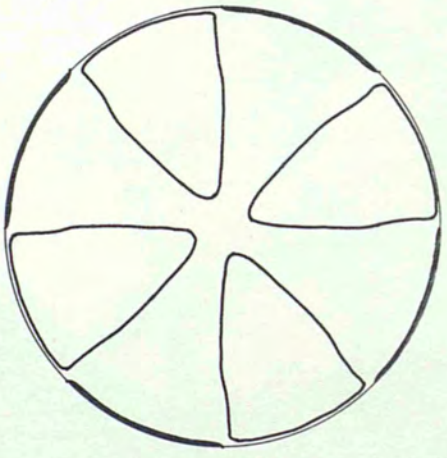

14.78

$\psi = 5°$

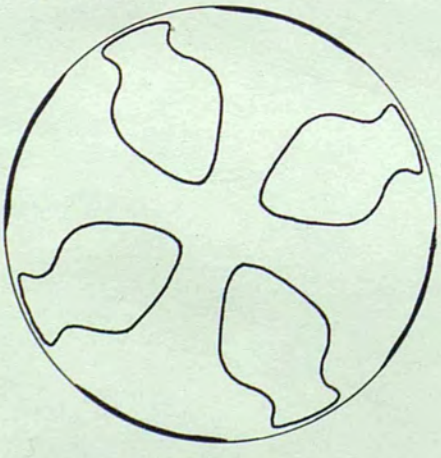

14.79

$\psi = 6°$

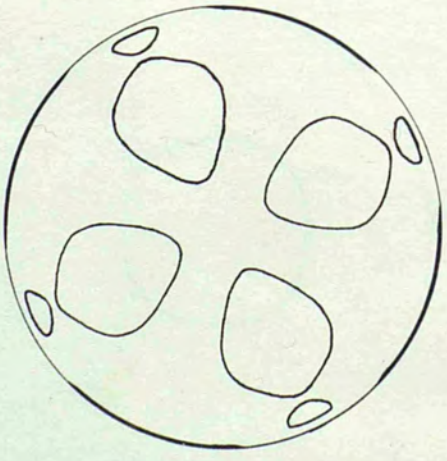

14.80

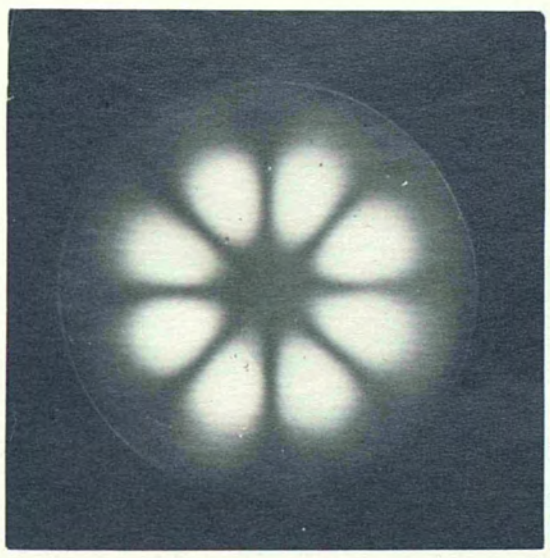

14.81

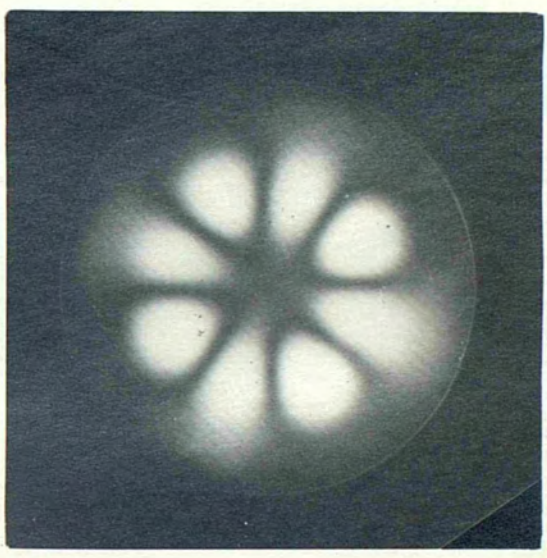

14.82

Figs 14.83-86

(overleaf)

n=2 m=5

$\psi = 10^\circ$

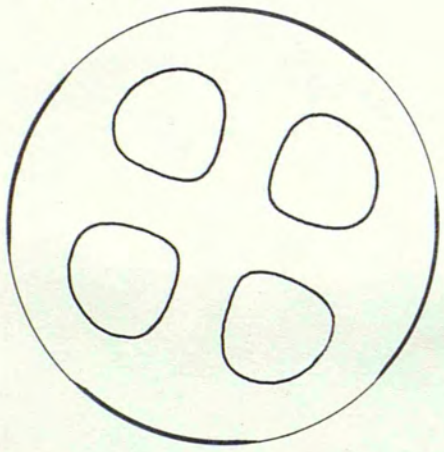

14.83

$\psi = 25^\circ$

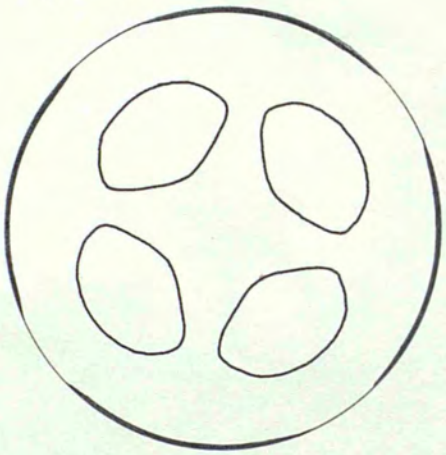

14.84

$\psi = 35^\circ$

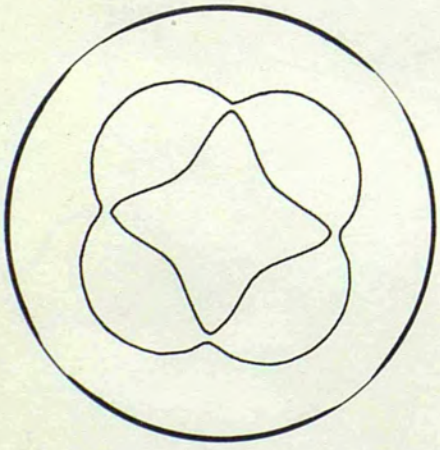

14.85

$\psi = 45^\circ$

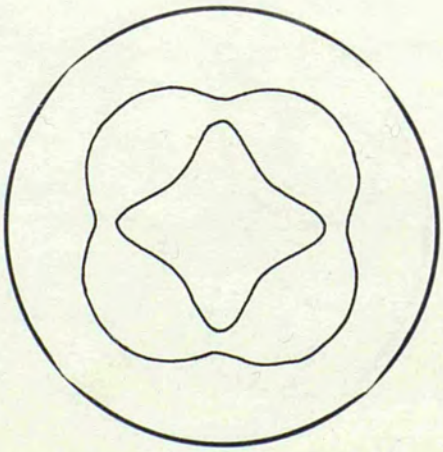

14.86

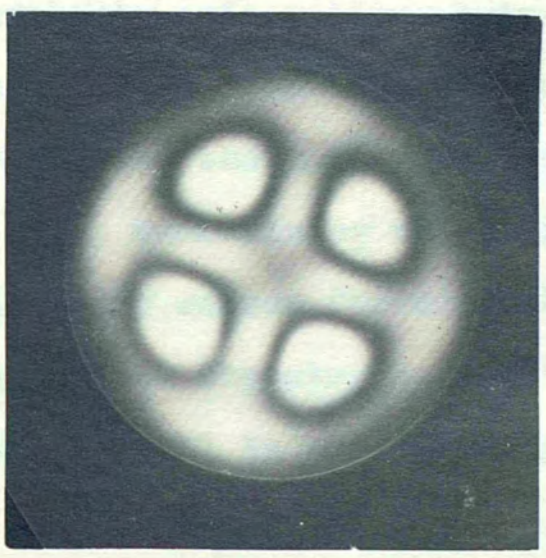

14.87

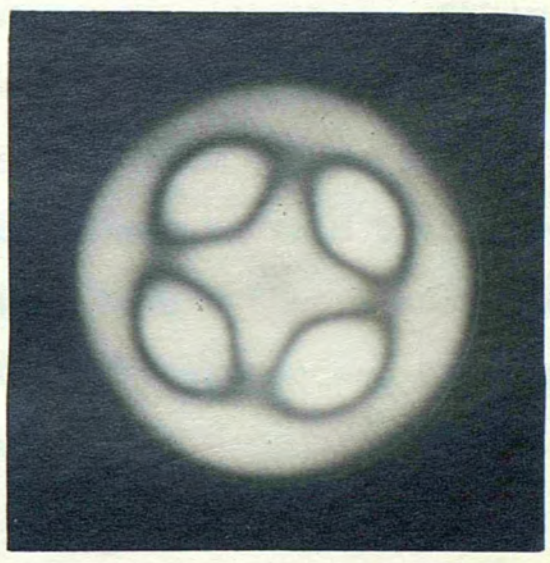

14.88

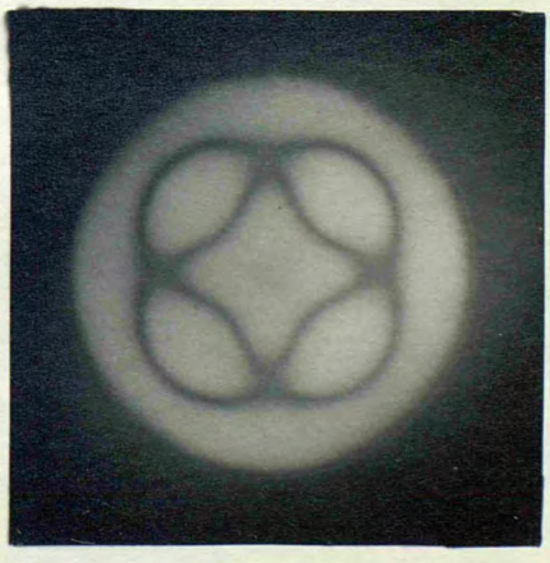

14.89

each mode, this time differing by 45°. These were not quite so definite as previously, however, and there seemed to be unstable orientations between these two extremes. Other $n = 2$ modes were also examined and, of the first 9, most were like the $m = 1$ mode and the rest like the $m = 5$ mode.

Summarizing this chapter, it may be said that there is every reason for supposing that Love's theory adequately describes the stress distribution of these modes, provided the crystal is sufficiently thin.

CHAPTER 15

OBSERVATIONS BY INTERNAL INTERFERENCE

For the reasons mentioned in Chapter 6, the work described in this chapter is necessarily of an empirical nature. The effects due to the magnitude of the sum of the principal stresses will be regarded as the primary cause of the observed fringe shift and other effects will be regarded as modifying influences. The experimental arrangements have already been fully described in Chapters 9 and 11.

15.1 Symmetrical modes (n = 0)

a) Type A. Here the nodal system is that summarized in Table 13.1; the radii given there are those at which the sum of the principal stresses, the areal dilatation and the normal displacement all vanish. Now any fringe splitting effects are due to the difference between the principal stresses, and the radii at which this is zero have been given in Table 14.1. Since the roots of $J_o(kr)$, apart from the first, are near to those of $J_2(kr)$, it follows that the nodes, apart from the first, should be fairly clearly defined.

Figs 15.1-4 show the first four modes of the specially worked 2.0 mm crystal. There is, in fact, very little evidence of any fringe splitting, even for the first

15.1

15.2

15.3

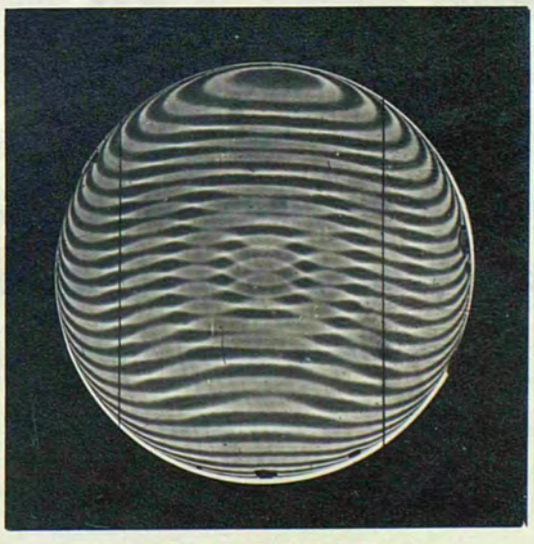

15.4

node, or indeed anywhere on the whole surface. The nodal radii agree well with the expected values.

It was hoped to compare the fringe displacement observed by simple interference with that due to internal interference. This did not prove worthwhile, however, as the former fringe displacement is extremely small compared with the latter. Fig 15.5 shows the two types of interference simultaneously for the A.1 mode. This was achieved by resting the doubly coated crystal on a similarly coated reference flat. It is seen that for a substantial displacement of the internal interference fringes, the displacement of the simple interference fringes is negligible.

This result is in agreement with a subsequent calculation based on Pockels' values for the stress-optic coefficients. The change of mean path difference between successively reflected beams, due to the stress-optic effect, was found to be about 2.5 times that due to the change of thickness of the crystal. Since these effects are additive and the change of optical thickness of the crystal is about 3 times the displacement of either surface relative to the median plane, it follows that the displacement of the internal interference fringes is more than 10 times as great as that of the simple interference fringes over the same

Fig 15.5

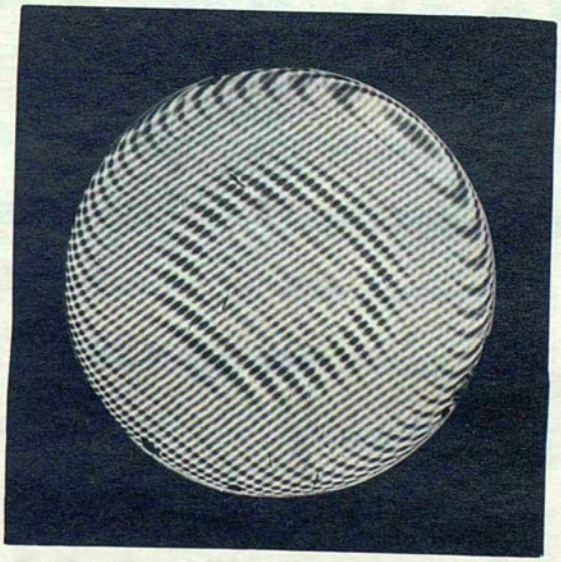

region. Moreover it has been calculated that if the quartz were devoid of rotatory power, the distance between the two components of a split fringe due to a given principal stress difference would be less than one third of the bodily displacement of the fringe due to a principal stress sum of the same magnitude.

b) Type B. Here $(P+Q)=0$, so the movement of the fringes is entirely due to the birefringent effect. The fringe splitting is thus symmetrical about the rest position and the fringes should be completely undisturbed where $(P-Q)=0$. This occurs in the isotropic regions and the nodes are thus found from the roots of $J_2(k_1 r)$ and coincide with the zero order stress fringes. The radii are those shown in Table 14.2.

Figs 15.6-9 show the experimental patterns for the B.0 - 3 modes of the 2.0 mm crystal. The observed nodal radii agree well with the theory. There is, however, some evidence of fringe doubling, showing that the fringe splitting is not quite symmetrical and implying that $(P+Q)$ is not zero. This is particularly noticeable for the B.1 mode. It will be remembered that the surface displacement for this mode (Fig 13.23) showed a much more distorted pattern than the other type B modes.

15.6

15.7

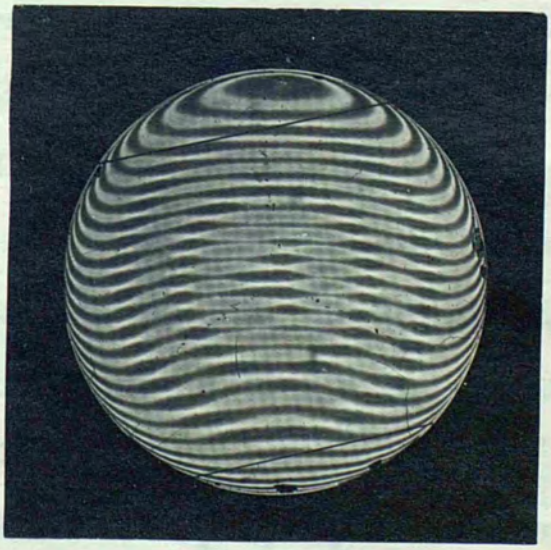

15.8

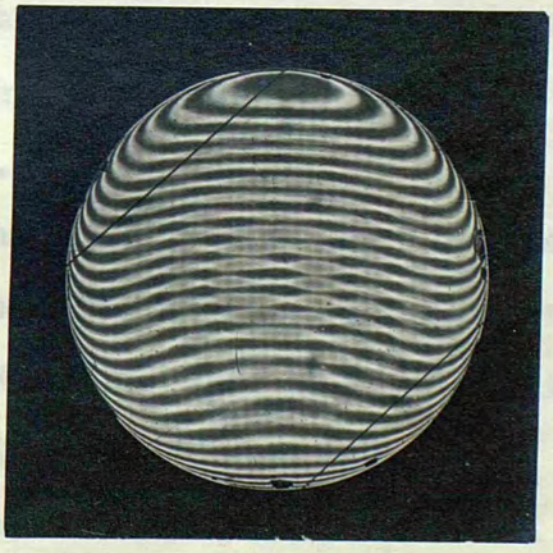

15.9

The general appearance of the oscillating fringe envelopes for these modes is little different from that of simple interference fringe envelopes. This is surprising in view of the fact that the birefringence present in the crystal when vibrating with the amplitude shown in the photographs must have caused a considerable change in the apparent rotatory power of the quartz.

15.2 Type C modes

a) n = 1 modes. The nodes of (P+Q) consist of a single diameter and a number of circles whose radii have been given in Table 13.2. Figs 15.10-12 show the observed patterns for the 2.0 mm crystal. These were the only modes strong enough to show any noticeable fringe displacement. The values of m are 0, 1 and 4, respectively. The nodal radius for m = 4 agrees well with theory. Fringe splitting is very slight for this mode but is comparable with the displacement for the m = 1 mode.

b) n = 2 modes. Here there are two diametral nodes and various circular nodes, the radii having already been given in Table 13.3. These modes were more readily excited than the n = 1 modes. Figs 15.13-17 show the modes for which m = 0, 2, 3, 5 and 7 respectively. The nodal radii fit the theoretical values very well. The amount of fringe

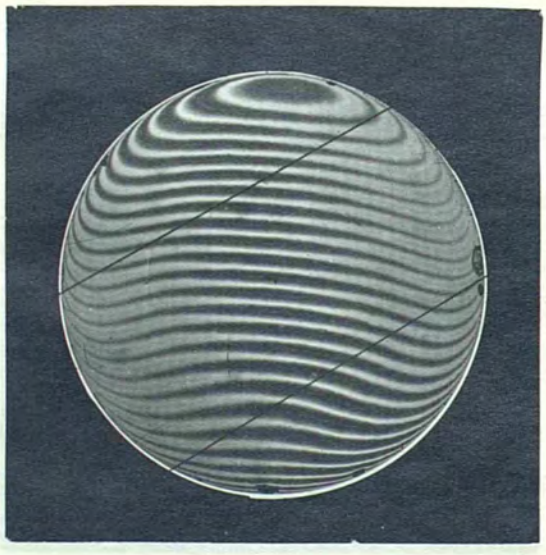

15.10

15.11

15.12

15.13

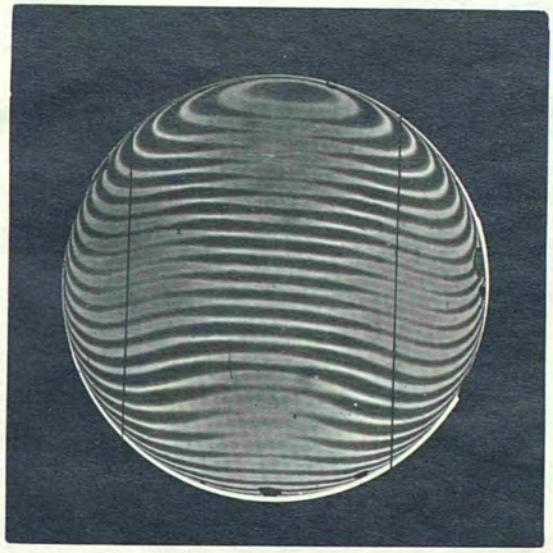

15.14

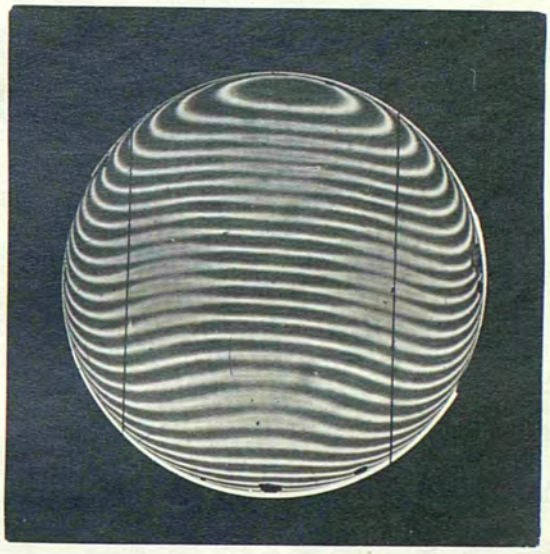

15.15

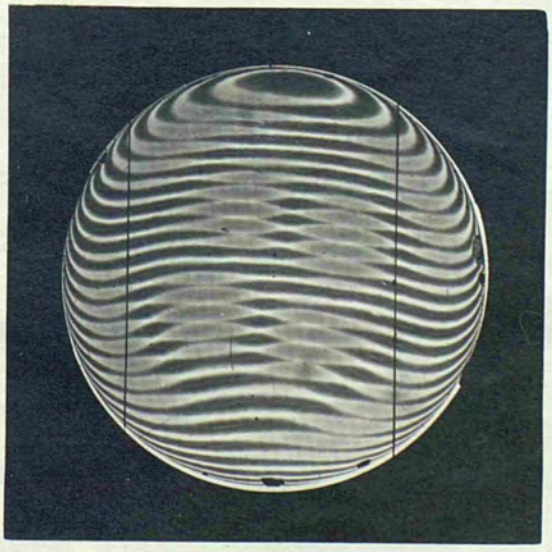

15.16

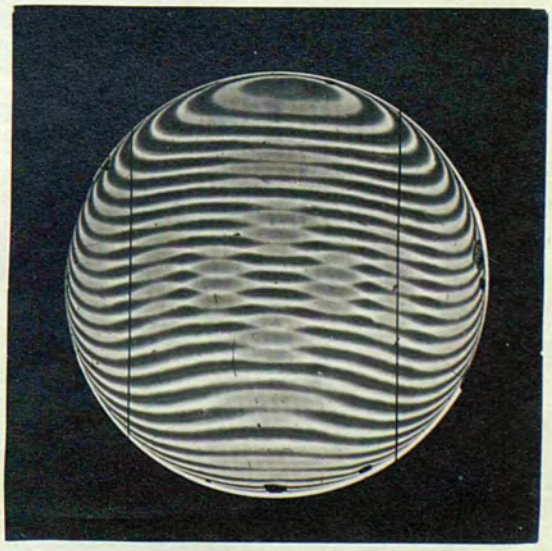

15.17

splitting varies from mode to mode, but a precise analysis of the behaviour of multiple-beam fringes under these conditions is required before the magnitude of the fringe splitting may be interpreted quantitatively.

CHAPTER 16

CALCULATION OF THE LONGITUDINAL DISPLACEMENT AND LYCOPODIUM POWDER PATTERNS

16.1 Symmetrical modes (n = 0)

a) Type A. Here the tangential displacement is everywhere zero. The radial displacement, as given by eqn 5.14 is:

16.1 $$U = A' J_1(kr)$$

Fig 16.1(a) shows the variation of the radial displacements with r for the first four modes. The nodes are a series of circles, their radii being given in Table 16.1 as fractions of the disc radius.

For this type of vibration the normal displacement is entirely due to the Poisson contraction; it follows, from the reasoning of Chapter 8, that all of the nodes of longitudinal displacement should be indicated by the lycopodium powder and none of the nodes of normal displacement.

Figs 16.2-5 show the lycopodium patterns on a 2.0 mm crystal for the m = 0 - 3 modes. The patterns are very little like the theoretical ones. As thinner crystals gave still more complex patterns than those shown, only the experiments with this crystal will be described, in order that the interpretation may not be too involved. The patterns on the

Figs 16.1(a)-(b)

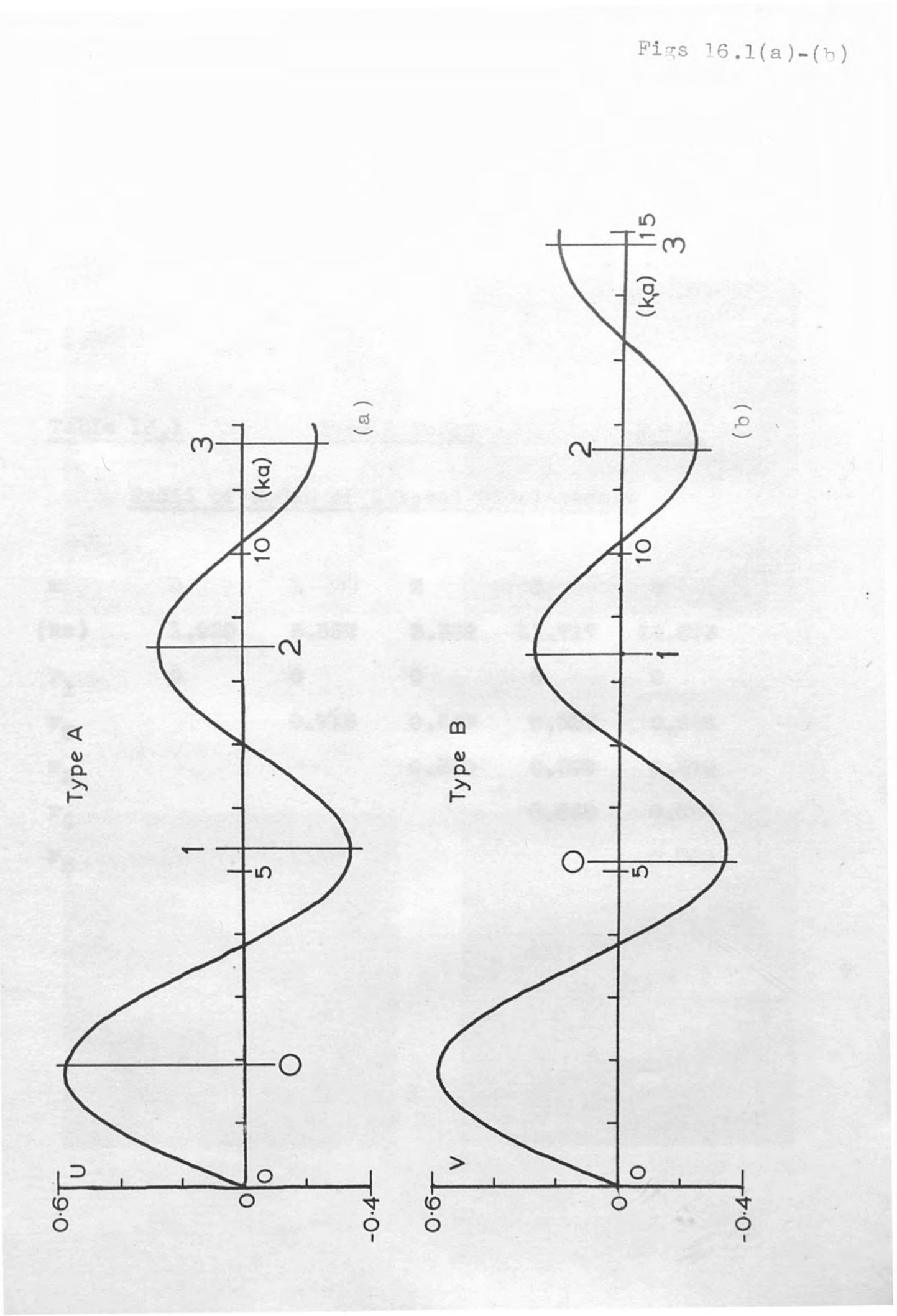

Table 16.1 Type A Modes V = 0

Radii of Nodes of Lateral Displacement

m	0	1	2	3	4
(ka)	1.939	5.362	8.552	11.717	14.873
r_1	0	0	0	0	0
r_2		0.715	0.448	0.327	0.258
r_3			0.820	0.599	0.472
r_4				0.868	0.684
r_5					0.890

A modes, side 1

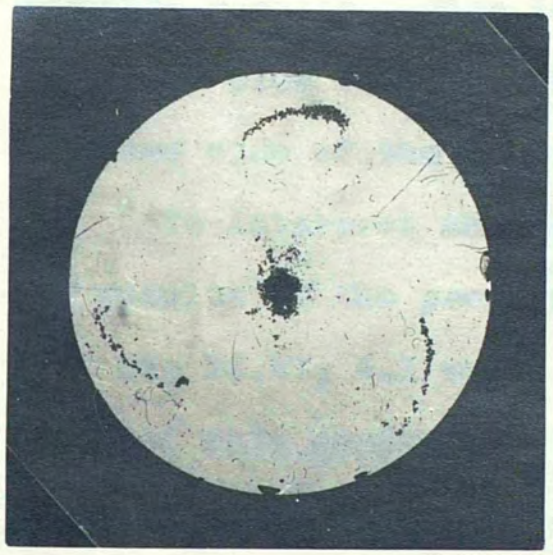

16.2

16.3

16.4

16.5

reverse side are complementary, and when the two patterns for a given mode are superposed a figure with six-fold symmetry results. Figs 16.6 and 16.7 show the patterns on the other side for the A.0 and A.1 modes, as viewed from the same side of the crystal as Figs 16.2 and 16.3.

To interpret the motion, reference will be made to the results of the previous chapters. In Chapter 14 (see Fig 14.27, A.1 mode) it was shown that even in the cause of this comparatively thick crystal the primary stress, namely radial compression, was nearly perfect. In Chapter 13 we saw that the displacements normal to the surface were invariably complicated by what were assumed to be flexural modes. In the interference patterns shown by the doubly coated crystal, which should not show up the effects of flexural motions, the observed patterns were very much as expected.

It is assumed from these observations that the theoretical mode of vibration with all its attendant stresses and strains does in fact occur, but that a flexural mode, with its own system of stresses and strains, is superposed. For the A.1 mode, Fig 16.3, which will now be discussed in detail, this flexure has three diametral nodes and two circular ones and accounts satisfactorily for the observed

interferometric pattern.

At the centre, the flexural amplitude must be zero, and the motion of the powder near the centre should be towards the centre, on both sides of the crystal, as in the case of the pure uncoupled motion discussed previously. Using this fact as a starting point, the direction of movement of the powder will be reversed every time a node of either normal or lateral displacement is crossed. Fig 16.8 shows a tracing of the nodes of the normal displacement, as revealed by the interferometric pattern, Fig 13.10, with the theoretical nodes of the longitudinal displacement superposed. Arrows are shown directed toward the centre to indicate the motion of the powder there and all the other arrows have been drawn to conform to the rules given. This diagram explains the presence of all the lines shown up by the lycopodium powder. Of particular interest is the fact that some of the regions where the powder remains undergo large normal displacements. This emphasises the danger of using the lycopodium powder method to indicate nodes without any corroborative evidence, as numerous previous workers have done.

The pattern on the reverse side of the crystal can be explained similarly. It is partly complementary to that on the first side, owing to the complementary nature of the

normal displacements on the two sides, the latter being a fundamental property of a combination of longitudinal and flexural displacements.

b) Type B. Here U is everywhere zero and the longitudinal displacement is tangential, that is:

16.2 $$V = B'J_1(k,r)$$

Fig 16.1(b), after page 122, shows the variation of V with r and Table 16.2 gives the nodal radii for the first four modes.

Since the normal displacement w is everywhere zero, the lycopodium spores will slip for all but the extremely small fraction of the cycle when $|\omega^2 V| \leq \mu g$. The particles will slither about aimlessly but will be at the mercy of air currents and in any case will inevitably find themselves at a node, after a sufficient lapse of time, and remain there. However, this idealized version of the motion is nullified by the presence of the coupled modes.

Figs 16.9-12 show the first four modes of this type. As was the case for type A, many more nodes are shown than predicted by theory. As the longitudinal displacement is parallel to its nodes, these nodes are shown up only faintly, as there is no direct motion of the powder towards them; in fact they are rendered visible mainly by the

Table 16.2 Type B Modes U = 0

Radii of Nodes of Lateral Displacement

m	0	1	2	3	4
(k;a)	5.135	8.417	11.620	14.796	17.960
r_1	0	0	0	0	0
r_2	0.746	0.455	0.330	0.259	0.213
r_3		0.834	0.604	0.474	0.391
r_4			0.875	0.688	0.566
r_5				0.903	0.742
r_6					0.917

B modes, side 1

16.9

16.10

16.11

16.12

discontinuities in the radial nodes. The latter are superfluous to the theory and are assumed to be due to flexural modes as for Type A. This is again supported by the complementary nature of the pattern on the reverse side. Figs 16.13 and 16.14 show the reverse side of the crystal for the B.0 and B.1 modes, as seen from the same side of the crystal as Figs 16.9 and 16.10. In Fig 16.15 the nodes of the lateral displacement for the B.0 mode are superposed on the observed nodes of the normal displacement and arrows are drawn to indicate the motion of the lycopodium powder. This completely explains the observed lycopodium pattern and doubtless all the other patterns may be analysed in the same way.

16.2 Type C modes

Here we have to contend with two components of longitudinal displacement, parallel and perpendicular to the radius vector at any point, each one having its own nodal system.

a) $n = 1$ modes. The longitudinal displacements may be written in the form:

16.3 $$U = U'\cos\theta \qquad (1)$$

$$V = V'\sin\theta \qquad (2)$$

The nodes of each consist of a single diameter plus

B modes, side 2

16.13

16.14

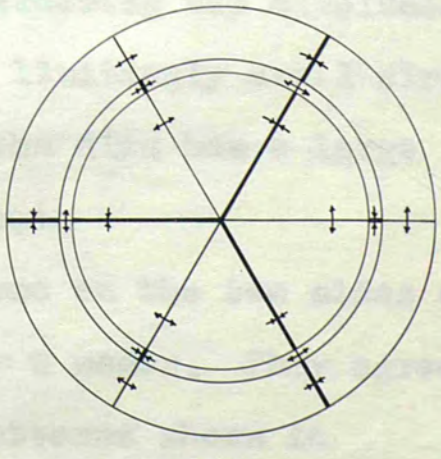

16.15

a set of circles whose radii are found from the roots of U' and V'. The diametral nodes of the two displacements are mutually perpendicular and in general the circular nodes do not coincide. The circular nodes have to be found graphically by plotting U' and V' against r.

The displacements have been calculated for the first two modes only and are shown in Figs 16.16 and 16.17. The radii of the nodal circles do not form a regular series as in the case of the type A and B modes. All that can be said is that the number of circles increases with mode order and for a given mode there are usually more nodes of the tangential than of the radial displacement. At the first sight the centre would appear to be an absolute node of longitudinal displacement, as the nodal diameters of U and V intersect there. But the graphs of U' and V' against r have a maximum at r = 0 and by considering the displacements at points on the circumference of a limitingly small circle, it may be shown that the centre of the disc has a large amplitude of longitudinal displacement.

Figs 16.18-21 show the patterns on the two sides of the crystal for the two different m = 0 modes. They agree well with the normal displacement patterns shown in Figs 13.26, 13.28 and 13.30. The nodes which are actually

Longitudinal Displacement n = 1 modes

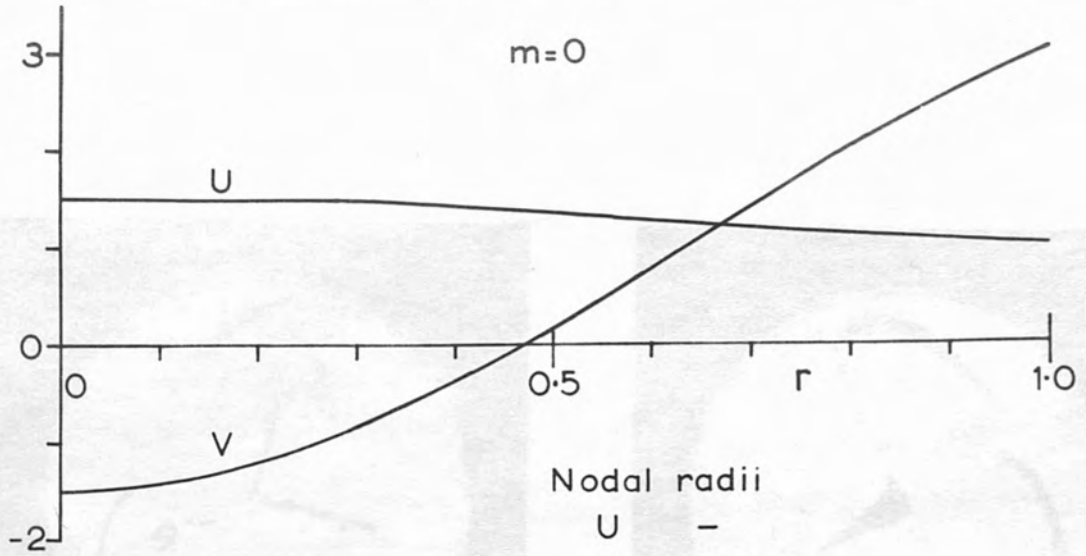

Nodal radii

U	–
V	0·47

16.16

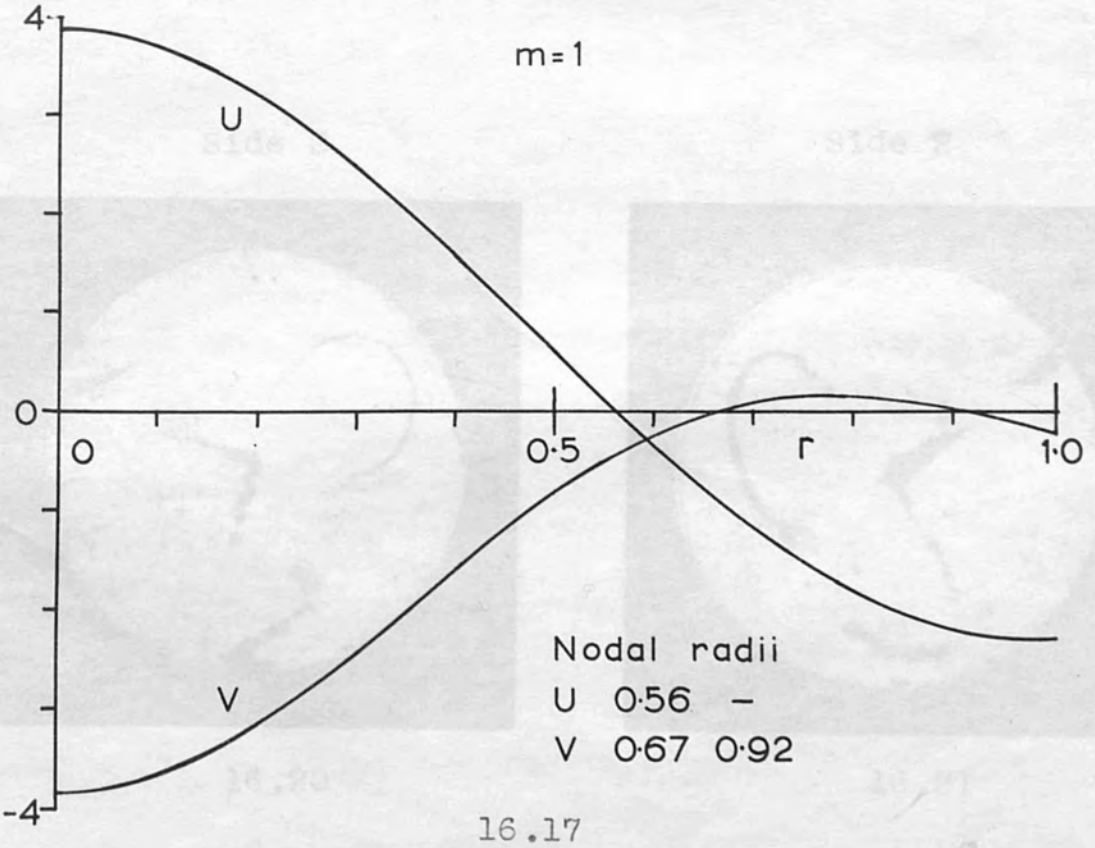

Nodal radii

U	0·56	–
V	0·67	0·92

16.17

n = 1, m = 0 mode

117.9 Kc/s

Side 1

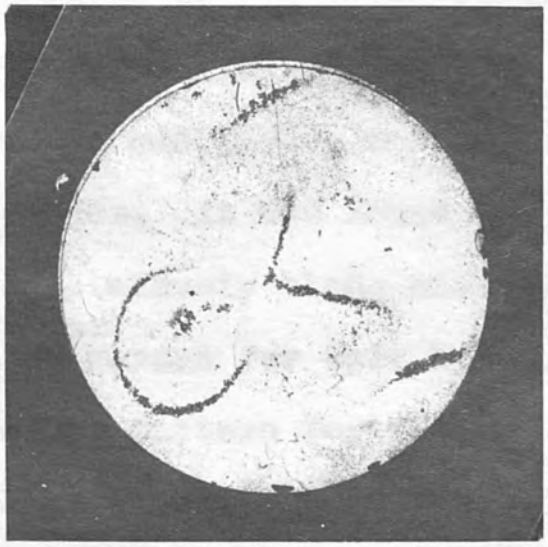

16.18

117.7 Kc/s

Side 1

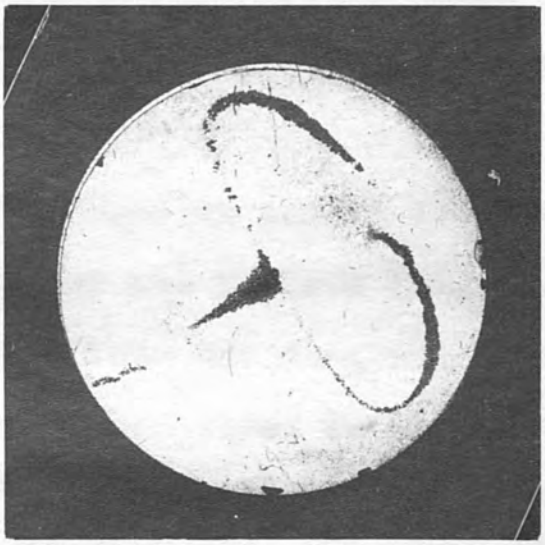

16.19

Side 2

16.20

Side 2

16.21

shown up by the lycopodium powder may be explained in the same way as for the A and B modes. Fig 16.22 shows a tracing of the nodes of one of the normal displacement patterns (Fig 13.30) with the nodes of longitudinal motion added and arrows showing the direction of motion of the powder. It was found that the lycopodium powder streamed continuously along certain parts of the pattern (Fig 16.19), the reason for this being obvious from the diagram. The other pattern for this mode can be explained in the same way. Figs 16.23-26 show the pattern on both sides of the crystal for the two types of vibration corresponding to $m = 1$.

b) $n = 2$ modes. Figs 16.27-30 show the patterns observed on the two sides of the crystal for the two modes corresponding to $m=0$. No analysis is given here but, in general, the nodes correspond to parts of the nodal system of the normal displacement and the rules given for the motion of the lycopodium powder apply in these cases also.

Fig 16.22

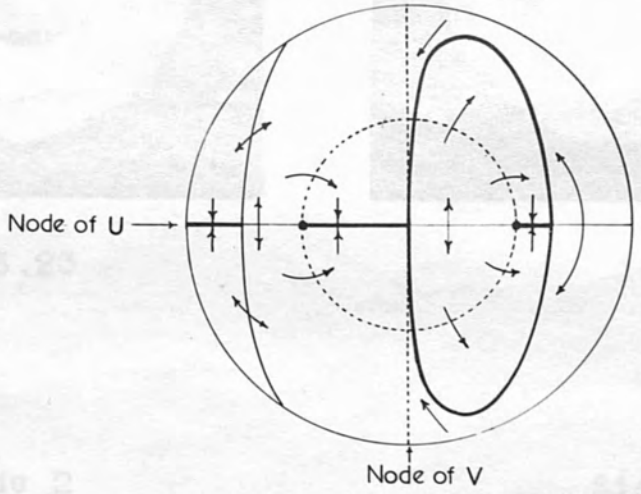

Radius of circular node of V is 0·47a

n = 1, m = 1 mode

243.6 Kc/s

Side 1

16.23

243.7 Kc/s

Side 1

16.24

Side 2

16.25

Side 2

16.26

n = 2, m = 0 mode

105.8 Kc/s

Side 1

16.27

105.6 Kc/s

Side 1

16.28

Side 2

16.29

Side 2

16.30

CHAPTER 17

DISCUSSION OF RESULTS

17.1 Mechanism of the coupling between modes

a) General theory. Since performing these experiments it has been found possible to explain most of the observed coupling effects by considering the nature of the secondary shear strains due to the particular symmetry of crystalline quartz which have, so far, been ignored. From eqn 5.3 these strains are:

17.1 $y_z = s_{14}(X_x - Y_y)$ (1) $z_x = 2s_{14}X_y$ (2)

and are equivalent to a shear strain of magnitude $\sqrt{y_z^2 + z_x^2}$ acting in a plane normal to an axis in the XY-plane at an angle $-\tan^{-1}(z_x/y_z)$ to the X-axis. If the stresses X_x, Y_y and X_y are expressed in terms of the stress resultants and the latter are written in the form:

17.2 $(T_r - T_\theta)/2h = T\cos(n\theta)$ (1) $2S_{r\theta}/2h = S\sin(n\theta)$ (2)

then it may easily be shown that:

17.3 $y_z = (s_{44}/2)\left[(T+S)\cos(n+2) + (T-S)\cos(n-2)\right]$ (1)

$z_x = (s_{14}/2)\left[(T+S)\sin(n+2) - (T-S)\sin(n-2)\right]$ (2)

the X-axis of the quartz crystal being taken as initial line.

At any point on a circle for which $T - S = 0$, the resultant shear strain is $\frac{1}{2}s_{14}(T+S)$ and the axis of shear (i.e. the line normal to the plane of shear) makes an angle

$-(n+2)\theta$ with the X-axis, that is $-(n+3)\theta$ with the radius vector. Thus the resulting strain system has $(n+3)$-fold symmetry and there are $(n+3)$ values of θ for which the axis of shear is parallel to the radius vector. These directions are favourable for the formation of the diametral nodes of a flexural vibration, since the shear strain about the radius vector has a maximum value in these directions.

Alternatively, at any point on a circle for which $T+S=0$, the resultant strain is $\frac{1}{2}s_{14}(T-S)$ and the axis of shear makes an angle $+(n-2)\theta$ with the X-axis, that is $+(n-3)\theta$ with the radius vector. In general, when T and S have any values, there will be a tendency for coupling to flexural modes (or shear modes in the case of thick crystals) having $(n\pm3)$ diametral nodes, and a number of circular nodes which depends upon the frequency of vibration in the way already discussed in Section 13.1(a).

b) Symmetrical modes $(n=0)$. For type A modes $S=0$, and the axis of shear makes an angle -3θ with the X-axis. Thus the axis of shear is parallel to the radius vector along the three X-axes and conditions are favourable for a coupled flexure having three diametral nodes along these axes. It is seen from Figs 13.17 and 16.8 that the axes of symmetry of the interferometric and lycopodium powder patterns for

the A type modes bisect the angles between the nodes of the coupled flexure and should thus lie along the Y-axes. This is precisely what has been observed and commented upon by Petrzilka (1935a).

For the type B modes, it is found that the axis of shear makes an angle $\pi/2 - 3\theta$ with the radius vector and is thus parallel to it along the three Y-axes. This favours a coupled flexure having three diametral nodes along the Y-axes. For these modes the axes of symmetry of the interference or powder patterns are coincident with the flexural nodes and thus lie along the Y-axes, as for Type A. Petrzilka observed this effect also.

c) Type C modes. For the symmetrical modes the choice of initial line is arbitrary, but for Type C modes a more general theory is required. If the initial line of the cylindrical coordinates to which the vibratory system is referred makes an angle α with the X-axis of the crystal, then it is easily shown that the coupled shear strain system with $(n+3)$-fold symmetry is turned through an angle $n\alpha/(n+3)$ and the system with $(n-3)$-fold symmetry through an angle $n\alpha/(n-3)$ relative to their former positions; if the angle between the initial line and the X-axis alters by α then the shear strain systems change their orientations by

these angles also.

According to this theory, the flexures favoured by the n = 1 modes have two or four diametral nodes. The relative magnitudes of these flexures depend upon the way in which T- S and T+ S vary throughout the crystal for the particular mode concerned; the radii of the circular flexural nodes depend upon the value of the frequency of vibration in relation to the frequencies of free flexures having these numbers of diametral nodes. If we accept the fact that there are two possible vibration states for each of the type C modes, whose orientations relative to the crystal differ by 90°, then it follows automatically from the theory just given that whatever are the orientations of the coupled flexures for the one state, those for the other will differ by -45° and +22½° respectively. It has already been mentioned in Chapter 13 that flexures with two and four diametral nodes are in fact coupled to the n = 1 modes and there was also evidence that the two diametral node flexure turned through an angle of 45° for the second vibratory state.

When n = 2, the favoured flexures have one or five diametral nodes. This is precisely what was observed in Chapter 13. Moreover, if the primary longitudinal mode changes its orientation by 45° for the second vibratory state,

which has been observed experimentally and is supported by Rayleigh's theory (see Section 14.5), then the coupled flexures turn through -90° and $+18^{\circ}$ respectively. In general, for the two vibration states of any type C mode which are allowed by Rayleigh's theory, the two coupled flexural modes take up orientations which differ by the angles allowed for by the same theory, supposing that they were free.

There is a great deal of information inherent in this theory which is capable of direct verification by observation with simple interference. The relative orientations of the primary longitudinal vibration and the coupled flexural vibration may be further checked by using the other methods of observation. The theory shows great promise of explaining most of the observed coupling phenomena.

17.2 Some comments on phenomena observed by previous workers

a) Polarized light phenomena. Moens and Verschaffelt (1927) found that a vibrating quartz bar showed an increase in the apparent rotatory power, this manifesting itself by a shift of the extinction band in the spectrum transmitted by the crystal when placed between crossed polarizer and analyser and illuminated by white light. They attributed this to some peculiar property of the quartz when vibrating, since they could not produce the effect by static mechanical or electric

stress. They considered that this failure confirmed Ny Tsi Ze's observation (1927a) that a quartz crystal is hardly strained in the Z-direction when subjected to an electric field in the XY-plane. This remark is irrelevant, however, since there is no connection between the strain in the Z-direction and the change of the optical properties for light propagated in this direction.

Their failure to observe the static effect was probably due to their not appreciating the truly enormous stresses, both mechanical and electrical, present in a resonating quartz crystal. Using the theory of Chapter 7 and the value of $(q_{11} - q_{12})$ given in Chapter 14, the stress necessary to produce their quoted change of 20°-30° in the rotation would necessitate a force of at least 200Kg applied to the face of the crystal which they used, as they attempted to produce the effect by uniform compression. From Pockels' values of the electro-optic constants of quartz, a potential difference of 10KV between the crystal faces would be required to produce the same effect. They do not mention the order of magnitude of the stresses which they applied but evidently they did not go to these extremes. It has already been shown in Chapter 14 that the requisite stresses are easily produced by simple bending.

Pan Tcheng Kao (1935) noticed that the high order modes of a vibrating rectangular Z-cut quartz crystal had the appearance of a regular array of red and green spots when the crystal was examined in reflection by white plane polarized light, using a crossed analyser. Now under these conditions he was, although he did not realize it, observing the isoclinic patterns corresponding to principal stress directions differing by half the optical rotation of the quartz from the directions of the axes of polarizer and analyser. Since he used white light, the isoclinic parameter varied for each colour, owing to the rotatory dispersion of the quartz. Thus at any point of the crystal where there was the correct relation between the principal stress directions and the rotation for a particular colour, this colour would be stopped by the analyser and the complementary colour would show up. Thus the general appearance was that of diffuse isoclinics coloured red on one side and green or blue on the other.

b) Petrzilka's observations of longitudinal vibrations by the lycopodium powder method. In Petrzilka's experiments on tourmaline (1932), since the electric and optic axes coincide, the electrodes consisted of two discs parallel to the circular faces of the crystal. He noticed that although the type A modes were easily excited, the B modes were excited

with great difficulty unless the disc protruded slightly from the electrodes, in which case excitation was as easy as for type A. He did not offer an explanation for this effect but the reason is obvious on inspecting the piezoelectric constants for tourmaline (See, for example, Cady (1946) p.225). An electric field along the Z-axis produces only longitudinal stresses along X,Y or Z. To produce the shearing stress in the XY-plane necessary for type B modes, a field component along the X or Y-axis is required. If the disc is displaced slightly, so that part of it lies in the curved field between the edges of the electrodes, then such a component comes into play. Piezoelectric effects have been largely ignored in this work but since the alternating electric field between the electrodes provides the driving force, then however slight its effect on the resulting motion, it must have a component which produces the right type of stress before resonance can occur.

For the type C modes the radial and tangential displacements are:

17.4 $U = U'\cos(n\theta)$ (1) $V = V'\sin(n\theta)$ (2)

Petrzilka (1935a) interpreted these equations by saying that, at the frequency corresponding to any given mode, there are three possible nodal patterns, given by:

17.5 $U' = 0, \quad \sin(n\theta) = 0 \quad (1)$

$V' = 0, \quad \cos(n\theta) = 0 \quad (2)$

$U' = 0, \quad V' = 0 \quad (3)$

This is entirely incorrect. The two relations (1) and (2), taken together, define all possible absolute nodes of longitudinal displacement. They exist simultaneously and cannot be established separately. The third relation is impossible, in general, although it is occasionally possible that a root of $U' = 0$ nearly coincides with a root of $V' = 0$. It would have been just as logical to give $\sin(n\theta) = 0, \cos(n\theta) = 0$ as a fourth nodal system, which is clearly meaningless. But what must be explained is the fact that Petrzilka actually did obtain three different nodal patterns at the expected frequencies of the type C modes.

As described in Chapter 16, the present author has found two patterns for each mode and these fit in with the normal displacement patterns shown in Chapter 13, the origin of which has already been discussed. These account for two of Petrzilka's observed powder patterns and are in fact very similar to his. The third pattern which he observed was of an entirely different character from the first two, usually consisting of discrete heaps of powder. It was found in the present experiments that if, having established one

of the two patterns for a given mode, the frequency was altered to the value required for the production of the alternative pattern, the powder rearranged itself into heaps whose configuration was similar to that of the third type of pattern shown by Petrzilka and seemed to indicate points common to both patterns. This phenomenon could be produced by a transition in either direction. If the surface was subsequently sprinkled with lycopodium powder the rest of the pattern could, of course, be defined.

17.3 Further comments on the methods of observation

a) Multiple-beam interference. This is the only method capable of giving the numerical magnitude of one of the variables associated with vibrations. Although it has not actually been used for measurement in the present work, but only to indicate the nodal regions, it is capable of a high degree of accuracy and requires no calibration, all the information necessary for a calculation of amplitude being present on one photographic plate. As there is no possible doubt as to the meaning of the fringe displacement, apart from the small uncertainty of the amplitude, mentioned in Section 6.3, the results given by the other methods of observation must be so interpreted as to conform with the results of the interferometric study.

While the multiple-beam method offers great advantages for the purpose of amplitude measurement, the author considers that a dark field two-beam method such as that of Straubel (see Section 4.1) gives a better indication of the nodal regions. It sometimes happens, when two modes are coupled, that large areas of the surface have only a small amplitude of normal displacement and it is difficult to say just where the fringe displacement is zero. In the case of the dark field two-beam method, however, only the nodes remain completely dark and it is much simpler to see the general configuration of the nodal pattern. These patterns have the same type of intensity distribution as the stress patterns of Chapter 14 but are more sharply defined as the phase differences between the two interfering beams are generally much larger.

b) Polarized light. This method has been used very successfully in this work but there are still a number of features which require a fuller explanation. In the special case of the Z-cut crystals used here, the general principles of photo-elastic stress analysis may be applied, with the reservations mentioned at the end of Chapter 7, when examining longitudinal vibrations in the XY-plane.

For very thin crystals there is practically perfect agreement between the theoretical and observed stress patterns,

while for thicker crystals the patterns are distorted, those for the A and B modes no longer indicating circular symmetry of the stress system. Now the cross shear strains discussed in Section 17.1 serve merely as a means of excitation of the favoured flexural modes. The additional normal displacement, superfluous to Love's theory, is not the manifestation of these strains, since the distribution of the normal displacement due to these is independent of the crystal thickness, and we have seen that the nature of the coupled normal displacement varies with this thickness. The coupled flexural modes are complete in themselves, although forced, and consequently additional stresses must exist, their magnitude depending upon the differences between cross shear strains due to the primary longitudinal stresses and the strains, both longitudinal and shear, due to the flexural vibrations. These stresses give rise to the discrepancies between the calculated and observed stress patterns.

It is, perhaps, surprising that the stress patterns for the thin crystals should not be distorted, in spite of the fact that the coupled flexural displacements are as great as, or greater than, those of the thicker crystals.

The reason for this lies in the nature of the flexural vibrations. It is well known that when lateral waves are propagated in a lamina, if the frequency is increased until the wavelength is no longer very great compared with the thickness of the lamina, there is a gradual transition from pure bending waves, for which the stresses are entirely longitudinal, to shear waves, which are accompanied by shear stresses acting about axes in the lamina parallel to the wavefronts. Experiments on this subject by previous workers have been mentioned in Section 2.1.

Now the overall birefringence of an isotropic lamina to light traversing it normally is zero, when vibrating flexurally, since the retardations due to the longitudinal stresses in elements which are symmetrically disposed about the median plane are equal and opposite, and moreover no birefringence is produced by shear stress acting in planes parallel to the direction of propagation.

In quartz there is bound to be a small net retardation due to the longitudinal stresses, on account of the optical activity. This is difficult to discuss analytically but is simply explained qualitatively by reference to the Poincaré sphere; Jerrard (1954) has given a concise account of the theory and uses of this elegant method for representing the properties of birefringent, optically active media. These effects are of

the second order only, however, the main difference between quartz and an isotropic medium being the presence of the stress optic coefficients $q_{65} = -q_{24} = q_{14}$.

The effect of these coefficients, considered alone, is that if a given shear stress acts about an axis in the XY-plane at an angle θ to the X-axis, then the resultant birefringence in the Z-direction is independent of θ, but one axis of the section of the index ellipsoid by the XY-plane makes an angle $-3\theta/2$ with the axis of shear. As a consequence, the shear stresses due to the coupled flexural modes alter the configuration of the stress patterns. The 'isoclinics' in this case will not represent points at which the principal stresses have a fixed direction, but points at which there is a particular relation between the magnitudes and directions of the primary longitudinal and secondary shear stresses.

c) Lycopodium powder patterns. This method, although regarded by the author with some suspicion, at first, has proved to be as valuable as the other methods for establishing the true nature of a given vibratory system. It can be used to find the phase relation between the longitudinal and normal components of displacement, and thus proves useful for empirical investigation in cases where the nature of a coupled mode is not known. The simple theory of the motion of the lycopodium

spores, outlined in Chapter 8, has proved adequate for an explanation of all the patterns so far observed.

17.4 Conclusions and future work

From the experimental evidence presented here, it is true to say that Love's theory satisfactorily describes the longitudinal vibrations of thin isotropic discs. The anomalies observed by Petrzilka, and confirmed by the present author, are entirely due to the crystal structure of the quartz and may be explained adequately in terms of the cross shear strains due to the primary plane stress system. There is scope for a more extensive and mathematical study of the phenomenon of coupling and it may be possible to calculate the amplitude of the coupled modes in terms of the amplitude of the longitudinal modes.

It will be interesting to extend the calculations of frequencies, stresses and displacements to type C modes for which n is greater than two. The $n=3$ modes are particularly interesting, as these favour coupled flexural modes having no diametral nodes or six diametral nodes and may be simpler to interpret than the others. An investigation of the longitudinal vibrations of rectangular Z-cut quartz crystals, already studied by Petrzilka using lycopodium powder (1935b), should also be worthwhile, and it would be

interesting to determine the nature of the coupled flexural modes in this case. It may be possible to study the free flexural vibrations of Z-cut quartz laminae by means of the optical effects caused by the shear stresses, discussed in the previous section.

As regards the correlation between the various methods of observation, which was the primary object of the work described here, there has been excellent correspondence of the results, and no serious discrepancies have been observed. The three methods have been regarded as complementary throughout and the empirical explanation of the coupling phenomenon was the logical outcome of a constant comparison of the information yielded by them.

Finally, these experiments have shown that it is generally unreasonable to expect any one method of observation to give a reliable guide to the type of motion of a vibrating body. This has been one of the pitfalls of previous experimenters. Most of the optical methods of investigation present the results in an extremely elegant manner but, by themselves, such results are of limited value. When discussing the results of empirical experiments, previous workers have emphazised the need for applying their methods to large numbers of crystals, in order to recognize the

various types of vibration and the influence of crystal shape on the nodal patterns. The author is of the opinion that this point of view should be reversed, and the largest possible number of methods of observation should be applied to the examination of a single type of vibratory mode, using the same crystal for all the experiments.

REFERENCES

AIREY,J.R.(1913) Arch.Math.Phys.,Lpz.20,289.

AIRY,G.B. (1831) Math.Tracts.

ANDRADE,E.N.da C.and SMITH,D.H.(1931)Proc.Phys.Soc.Lond. 43,405.

BARDSLEY,W.(1951)Ph.D.Thesis,London.

BELK,J.A.,TOLANSKY,S.and TURNBULL,D.T.(1954)J.Opt.Soc.Amer. 44,5.

BERGMANN,L.(1949)Z.Phys.125,405.

BORODOVSKAYA,L.N.and SALOMONOVICH,A.E.(1951)J.Tech.Phys.U.S.S.R. 21,221.

BREWSTER,D.(1815)Phil.Trans.60.
(1818)Trans.Roy.Soc.Edinb.8,281.

BROSSEL,J.(1947)Proc.Phys.Soc.Lond.59,224.

BRUCE,C.F.,MACINANTE,J.A.and KELLY,J.C.(1951)Nature Lond. 167,52.

BRUNINGHAUS,L.(1935)J.Phys.Radium 6,159.

BÜCKING,H.(1883)Z.Kristallogr.7,555.

CADY,W.G.(1946)Piezoelectricity,Mcgraw-Hill.

CHLADNI,E.F.F.(1787)Entdeckungen über die Theorie des Klanges,Leipzig.

COLWELL,R.C.(1931)Phil.Mag.12,320.

COLWELL,R.C.and HILL,L.R.(1937)J.Appl.Phys.8,68.

CORTEZ,S.H.(1934)J.Opt.Soc.Amer.24,127.

DOERFFLER,H.(1930)Z.Phys.63,30.

DRUDE,P.(1905)The Theory of Optics,Longmans Green.

DYE,D.W.(1932)Proc.Roy.Soc.138,1.

EICHHORN,K.(1936)Z.Tech.Phys.17,276.

GÜNTHER,N.(1932)Ann.Phys.,Lpz.13,783.

HARDING,J.W.and WHITE,F.W.G.(1929)Phil.Mag.8,169.

HUND,A.(1926)Proc.Inst.Radio Engrs,N.Y.14,447.

JERRARD,H.G.(1954)J.Opt.Soc.Amer.44,634.

KAO,P.C.(1935)C.R.Acad.Sci.,Paris 200,563.

KIRCHOFF,G.(1850)J.reine angew.Math.40,51.

KOTLYAREVSKI,M.L.and PUMPER,E.Ya.(1941)J.Phys.U.S.S.R. 4,67.

KRISTA,F.(1939)Z.Phys.112,326.

KUNDT,A.(1883)Ann.Phys.,Lpz.18,228.

LISSAJOUS,J.A.(1858)C.R.Acad.Sci.,Paris 46,846.

LISSÜTIN,A.(1930)Z.Phys.59,265.

LONN,E.(1937)Ann.Phys.,Lpz.30,420.

LOVE,A.E.H.(1927)The Mathematical Theory of Elasticity,Cambridge.

MOENS,R.and VERSCHAFFELT,J.E.(1927)C.R.Acad.Sci.,Paris 184,1645.

MOIGNO and SOLEIL(1850)C.R.Acad.Sci.,Paris 30,361.

MURRAY,W.M.(1941)J.Appl.Phys.12,617.

NEUMANN,F.(1841)Ann.Phys.,Lpz.54,449.

OSTERBERG,H.(1929)Proc.Nat.Acad.Sci.,Wash.15,892.
(1932)J.Opt.Soc.Amer.22,19.
(1933)Phys.Rev.43,819.
(1934)Rev.Sci.Instrum.5,183.

PAVLIK,B.(1936)Ann.Phys.,Lpz.26,625.

PETRZILKA,V.(1931) Ann.Phys.,Lpz.11,623.
(1932) Ann.Phys.,Lpz.15,881.
(1935a)Ann.Phys.,Lpz.23,156.
(1935b)Z.Phys.97,436.

POCKELS,F.(1889)Ann.Phys.,Lpz.37,144.
(1890)N.Jahrb.f.Miner.Beil.7,224.

PRESTON,T.(1901)The Theory of Light,Macmillan.

RAYLEIGH,Lord(1894)Theory of Sound,Macmillan

RITZ,W.(1909)Ann.Phys.,Lpz.28,737.

RÖNTGEN,W.C.(1883)Ann.Phys.,Lpz.18,213.

SAVART,F.(1820)Ann.Chim.(Phys.)14,113.

SCHULZE,F.A.(1907)Ann.Phys.,Lpz.24,785.

SCHUMACHER,R.O.(1937)Telef.Z.18,16.

STRAUBEL,H.(1933)Phys.Z.34,894.
(1934)Phys.Z.35,179.

TAWIL,E.P.(1926)C.R.Acad.Sci.,Paris 183,1099.
(1929)C.R.Acad.Sci.,Paris 189,163.

TERQUEM,A.(1858)C.R.Acad.Sci.,Paris 46,775.

THOMAS,H.A.and WARREN,G.W.(1928)Phil.Mag.5,1125.

TOLANSKY,S.(1948)Multiple-beam Interferometry,Oxford.

TOLANSKY,S.and BARDSLEY,W.(1948)Nature,Lond.161,925.
(1951)Proc.Phys.Soc.,Lond.B 64,224.

WACHSMUTH,R.and AUER,H.(1928)Z.Phys.47,323.

WALLER,M.D.(1937)Proc.Phys.Soc.,Lond.49,522.
(1949)Proc.Phys.Soc.,Lond.B 62,277.

WRIGHT,R.B.and STUART,D.M.(1931)J.Res.Nat.Bur.Stand. 7,519.

ZACEK,A.and PETRZILKA,V.(1938)Phil.Mag.25,164.

ZE,N.T.(1927a)C.R.Acad.Sci.,Paris 184,1645.
(1927b)C.R.Acad.Sci.,Paris 185,195.

ZE,N.T.et al.(1936)Proc.Inst.Radio Engrs.N.Y.24,1484.

ACKNOWLEDGEMENTS

I wish to express my gratitude to Professor Tolansky for his encouragement throughout this work, to my colleagues for their helpful discussion, and to the laboratory staff for assistance with the apparatus.

I am grateful to the Department of Scientific and Industrial Research for the provision of a maintenance grant during part of the work.